HIGH-SHEAR DEFORMATION PROCESSING ON ALUMINUM ALLOY FOR SHEET PRODUCTION

by

Xiaolong Bai

A Dissertation

Submitted to the Faculty of Purdue University

In Partial Fulfillment of the Requirements for the degree of

Doctor of Philosophy

School of Materials Engineering

West Lafayette, Indiana

December 2018

THE PURDUE UNIVERSITY GRADUATE SCHOOL
STATEMENT OF COMMITTEE APPROVAL

Dr. Kevin P Trumble, Co-chair
School of Materials Engineering
Dr. Srinivasan Chandrasekar, Co-chair
School of Industrial Engineering
Dr. Matthew J M Krane
School of Materials Engineering
Dr. David R Johnson
School of Materials Engineering

Approved by:
Dr. David F Bahr
Head of the Graduate Program

To my family, with love

ACKNOWLEDGMENTS

The author would like first to thank his advisors, Prof. Kevin Trumble and Prof. Srinivasan Chandrasekar for their excellent guidance, constant support and invaluable discussion. He is also grateful to his committee members, Prof. Matthew Krane and David Johnson for their excellent suggestions on the research, which broaden his horizon on deformation processing.

The author also acknowledges his colleagues and friends for support throughout graduate school, Andrew Kustus, Yiwei Sun, Mojib Saei, Anirudh Udupa, Daniel Klenosky, Rui Tu, Xianyi Hu, and Yunze Dai. Special thanks to Andrew Kustus for the guidance on machining process and texture analysis; Yiwei Sun, for the help with rolling and discussion on texture; Lab manager in Industrial Engineering, Marc Williams, for the assistance with making small scale samples.

Finally, the author would like to express his deepest gratitude to his mother, father and brother, Caiyun Zhu, Chaotian Bai and Yifan Bai, for their unconditional support throughout graduate degree, and girlfriend Xiaomeng Zhang, who makes the graduate life enjoyable and memorable.

TABLE OF CONTENTS

LIST OF TABLES VIII
LIST OF FIGURES IX
ABSTRACT XIV
1. INTRODUCTION 1
1.1 Aluminum and aluminum alloys 1
1.1.1 General features 1
1.1.2 Alloy categories and tempers 2
1.1.2.1 Alloy categories 2
1.1.2.2 Aluminum temper designation system 4
1.2 Industrial production of 6xxx aluminum alloy sheets 5
1.3 Problem statement 8
2. BACKGROUND 10
2.1 Texture characterization 10
2.1.1 Pole figure 10
2.1.2 Orientation distribution function 13
2.2 Texture evolution during rolling and annealing process 16
2.2.1 Texture evolution during commercial rolling process 16
2.2.2 Texture evolution during annealing process 18
2.3 Particle stimulated nucleation 20
3. MACHINING-BASED PROCESSES 23
3.1 Free machining 23
3.2 Large strain extrusion machining 23
3.2.1 Deformation strain and hydrostatic pressure 24
3.2.2 Deformation temperature 26
3.2.3 Deformation path and controlling on texture 28
4. THERMOMECHANICAL CONTROL OF MICROSTRUCTURE IN LARGE STRAIN EXTRUSION MACHINING ON AGE-HARDENED ALUMINUM ALLOY 31
4.1 Introduction 31
4.2 Experimental procedure 32

4.3 Results and discussions 34
4.3.1 Free machining at ambient temperature 34
4.3.2 LSEM strips at ambient temperature 37
4.3.3 LSEM strips at high temperature 40
4.3.4 Static recrystallization of LSEM strips 42
4.3.5 Cold rolling on LSEM strips 43
4.3.6 Comparison of LSEM and rolled strips 45
4.3.6.1 Microstructure of the rolled and annealed strips 45
4.3.6.2 Ageing response of the strips 46
4.3.6.3 Mechanical properties of the strips 47
4.4 Implications 49
4.4.1 Controlling microstructure in LSEM 49
4.4.2 Dynamic and static recrystallization 50
4.5 Conclusions 51
5. ENHANCED WORKABILITY OF ALUMINUM STRIPS PRODUCED BY CUTTING-EXTRUSION ON AS-CAST AA6013 53
5.1 Introduction 53
5.2 Experimental procedure 53
5.3 Results 55
5.3.1 Casting of AA6013 55
5.3.2 FM and LSEM of as-cast 6013 alloy 56
5.3.3 Cold rolling of LSEM strips 59
5.3.4 Texture of LSEM strips 64
5.3.5 Microstructure and texture of annealed LSEM strip 66
5.4 Discussion 68
5.4.1 LSEM vs Hot rolling 68
5.4.2 Cold rolling after LSEM 69
5.4.3 Shear texture and workability 69
5.4.4 Microstructure evolution of cold rolled strip 71
5.4.5 Shear texture and formability 72
5.5 Conclusions 74

6. A NOVEL WAY TO PRODUCE ALUMINUM STRIPS BY MACHINING AND ROLLING PROCESS 75
6.1 Introduction 75
6.2 Experimental procedure 75
6.3 Results and discussions 76
6.3.1 Casting of 6013 aluminum alloy 76
6.3.2 Warm rolling of as-cast alloy 77
6.3.3 Cold rolling of warm rolled strips 79
6.4 Discussion 83
6.4.1 LSEM vs warm rolling 83
6.4.2 Cold rolling of LSEM and warm-rolled strips 84
6.4.3 Homogenization and solution treatment of LSEM strips 85
6.5 Summary 88
7. CONCLUSIONS AND RECOMMENDATIONS FOR FUTURE WORK 90
7.1 Conclusions 90
7.2 Future work 92
REFERENCE 94
VITA 103

LIST OF TABLES

Table 1.1 Aluminum Association designation system for wrought aluminum alloy 3

Table 1.2 Aluminum Association designation system for cast aluminum alloy..... 4

Table 1.3 Basic aluminum alloy temper designations 5

Table 2.1 Miller indices and Euler angles of the most important orientations of aluminum sheets after rolling and annealing. 15

Table 4.1 Free machining parameters and results at room temperature 35

Table 4.2 LSEM parameters and results at room temperature..... 37

Table 4.3 Parameters and results of the high-temperature LSEM experiments 40

Table 4.4 Cold rolling parameters of LSEM 6013 aluminum strips..... 44

Table 5.1 FM and LSEM parameters at room temperature 57

Table 5.2 Rolling parameters of LSEM 6013 aluminum strips 60

Table 5.3 Calculated R values for common sheet texture components 73

Table 6.1 Warm rolling parameters on the as-cast 6013 workpieces 77

Table 6.2 Cold rolling parameters on warm-rolled 6013 aluminum strips..... 80

LIST OF FIGURES

Figure 1.1 Schematic diagram showing commercial production of aluminum alloy sheets. 6

Figure 1.2 Evolution of grain structure during the thermomechanical processing of AA6016 sheets. (a)-(e) are microstructures after (a) solidification; (b) reversible hot rolling; (c) multi-stand hot rolling; (d) cold rolling; (e) annealing process. (After [18], with permission of Elsevier) 7

Figure 2.1 Schematic illustration of the relationship between the crystal and specimen axis for the {100}<001> Cube orientation: (100) plane is parallel to the specimen normal plane and [001] is parallel to the specimen rolling direction. 10

Figure 2.2 Presentation of pole figure. (a) Stereographic projection of P in sample coordinate with RD (rolling direction), TD (transverse direction) and ND (normal direction); (b) pole figure of this crystallographic plane. 11

Figure 2.3 {100} poles of a cubic crystal in the stereographic projection. (a) Crystal in the unit sphere; (b) {100} pole figure on the equatorial plane. 11

Figure 2.4 Derivation of 2-D pole figure from EBSD measurement using OIM software, showing different intensities of certain texture component. 12

Figure 2.5 {111} pole figure of the most common rolling and annealing textures. 13

Figure 2.6 Diagram showing the rotation between the specimen and crystal axis through the Euler angles φ_1, Φ, φ_2 in order 1, 2, 3. 14

Figure 2.7 Standard 2-Dpresentation of ODF at φ_2 = 80°section and plotted with iso-intensity lines with the maximum intensity 20.299 ×. 15

Figure 2.8 Common textures in (a) 3-D Euler angle space; (b) 2-D ODF at φ_2 = 0-90° with 5° interval and textures at φ_2 = 0, 45, 65 and 90° are labeled. The intensity contour values are in the lower right corner and the inside contour has the largest intensity. (After [18], with permission of Elsevier) 16

Figure 2.9 ODF showing texture after (a) reversible hot rolling; (b) multi-stand hot rolling and (c) cold rolling. Intensity contour values are in the lower right corner and the inside contour has the largest intensity. (From [18], with permission of Elsevier)..... 18

Figure 2.10 Typical annealing texture of 6xxx aluminum alloy. (From [18], with permission of Elsevier) 19

Figure 2.11 Materials are pre-heated to obtain coarsened Mg_2Si particles, resulting in a characteristic weak PSN recrystallization texture. (From [18], with permission of Elsevier) 21

Figure 3.1 Schematic of rotary free machining process with inset showing relative geometric parameters, where CFD, RFN and TD indicate chip flow direction, rake face normal and transverse direction..... 23

Figure 3.2 Schematic of rotary large strain extrusion machining process with inset showing relative geometric parameters. CFD, chip flow direction; RFN, rake face normal; TD, transverse direction. 24

Figure 3.3 Plot showing effect α and λ on effective ε (in red line) and hydro static pressure *p/2k* (in blue line). (After [55], with permission of Elsevier) 26

Figure 3.4 Dependence of T on V_0, T_0 and λ in LSEM of Mg AZ31B alloy. The machining parameters were: $t = 250$ μm, $\alpha = 5°$ (After [55], with permission of Elsevier)..... 27

Figure 3.5 PIV analysis showing side view of shear deformation in FM and LSEM. The top four images indicate material flow in machining process and the bottom four show the resultant stain rate fields. The strain rate tensor and shear direction for point c are compared (After [51], with permission of Elsevier) 29

Figure 4.1 Microstructure of polished and etched cross-sections of (a) as-received 6013-T6 plate showing (b) fine-grain structure near surfaces and (c) coarse-grain structure in the middle. Half-thickness of plate removed to produce workpieces containing adjacent fine- and coarse-grain regions as indicated in (a). 34

Figure 4.2 Microstructures of FM 6013-T6 strips. (a) fine-grain (b) coarse-grain side at V_0 = 0.5 m/s; (c) fine-grain (d) coarse-grain side at V_0 = 3 m/s. 36

Figure 4.3 Microstructures of LSEM 6013-T6 strips at λ = 1.5. (a) fine-grain (b) coarse-grain side at V_0 = 0.5 m/s; (c) fine-grain (d) coarse-grain side at V_0 = 3 m/s. 38

Figure 4.4 Microstructures of LSEM 6013-T6 strips at λ = 0.8. (a) fine-grain (b) coarse-grain side at V_0 = 0.5 m/s; (c) fine-grain (d) coarse-grain side at V_0 = 3 m/s. 39

Figure 4.5 Microstructures of LSEM 6013-T6 strips at λ = 1.5. (a) fine-grain (b) coarse-grain side at T_0 = 400 ℃; (c) fine-grain (d) coarse-grain side at T_0 = 300 ℃; (e) fine-grain (f) coarse-grain side at T_0 = 135 ℃. 41

Figure 4.6 Microstructures of annealed LSEM 6013-T6 strips at 572 ℃. (a) fine-grain (b) coarse-grain side for 1 min. 43

Figure 4.7 Top view of LSEM strips after different amount of cold rolling reduction. 44

Figure 4.8 Microstructures of (a) LSEM strips after (b) 10%, (c) 28%, (d) 60% and (e) 78% reduction. After rolling, the chip flow direction (CFD) becomes rolling direction (RD) and rake face normal (RFN) becomes normal direction (ND). 45

Figure 4.9 Microstructure of the strips after (a) warm-rolled with the same effective strain as LSEM strips and then (b) annealing, where ND and RD are normal and rolling direction. 46

Figure 4.10 Ageing response of the LSEM and warm-rolled strips after heat treatment at 190 ℃ for up to 420 min. 47

Figure 4.11 Engineering stress-strain curve of the LSEM and warm-rolled strips after solution treatment at 472 ℃ for 2 min. 48

Figure 5.1 Microstructure of the as-cast 6013 alloy: (a) EBSD inverse pole figure map, clearly showing grain size, (b) optical micrograph showing dendritic grain structure and porosity, and (c) showing the morphology of interdentritic phase α-AlFeSi and β-AlFeSi. 55

Figure 5.2 (a) Continuous strip produced by LSEM on as-cast 6013 alloy with effective strain 1.6 and surface roughness of (b) top surface and (c) rake face. 57

Figure 5.3 Microstructures of strips produced by FM and LSEM. (a) and (b) are microstructures of FM strips at 3 and 6 m/s, respectively, (c) is the microstructure of LSEM strip at $V0$ = 6 m/s with λ = 2.5. 59

Figure 5.4 Top view of LSEM strips after cold rolling for 17%, 44%, 65% and 73% reduction and surface roughness of the top surface after (b) 44% and (c) 73% reduction. 61

Figure 5.5 Microstructures of (a) LSEM strips after cold rolling for (b) 17% (c) 44% (d) 65% and (e) 73% reduction in a single step at room temperature..... 62

Figure 5.6 Relative thickness of constrained and primary shear zone of the LSEM strips after 17%, 44%, 65%, and 73% reduction..... 63

Figure 5.7 EBSD analysis showing texture data in constrained, primary shear and secondary shear zone in LSEM 6013 strip. The {111} and <110> shear texture fibers are highlighted in the (111) pole figures by black and magenta dotted lines, respectively. 65

Figure 5.8 Microstructure of LSEM strip annealed at 568 ℃ for 2 min, showing uniform structure with grain size around 20 μm. 67

Figure 5.9 Schematic showing flow line-type microstructure after LSEM process. Here σ, the compression imposed on the strip during rolling; σs, resolved shear stress along shear plane direction; β and θ are rotation angles of textures in constrained and primary shear zone..... 72

Figure 6.1 Microstructure of the as-cast 6013 alloy with (a) dendritic grain structure and (b) precipitations along grain boundary..... 77

Figure 6.2 (a) Top view of warm-rolled strips with 12% and 16% reduction per pass; (b) fracture surface of the sample rolled with 16%/pass; (c) through-thickness microstructure of the warm-rolled sample with 16%/pass, showing wavy grain structure along RD. 79

Figure 6.3 Top view of strips after cold rolling with (a) 17% and 26% (b) 46%, and (c) 65% reduction, showing the development of crack during cold rolling..... 81

Figure 6.4 Cross-section microstructures of warm-rolled strips (12%/pass) after cold rolling for (a) 17% and (b) 65% reduction. 82

Figure 6.5 Slip patterns of the (a) cold rolled of warm-rolled strips and (b) LSEM strips after 44% reduction in a single step. 83

Figure 6.6 Novel way to make aluminum strips by machining and rolling process. 88

ABSTRACT

Author: Bai, Xiaolong. PhD
Institution: Purdue University
Degree Received: December 2018
Title: High-Shear Deformation Processing on Aluminum Alloy for Sheet Production
Major Professor: Kevin P Trumble, Srinivasan Chandrasekar

Aluminum alloy sheets are typically manufactured from cast slabs by multi-step rolling and annealing process. This process is very energy intensive, especially in the homogenization process after casting, which usually is conducted at 480 to 580 ℃ for up to 48 h. To reduce the processing steps and energy, a shear-based single-step deformation process, large strain extrusion machining (LSEM), was used to create strips from AA6013-T6 with and without preheating of the workpiece. Continuous strips were obtained from this alloy with low workability. Flow patterns through the thickness of the strips exhibited primary shear with grains inclined steeply to the faces of the strips, modified to varying degrees by secondary shear from friction with the tools at the surfaces. Through control of the deformation parameters (strain, strain rate and temperature), a wide range of microstructure could be achieved. In high-temperature LSEM, dynamic recrystallization occurs at lower temperatures than in commercial hot rolling processes.

LSEM was performed directly on the as-cast AA6013 without homogenization. By appropriate combination of strain and strain rate, continuous strips were obtained in a single step without preheating directly from the as-cast workpiece. The highly deformed LSEM strip has enhanced workability. It can be cold rolled with at least 73% reduction in a single step without cracking. The strips were characterized by strong shear texture with partial {111} and <110> fibers. After annealing, a mixed texture containing simple shear texture and other texture develops. The annealed strips are expected to have better formability than commercial ones made by rolling.

In comparison, multi-step warm-rolling and cold rolling were performed on the as-cast AA6013. The as-cast material was preheated to 300 ℃ and rolled with 12% reduction per pass till the same effective strain as the LSEM. The warm-rolled strips were then cold-rolled with the same reductions as those on LSEM strips. The results showed that during warm rolling process, cracking occurs on the strips before reaching the same effective strain and the warm-rolled strips can only be further cold rolled with reduction less than 26% before cracking, compared with 73% reduction without cracking for LSEM strips.

Based on the simple shear LSEM process, a novel way to produce aluminum strip/sheet material is introduced. The alloys are cast into disk-shape workpiece and then transferred to the LSEM line. In this line, continuous strips/sheets are obtained in a single step at room temperature. The materials are then coiled if needed and cold rolled to the final gauge. Finally, the strips/sheets are solution treated for further deformation processing. In this method, the conventional homogenization and hot rolling, including reversing and multi-stand hot rolling, are replaced by a single-step LSEM process at room temperature.

1. INTRODUCTION

1.1 Aluminum and aluminum alloys

1.1.1 General features

Aluminum is the world's most abundant metal and third most common element, comprising 8% of the crust, as opposed to 5% of iron. The unique combination of properties, such as light weighting, oxidation and corrosion resistance, excellent electrical and thermal conductivity, and recyclability, makes it one of the most widely used metallic materials. Aluminum alloys are second only to steels in application as structural materials.

The most attractive property of aluminum is the low density 2.69 g/cm^3, which is approximately 1/3 that of steel (7.8 g/cm^3). Aluminum can be alloyed and strengthened by cold working and/or heat treatment to achieve a high strength, allowing designing and production of strong and lightweight structures that are applied in aerospace and automotive industries. It is estimated that a 10% reduction in vehicle weight leads to a reduction in fuel saving about 5~6% [1].

The exposed aluminum surface reacts with oxygen and form an inert oxidation film, preventing the progressive oxidation which causes steel to rust away. By appropriate treatment, aluminum can withstand corrosion by water, salt and a wide range of other chemical and physical agents. Aluminum displays excellent electrical and thermal conductivity. The electrical conductivity of aluminum is nearly two times as large as copper on an equivalent weight basis.

The oxidation and corrosion resistance of aluminum alloys make it more recyclable than steel. Although it takes more energy to win aluminum metal from its ore than it does for iron, recycling aluminum only need 5% energy of producing primary aluminum and 95% of aluminum

in scrapped cars are recycled, which offers a significant reduction in greenhouse gas emission [2-4].

Aluminum alloys may be processed into any form. They can be cast into complicated shapes or rolled to any desired thickness down to foil used for packaging. Aluminum sheet can be stamped and deep drawn. The metal also may be hammered or forged. It can be drawn into wire shape. There is almost no limit to the shapes in which the metal can be extruded.

1.1.2 Alloy categories and tempers

1.1.2.1 Alloy categories

Generally, aluminum alloys are divided into two major categories: wrought alloys and cast alloys. For each category, based on different strengthening mechanism, it can be subdivided into two groups: heat treatable alloys (precipitation-hardenable) alloys and non-heat treatable (work-hardenable) alloys.

The Aluminum Association system nomenclature is the most widely used system in USA for cast and wrought aluminum alloys. According to this system, a four-digit system is used to present wrought alloys and a list of wrought composition families are shown in Table 1.1[5-7].

Table 1.1 Aluminum Association designation system for wrought aluminum alloy

Alloy designation	Main alloy elements
1xxx	Pure Al (99.00% or greater)
2xxx	Al-Cu alloys
3xxx	Al-Mn alloys
4xxx	Al-Si alloys
5xxx	Al-Mg alloys
6xxx	Al-Mg-Si alloys
7xxx	Al-Zn alloys
8xxx	Al+other elements
9xxx	Unused series

In this designation, 2xxx, 6xxx, 7xxx and some of the 8xxx alloys are classified as heat-treatable aluminum alloys; while 1xxx, 3xxx, 4xxx, 5xxx and remaining 8xxx alloys are work-hardenable alloys.

Casting aluminum alloys are represented by a three-digit system followed by a decimal value. The first digit indicates the main alloying element added to the aluminum alloy. The second and third digits are arbitrary numbers to identify a specific alloy. The number following the decimal point indicates whether the alloy is a casting (.0) or an ingot (.1 or .2). A capital letter prefix (A, B and C) indicates a modification to a certain alloy. Table 1.2 [6-7] shows the Aluminum Association designation system for cast aluminum alloy. In this system, 2xx.x, 3xx.x 7xx.x series alloys are heat-treatable aluminum alloys.

Table 1.2 Aluminum Association designation system for cast aluminum alloy

Alloy designation	Main alloy elements
1xx.x	Pure Al (99.00% or greater)
2xx.x	Al-Cu alloys
3xx.x	Al-Si + Cu and/or Mg alloys
4xx.x	Al-Si alloys
5xx.x	Al-Mg alloys
7xx.x	Al-Zn alloys
8xx.x	Al-Sn alloys
9xx.x	Al+other elements
6xx.x	Unused series

1.1.2.2 Aluminum temper designation system

The heat-treatable alloys obtain their maximum mechanical properties through a series of heat treatment process, the most common heat treatments are solution heat treatment followed by artificial ageing. Solution heat treatment is the process of heating the alloys to elevated temperatures in order to dissolve the alloying elements or compounds into solid solution. Then the alloys are quenched, usually in water, to produce a supersaturated solution at room temperature. Finally, the alloys are artificial aged at proper temperatures for certain amount of time to acquired desirable properties.

The non-heat treatable alloys acquire their optimum mechanical properties through strain hardening. Strain hardening is the method of increasing strength through the application of cold working. Different thermomechanical processing of alloys is called temper. The temper designation system is an extension of the alloy designation system and consists of a series of letters and numbers which follow the alloy designation by a hyphen. Examples: 6061-T6, 6063-T4, 5052-H32, 5083-H112. The common temper designations are shown in Table 1.3 [5-7].

Table 1.3 Basic aluminum alloy temper designations

Designation	Meaning
F	As fabricated
O	Annealed
H	Strain hardened
W	Solution treated
T	Thermally treated

Numeric additions after “H” and “T” tempers indicate specific variations. For example, H14 stands for strain hardened for half hard, H18 for full hard; T4 means solution treated and naturally aged; T6 indicates solution treated and artificial aged.

1.2 Industrial production of 6xxx aluminum alloy sheets

In order to decrease the fuel consumption and emission of toxic gases, US government sets a goal for automakers that the auto fuel economy rises from 35.5 mile per gallon in 2016 to 50.8 by the year 2025. High-efficiency engine system and light weight bodywork are two main ways to achieve this target. Aluminum alloys have long been employed in aircraft construction since the 1930s because of high strength to weight ratio, good corrosion resistance and recycle potential [8-12]. And now it has been considered as potential substitute for conventional steel body sheet [13-15]. The Ford F-150, the best-selling light truck in north America auto market, has a better fuel efficiency, greater towing and payload capacities due to all-aluminum bodywork, which is 700 pounds lighter than the previous generation. Traditionally, solution strengthening 5xxx aluminum alloys are used for inner body parts with complicated shapes because of their good deep drawability. But Lüders bands appear during forming process due to discontinuous yielding phenomenon and even painting cannot cover this defect [16-17]. So 6xxx aluminum alloys are

usually employed for outer body panels. Now for recycling purpose, 6xxx aluminum alloys are used for both inner and outer panels.

The commercial production of aluminum alloy sheets consists of several thermomechanical steps before the final deformation processing (Figure 1.1) [18]. The alloys are usually direct-chill (DC) cast into large ingots (Figure 1.1a). During the solidification process, coarse Al(FeMn)Si constituent particles form at the grain boundaries (Figure 1.2a). The ingots are scalped on their rolling surface to remove the surface blemishes. Then the ingots are homogenized at temperatures around 550 ℃ for about 48 h (Figure 1.1b) to prepare for the following hot rolling process. During the homogenization process, the short-range intercellular segregation (coring) is reduced and soluble phases in the alloys are dissolved. The primary intermetallic particles change in shape, becoming more round and discrete, and their composition tends to shift to equilibrium, which are benefits for the following deformation process [19-23].

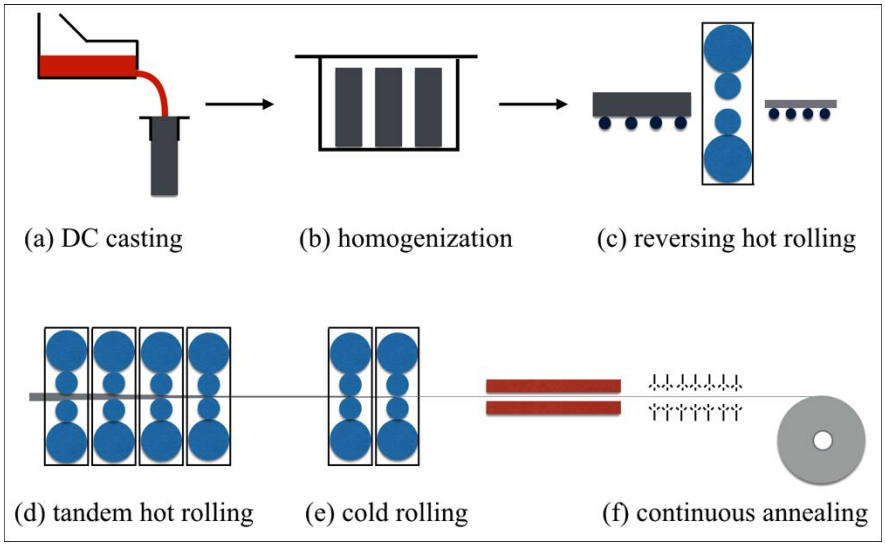

Figure 1.1 Schematic diagram showing commercial production of aluminum alloy sheets.

The hot ingots are then transferred to the hot rolling line, which typically consists of a reversing break-down mill (Figure 1.1c) and followed by a high-speed multi-stand tandem mill

(Figure 1.1d). In the break-down mill, the ingots are reversibly hot rolled in up to 25 passes to a thickness of around 30 mm at temperatures around 500 ℃, called transfer slab [24]. The microstructure of the transfer slab typically comprises slightly elongated recrystallized grains because of the high strain and deformation temperature, as shown in Figure 1.2b. In the following multi-stand hot rolling process, the transfer slab is hot rolled to a thickness around 5 mm, called hot band. The multi-stand hot rolling parameters change significantly compared to the reversing hot rolling: the rolling temperature reduces to about 400 ℃, while the strain and strain rate increase greatly. So, recrystallization is suppressed and the characteristic deformation structure - band structure - is dominant all through the hot band as shown in Figure 1.2c.

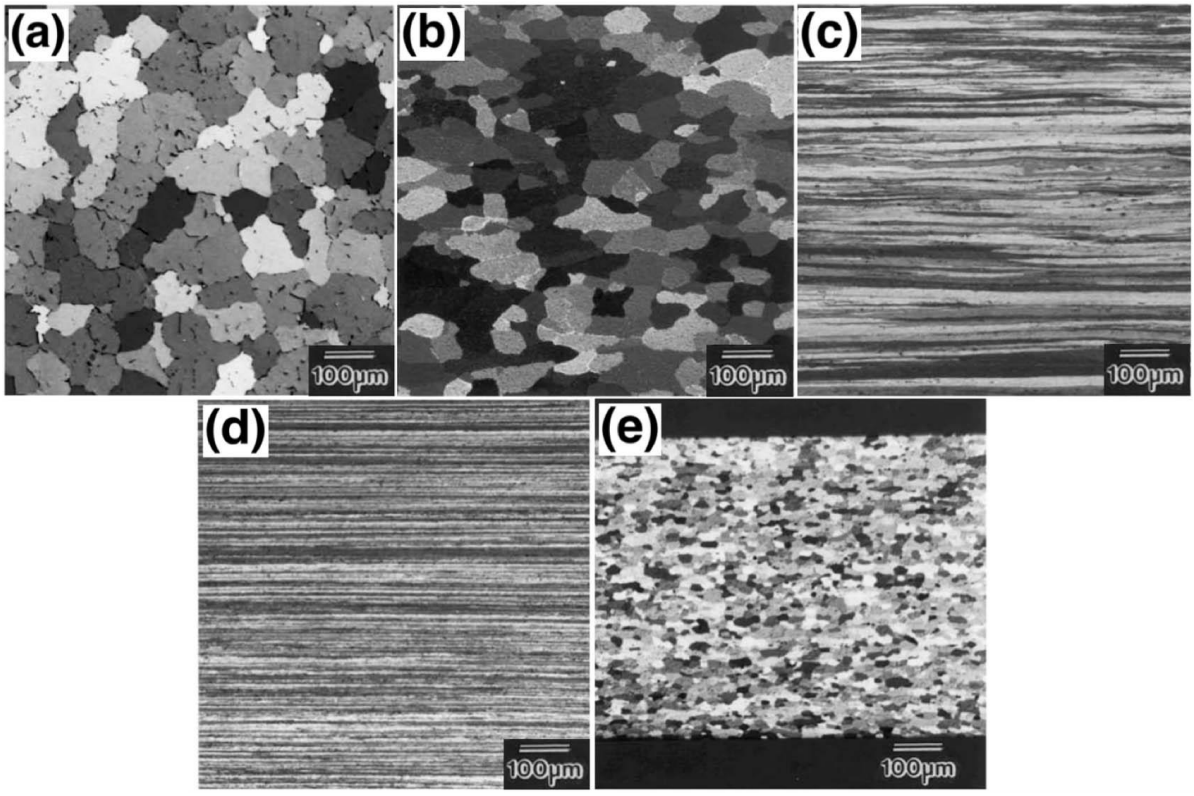

Figure 1.2 Evolution of grain structure during the thermomechanical processing of AA6016 sheets. (a)-(e) are microstructures after (a) solidification; (b) reversible hot rolling; (c) multi-stand hot rolling; (d) cold rolling; (e) annealing process. (After [18], with permission of Elsevier)

The hot band is then coiled and usually cooled before it is cold rolled to the final thickness of around 1 mm. After the cold rolling, the sheet consists of a highly elongated deformation structure (Figure 1.2d). In order to get the maximum age-hardening response and good formability, the sheet is then solution treated. The cold rolled sheet passes through a continuous annealing line as shown in Figure 1.1f. In this line, the sheet is rapidly heated to about 560 ℃ in order to dissolve the hardening phases (mainly Mg_2Si) that precipitated during the various preceding steps and then quenched to obtain the supersaturated solid solution. Complete recrystallization happens during this process and a fairly equiaxed microstructure with grain size about 20 μm develops as shown in Figure 1.2e. After the final annealing process, the sheet is flattened, possibly pre-aged for stabilization and maximization of the age-hardening response [25-26] in the paint bake cycle, and then pre-lubricated or pre-coated before blanking and the stamping process. After the forming process, the deformed sheet will undergo the paint bake cycle, which is usually at temperatures around 180 ℃ for about 1 h to achieve a higher strength.

1.3 Problem statement

Rolling process has many advantages. In hot rolling, large deformation can be accomplished rapidly and defects of the metal, such as porosity, can be considerably eliminated; in the following cold rolling, better dimension control and surface finish can be achieved. The disadvantages, however, are also obvious. Commercial rolling process of 6xxx aluminum alloy sheets is very energy intensive: first, homogenization of 6xxx usually occurs at temperatures around 550 ℃ for a cycle which may last for 2 days; second, in hot rolling process, the ingots are hot rolled at ~ 450 ℃ for multi-steps. The final sheet products have bad formability due to the resulting Cube and Goss texture developed in the annealing process. This is one of the main barrier that prevents the application of aluminum sheet materials on automotive outer body panels.

Besides, oxidation occurs and scale forms on the surface of the metal, leading to poor surface finish and loss of metal.

The goal of this thesis is to overcome the limitation of rolling by employing a single-step, shear-based technique to produce 6xxx sheet materials. Specific objectives include:

1. Examine the possibility to produce continuous sheets from aluminum alloys with low workability (T6 and as-cast condition).
2. Characterize the development of microstructures and texture of aluminum sheets produced by simple shear deformation.
3. Investigate the preliminary processing-structure-property relationships of aluminum sheet produced by simple shear and compare with commercial ones.
4. Develop new method to produce sheet materials based on simple shear deformation and compare with commercial rolling method.

2. BACKGROUND

2.1 Texture characterization

Texture is defined as the distribution of crystallographic orientations of polycrystalline materials. Samples with random orientations are thought to have no texture, but these are rare because any deformation/annealing process tends to align grains. Texture is usually denoted by Miller indices {hkl}<uvw>, where for the rolled sheet, {hkl} is the crystallographic plane parallel to specimen normal plane and <uvw> is the crystallographic direction parallel to specimen rolling direction as shown in Figure 2.1.

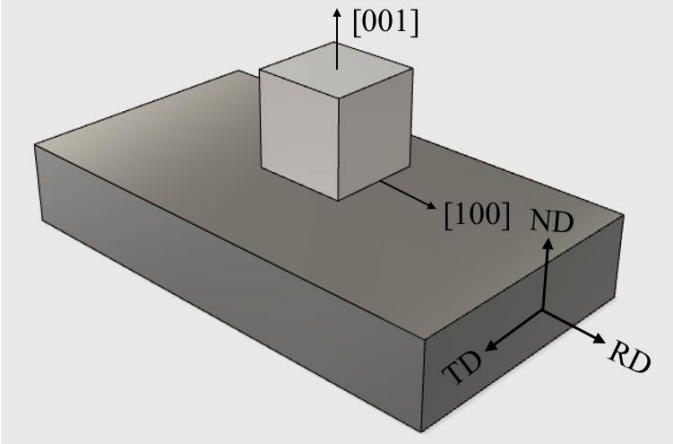

Figure 2.1 Schematic illustration of the relationship between the crystal and specimen axis for the {100}<001> Cube orientation: (100) plane is parallel to the specimen normal plane and [001] is parallel to the specimen rolling direction.

2.1.1 Pole figure

A pole is defined as the normal to the crystallographic plane. A stereographic projection of a pole is shown as Figure 2.2a where a crystal is imagined to be in the middle of the unit sphere O and the normal of a crystallographic plane (pole) intersects the sphere at P. Then P is projected from the 'South Pole' onto the equatorial plane at p′, so p′ is the stereographic projection of P. Figure 2.2b shows the orientation of this crystallographic plane at the equator plane and this is the

pole figure. Based on this definition, we can obtain the {100} pole figure of a certain crystal as shown in Figure 2.3.

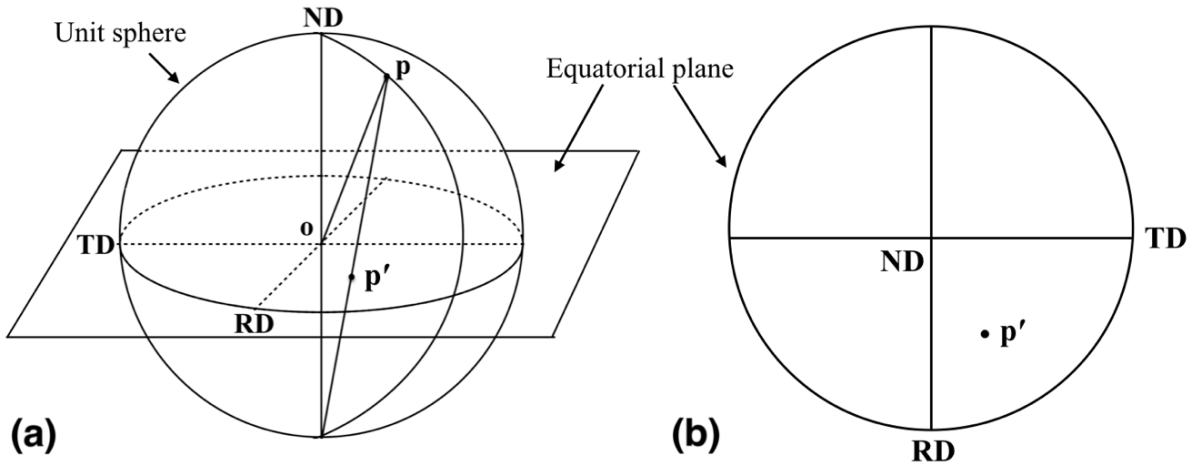

Figure 2.2 Presentation of pole figure. (a) Stereographic projection of P in sample coordinate with RD (rolling direction), TD (transverse direction) and ND (normal direction); (b) pole figure of this crystallographic plane.

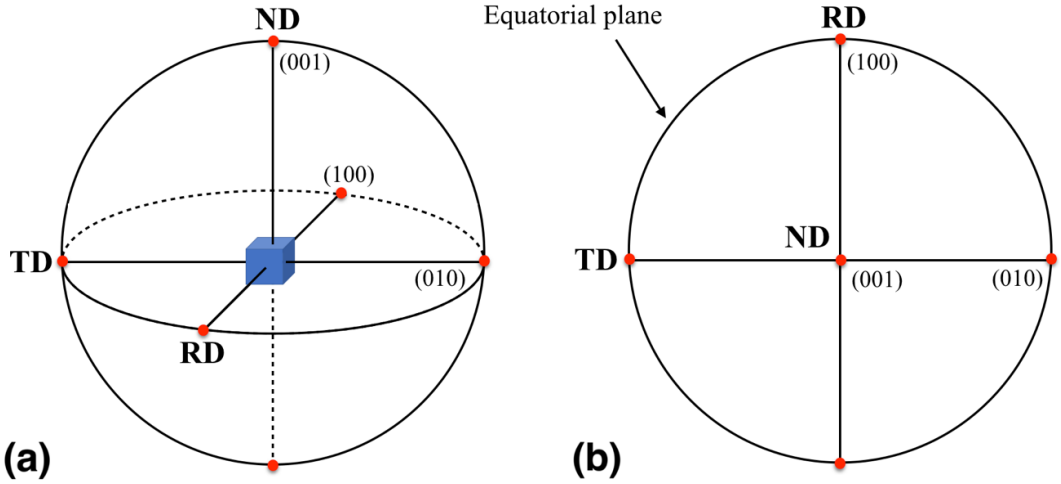

Figure 2.3 {100} poles of a cubic crystal in the stereographic projection. (a) Crystal in the unit sphere; (b) {100} pole figure on the equatorial plane.

In polycrystalline materials, even grains with the same texture seldom orient exactly the same, they may spread out about the ideal orientation and different textures may appear at similar

positions in one pole figure. So iso-intensity lines or contour lines are used to indicate the pole intensity around the ideal texture and each contour line represents a different pole intensity (Figure 2.4). The common unit to express the density of the texture is MRD (multiples of random distribution) of orientations, where MRD = 1 denotes random distribution, and a higher MRD number represents a stronger texture, as shown in Figure 2.4, where the inner loop has the strongest density 8.527 ×.

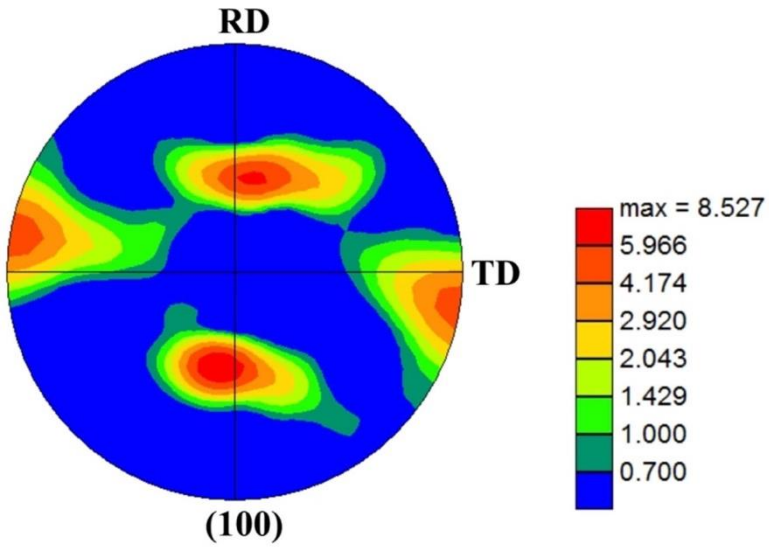

Figure 2.4 Derivation of 2-D pole figure from EBSD measurement using OIM software, showing different intensities of certain texture component.

There are two main kinds of textures during thermomechanical processing of aluminum alloy sheets: rolling texture (deformation texture) and annealing texture (recrystallization texture). The {111} pole figure of the most common textures from rolling and annealing is shown in Figure 2.5. In pole figures, different textures often overlap so it is hard to distinguish the intensity from each individual texture. This can be seen from the dotted circle in Figure 2.5, where the intensity actually results from the combination of Goss, S and Copper texture. So, we have to obtain as many pole figures as possible in order to separate different textures.

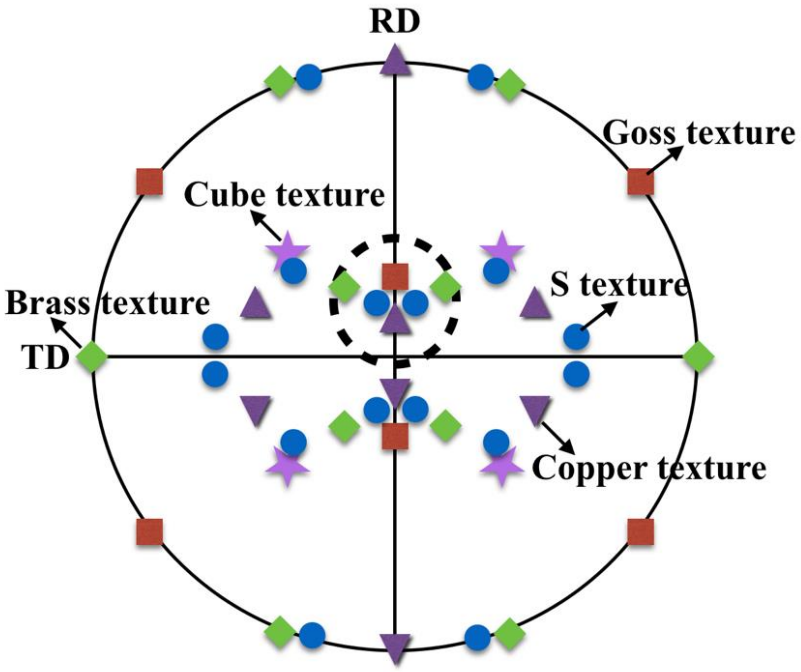

Figure 2.5 {111} pole figure of the most common rolling and annealing textures.

2.1.2 Orientation distribution function

Orientation distribution function (ODF) is a density function of the orientation and most commonly expressed by Euler angles φ_1, Φ, φ_2 formulated by H. J. Bunge [17, 18] ($0° \leq \varphi_1, \Phi, \varphi_2 \leq 90°$). The Euler anglers φ_1, Φ, φ_2 are the angles that are needed to rotate the sample axis to the crystal axis as shown in Figure 2.6. So, a certain texture corresponds to a specific group of Euler angles. For example, Cube texture {100}<001> appears in the Euler space at $\varphi_1 = 0°$, $\Phi = 0°$, $\varphi_2 = 0°/90°$.

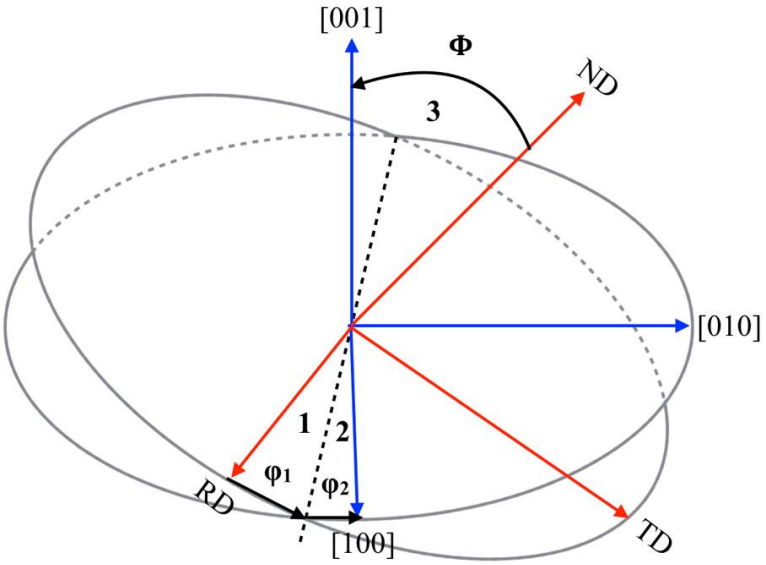

Figure 2.6 Diagram showing the rotation between the specimen and crystal axis through the Euler angles φ_1, Φ, φ_2 in order 1, 2, 3.

Similar to pole figure, a set of contour lines are used to denote the intensity around the ideal orientation as shown in Figure 2.7. So based on the ODF, the common textures and their ideal position in Euler space during rolling and annealing process are shown in Table 2.1 and Figure 2.8a. The ODF is a 3-D method to display the texture, which is complex, so 2-D ODF at certain φ_2 (0 - 90° with 5° interval) angles are usually employed to express the texture as shown in Figure 2.8b. Typically, ODF at φ_2 = 45, 65 and 90° are employed to display texture because most of the common textures shown in Table 2.1 are covered in these three sections. The actual position and intensity of the individual texture can be obtained separately by ODF at different groups of Euler angles (Table 2.1 and Figure 2.8), which benefits the investigation of the individual texture evolution during thermomechanical process. And that is the main advantage of ODF over pole figure.

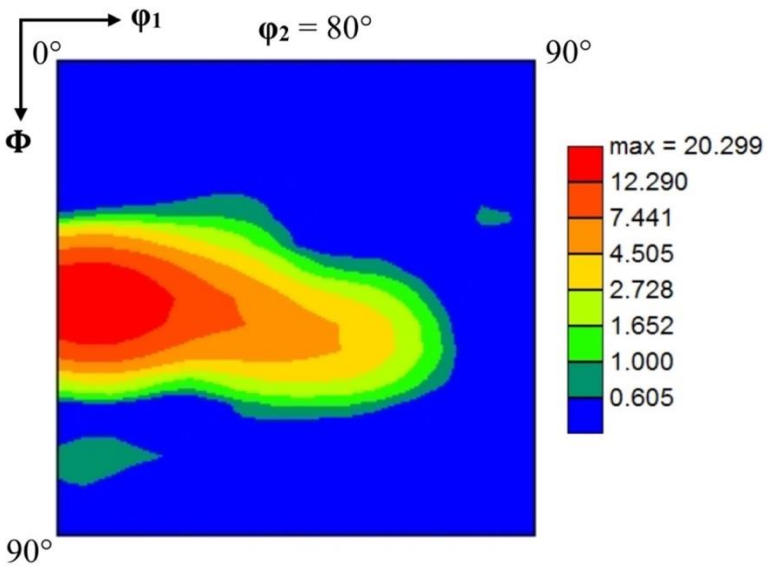

Figure 2.7 Standard 2-Dpresentation of ODF at $\varphi_2 = 80°$section and plotted with iso-intensity lines with the maximum intensity 20.299 ×.

Table 2.1 Miller indices and Euler angles of the most important orientations of aluminum sheets after rolling and annealing.

Designation	**Miller Indices {hkl}<uvw>**	**Euler angles**		
		φ_1	Φ	φ_2
Brass	{112} <111>	35°	45°	0°/90°
S	{123} <634>	59°	34°	65°
Copper	{110} <112>	90°	30°	45°
Cube	{100} <001>	0°	0°	0°/90°
R	{124} <211>	53°	36°	60°
Goss	{110} <100>	0°	45°	0°/90°

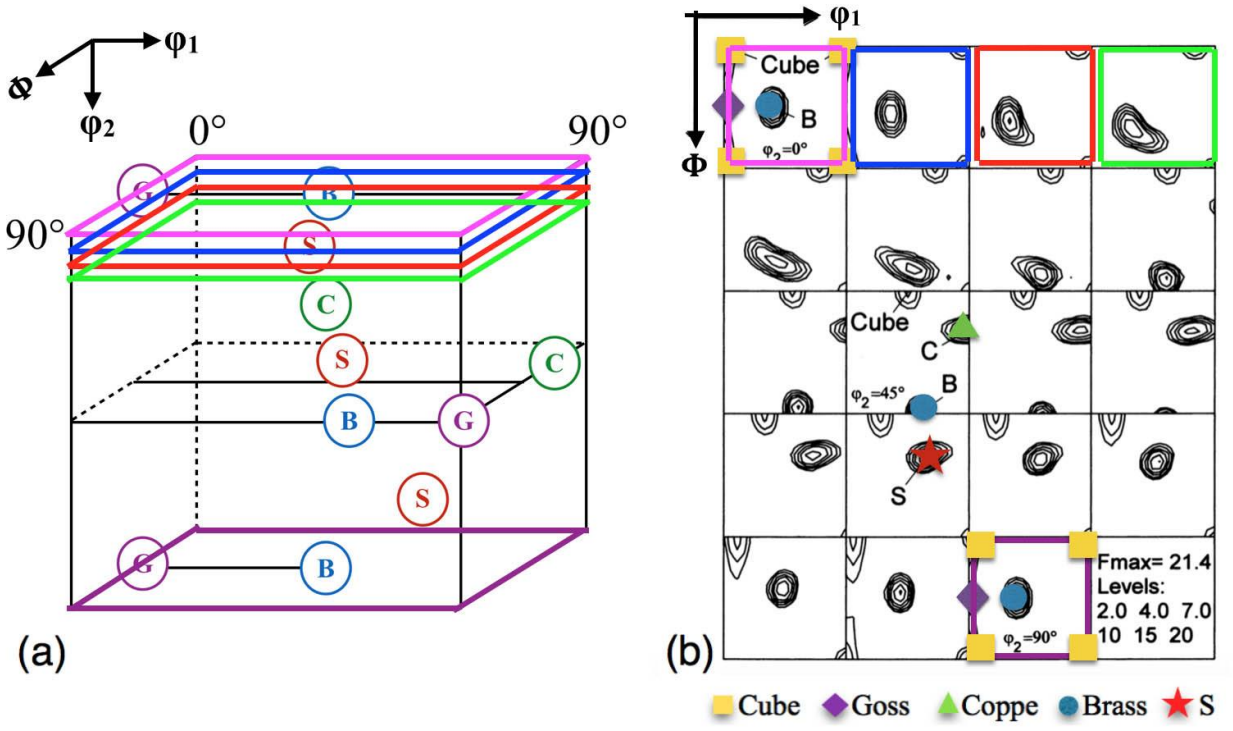

Figure 2.8 Common textures in (a) 3-D Euler angle space; (b) 2-D ODF at φ_2 = 0-90° with 5° interval and textures at φ_2 = 0, 45, 65 and 90° are labeled. The intensity contour values are in the lower right corner and the inside contour has the largest intensity. (After [18], with permission of Elsevier)

2.2 Texture evolution during rolling and annealing process

2.2.1 Texture evolution during commercial rolling process

During plane strain rolling process of aluminum alloys, all the initial textures rotate toward the stable end β fiber textures (Figure 2.8a), which runs through orientation space from Brass orientation {110}<112> (φ_1 = 35°, Φ = 45°, φ_2 = 0°/90°) along S orientation {123}<634> (φ = 59°, Φ = 340°, φ_2 = 65°) to Copper orientation {112}<111> (φ_1 = 90°, Φ = 30°, φ_2 = 45°) with increasing the rolling reduction [28-31].

Hot rolling usually consists of a reversible hot rolling mill and then followed by a multi-stand hot rolling mill. In reversible hot rolling, typically full recrystallization happens because of

the high strain and temperature, so Cube texture {100}<001> (φ_1 = 0°, Φ = 0°, φ_2 = 0°/90°) dominates, as shown in Figure 2.9a.

The microstructure and texture in multi-stand hot rolling, however, are totally different compared with the reversible hot rolling due to the decrease in rolling temperature and increase in strain and strain rate. The recrystallized structure is transformed into severely elongated band structure (Figure 1.2c) and the initial texture rotates to the β fiber rolling texture (Figure 2.9b). It is known that dynamic recrystallization is difficult in alloys with high stacking fault energy such as aluminum alloys. So, it is possible that the small amount of Cube texture develops due to the recrystallization that happens during the cooling process after hot rolling and the amount depends on the rolling parameters (rolling temperature, rolling strain). Larger rolling strain or lower rolling temperature leads to an increase in stored energy and thus a stronger Cube texture.

In the subsequent cold rolling process, the band structure sharpens and the β fiber rolling texture strengthens (Figure 2.9c) due to the further deformation. The cold rolling process weakens the intensity of Cube texture, but still the rolling reduction is not enough to eliminate them all due to the metastability of Cube texture.

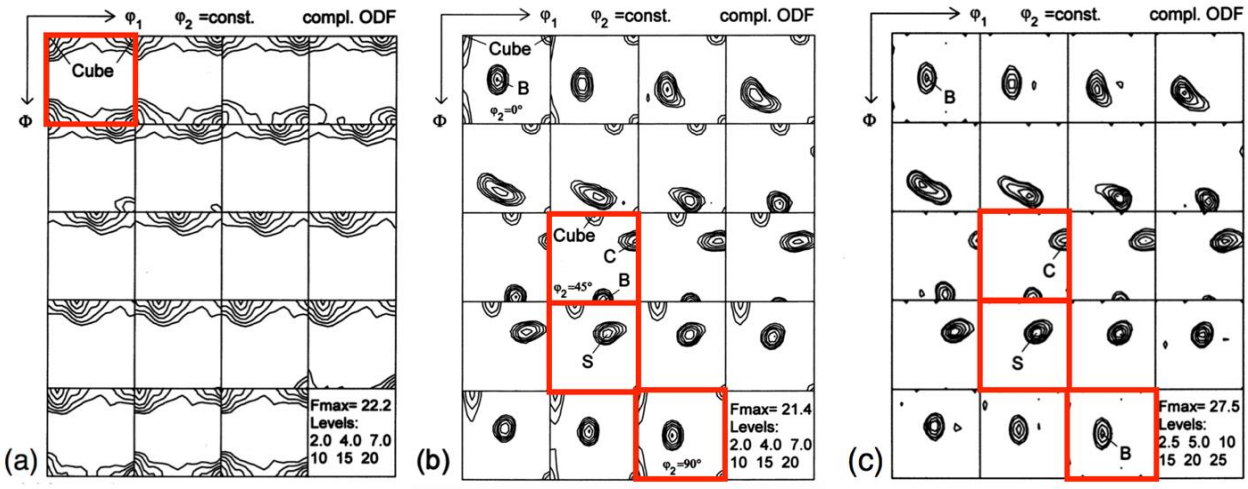

Figure 2.9 ODF showing texture after (a) reversible hot rolling; (b) multi-stand hot rolling and (c) cold rolling. Intensity contour values are in the lower right corner and the inside contour has the largest intensity. (From [18], with permission of Elsevier)

2.2.2 Texture evolution during annealing process

The annealing texture of most aluminum alloys after plane strain deformation consists of two main components, the Cube texture {001}<100> (φ_1 = 0°, Φ = 0°, φ_2 = 0°/90°), typically the strongest recrystallization texture, and the so-called R texture {124}<211> (φ_1 = 53°, Φ = 36°, φ_2 = 0°/90°), which originates from the former S rolling texture {123}<634> [32-34] as shown in Figure 2.10.

Cube texture is thought to come from the cube oriented grains in the initial material. During the rolling process, the cube grains are compressed into cube bands while their 'orientation metastability' is maintained [35-38], i.e., the orientation of the cube band may deviate a little from the ideal Cube texture during rolling, but ideal Cube texture develops in the subsequent annealing process. The sub-grains in the cube bands are found to be much larger than those in other orientated (B, S or C) grains and they have a higher growth rate, which makes cube bands very potent nucleation sites [39]. Apart from these nucleation advantages, the growth of cube oriented grain is also facilitated by the "orientation pinning" effect [40-42] that the growth is decided by the

possibility of encountering grains with similar orientations. Growth rate is retarded when encountering low angle grain boundaries, while enhanced by high angle grain boundaries. And cube oriented grains prevail with the lowest possibility to encounter a similar orientation.

R texture is another important annealing texture. During annealing, R oriented grains can be developed by both continuous and discontinuous recrystallization [43]. For continuous recrystallization, the R orientation emerges from the previous rolling texture (mainly S texture) by extended recovery; while for discontinuous recrystallization, the R orientation develops by nucleation at former S-oriented grain boundaries and growth under consumption of the deformation microstructure.

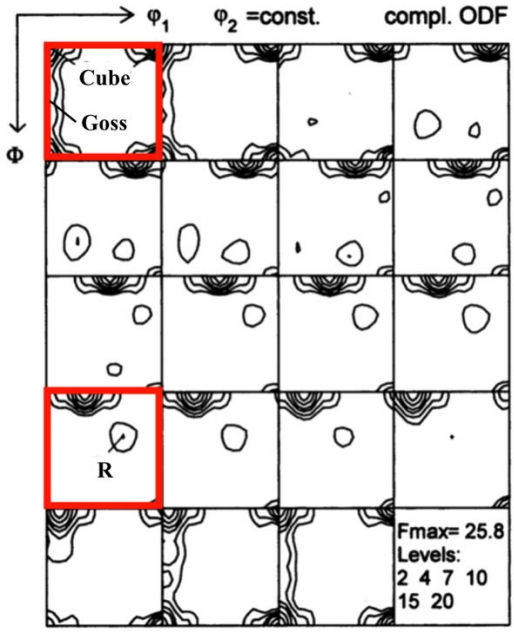

Figure 2.10 Typical annealing texture of 6xxx aluminum alloy. (From [18], with permission of Elsevier)

2.3 Particle stimulated nucleation

Generally, the recrystallization textures of 6xxx aluminum alloys are featured by the Cube texture with strong scattering along the RD toward the Goss texture, and R texture. Now it is well established that the nuclei of Cube and RD-rotated Cube orientation are formed in band-like structure (cube bands) which are present in the as-deformed microstructure [39, 41, 44]. During the subsequent growth of these nuclei, grains with the exact cube orientation prevail because of their favorable growth conditions by means of compromise growth effect [41-42]. Grain boundaries are also favorable nucleation sites. The nuclei formed at the grain boundaries will grow into the deformed structure and become the orientation similar to the deformation texture. During the subsequent growth, R oriented grains dominate because of their fast-growing orientation relationship with the S orientation in the rolling texture.

When the second-phase precipitations are present in aluminum alloys, the recrystallization process is somewhat influenced by the precipitation state, since large particles can promote recrystallization process by acting as nucleation sites. The particle stimulated nucleation (PSN) takes place in the so-called deformation zones that form around particles that are larger than 1 μm by interaction between dislocations and particles [45]. The resulting recrystallization textures of PSN are usually very weak, almost random. Accurate ODF analysis has established the occurrence of some characteristic PSN textures including the P orientation {011}<122> and significant rotation of the cube orientation by 20-30º about ND towards {001}<310> as shown in Figure 2.11 [41, 46].

Whether large particles can act as nucleation sites or not depends on the size of the particles, η, the driving pressure for recrystallization, P_D, and the Zener drag due to the dispersoids, P_Z [47]. Assume that the size of the deformation zone λ around the particle is about twice the size

of the particle, η, it follows that only the particles with a size larger than η^* will be able to initiate PSN process [18]:

$$\eta^* = \frac{1}{2}\lambda_{crit} = \frac{2\gamma_{GB}}{P_D - P_Z} \tag{2.1}$$

γ_{GB} refers to specific grain boundary energy, we can see that with increasing the Zener drag P_Z, the critical nucleation size λ_{crit} increases and so does the η^*. So, for PSN, η^* will eventually exceed the size of the particles present in the materials with increasing the Zener drag P_Z, so that PSN can no longer occur in the materials. In 6xxx aluminum alloy, the critical size of the particles is about 1 μm, which means that particles with a size larger than 1 μm can introduce additional nucleation sites and thus initiate the PSN process.

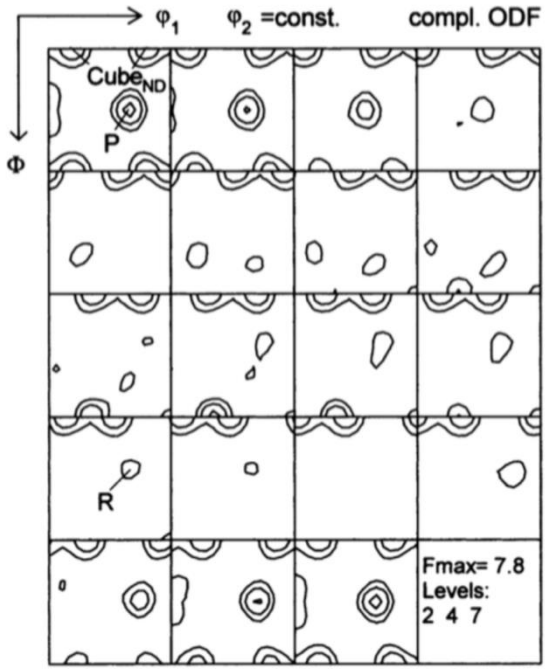

Figure 2.11 Materials are pre-heated to obtain coarsened Mg_2Si particles, resulting in a characteristic weak PSN recrystallization texture. (From [18], with permission of Elsevier)

Mg_2Si particles are the main precipitations in 6xxx aluminum alloys. So, the final recrystallization texture significantly depends on the precipitation state (size, volume and degree

of dispersion) of the Mg_2Si dispersoids. The material with the final recrystallization texture in Figure 2.10 was produced using the standard processing parameters, where the dispersoids formed during the coiling of the hot strip efficiently suppress the PSN, so that the recrystallization texture is dominated by the Cube orientation. In Figure 2.11, however, P texture and Cube-ND texture dominate. In this situation, the material was pre-treated. The precipitated Mg_2Si particles are too coarse to exert a significant Zener drag, which means a smaller η^*, so that Mg_2Si particles easily surpass this size and act as nucleation sites, leading to the characteristic PSN recrystallization texture [48]. By proper controlling on processing parameters where only part of the particles can initiate PSN, an intermediate state with a mixture of Cube and PSN recrystallization texture can be obtained.

Therefore, PSN is an effective method to modify the final recrystallization texture by controlling the precipitation state of the materials. And we can realize the controlling of the dispersion state by adjusting the parameters of the thermomechanical processing. This is very important in production of aluminum sheet materials since Cube and Goss textures are detrimental during forming process.

3. MACHINING-BASED PROCESSES

3.1 Free machining

Free machining (FM), which is also known as peeling, is a single-step, shear-based process to produced strip materials, as shown in Figure 3.1. A wedge-shaped cutting tool with rake angle α feeds at a constant rate (initial cutting depth (t_0)) with workpiece rotating at a preset surface velocity (V_0), producing continuous or segmented strips based on the material property. In free machining, the top surface of the produced strip is rough due to absence of constraint and the final chip thickness t_c is not controllable if the initial cutting depth t_0 and cutting velocity V_0 are fixed.

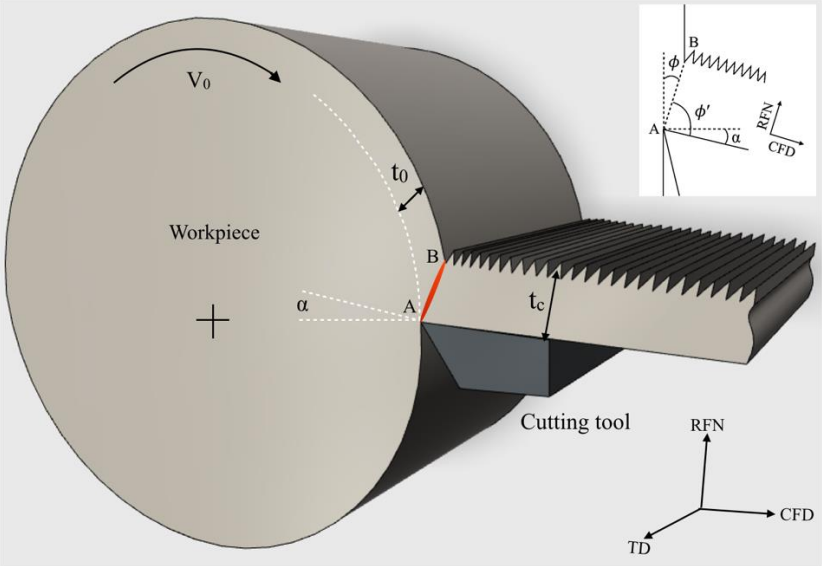

Figure 3.1 Schematic of rotary free machining process with inset showing relative geometric parameters, where CFD, RFN and TD indicate chip flow direction, rake face normal and transverse direction.

3.2 Large strain extrusion machining

In large strain extrusion machining, however, a constraint tool was employed to confine the flow of the materials on the top surface, so both surfaces of the strips are smooth, as shown in Figure 3.2. The level of confinement exerted by the constraint is defined via the chip thickness

ratio, $\lambda = {t_c}/{t_0}$, which is controllable, in contrast with the conventional free machining process. During cutting process, sheet materials were produced by intense, local shear deformation within a narrow deformation zone (thickness ~ 100 μm) [49-52]. Due to this narrow deformation zone and high velocity, strain rates as high as ~ 10^3 s^{-1} can be obtained in FM and LSEM in a single step.

LSEM offers control over deformation parameters such as strain, strain rate, deformation temperature and strain path, due to manageable λ, V_0 and α. They all can be used to control the microstructure and texture.

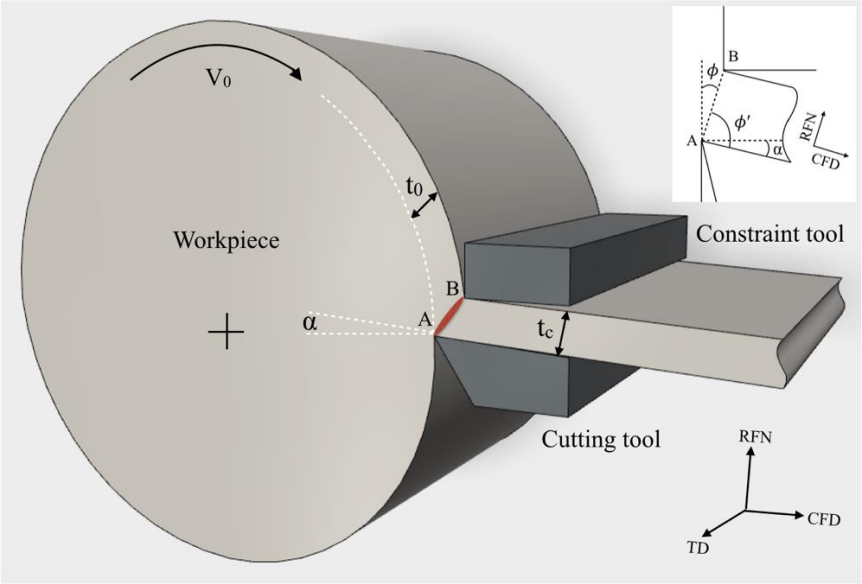

Figure 3.2 Schematic of rotary large strain extrusion machining process with inset showing relative geometric parameters. CFD, chip flow direction; RFN, rake face normal; TD, transverse direction.

3.2.1 Deformation strain and hydrostatic pressure

When idealizing the deformation zone as a single shear plane (Figure 3.2), the effective strain (ε) imposed on the sheet during machining process can be calculated by upper bound analysis and the equation is determined as:

$$\varepsilon = \frac{1}{\sqrt{3}}\left(\frac{\lambda}{\cos\alpha} + \frac{1}{\lambda\cos\alpha} - 2\tan\alpha\right) \quad 3.1$$

The strain developed in the machining process is a function of λ and α and the plot is shown in Figure 3.3. At a given λ, ε decreases with increasing α; at a given α, the minimum ε is achieved at $\lambda = 1$, then it increases with increasing or decreasing λ. The upper limit of λ is the natural λ, also called free λ, and is a material dependent parameter. In FM, only α and V_0 can be employed to control the strain. In LSEM, however, a wide range of λ can be controlled in a single step so that larger ranges of strain (as large as 10) can be achieved. In conventional rolling process, however, multiple rolling (cold or hot rolling) steps are required to achieve similar strain levels. This will be discussed in the next chapters.

Another factor that contributes to the formation of continuous strip during LSEM process is the hydrostatic pressure *P*. According to slip line field theory, the hydrostatic pressure in the narrow deformation zone can be estimated at near-zero rake angles by [55]:

$$\frac{P}{2k} = \frac{1}{2} + 2\tan^{-1}\left(\frac{1}{2\lambda}\right) \quad (3.2)$$

where *k* is the shear strength of the material. The dependence of *P/2k* is shown in blue line in Figure 3.3. With increasing λ, the hydrostatic pressure decreases monotonically. The maximum value of *P* is ~ 4*k* at $\lambda = 0.5$. In rolling process, however, the hydrostatic pressure is fixed at ~ *k*. This high level of hydrostatic pressure eliminates fracture effectively during LSEM of alloys with low workability, such as Fe-Si [53] and magnesium alloy [52], and enable the continuity of the strip without cracking. Due to this feature, the idea of producing sheet materials directly from as-cast aluminum alloy becomes feasible.

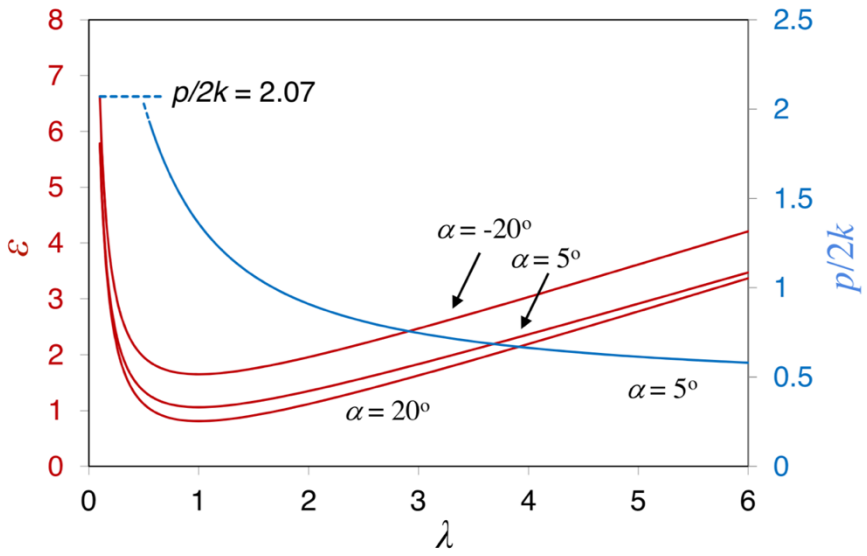

Figure 3.3 Plot showing effect α and λ on effective ε (in red line) and hydro static pressure *p/2k* (in blue line). (After [55], with permission of Elsevier)

3.2.2 Deformation temperature

As have mentioned in the previous section, intensive strain, strain rate and hydrostatic pressure localize within the narrow deformation zone, which inevitably increase the deformation temperature adiabatically during cutting process. The actual temperature can be determined by:

$$T = T_0 + \Delta T \tag{3.3}$$

T_0 in the equation is the initial temperature of the workpiece and it can be controlled by preheating the workpiece. ΔT is the adiabatic temperature rise and it can be estimated by the shear plane model, which simply assumes that the heat generated at the shear plane is divided into two parts: one part flows into the sheet and the other into workpiece. Based on this model, ΔT is given by: [54]

$$\Delta T = \frac{(1-\Gamma)u_s}{\rho c} \tag{3.4}$$

In the equation, Γ is the fraction of adiabatic heat flow into the workpiece and it is a function of strip geometry, material property, cutting velocity V_0 and chip thickness ratio λ, u_s is the energy

per unit volume dissipated at the shear plane during cutting and it is determined by the ratio of the cutting force to the strip cross-sectional area, and ρ and c are the density, specific heat capacity of the material. The deformation temperature during LSEM process on Mg alloy has been studied [55] and the effect of cutting velocity V_0, initial temperature T_0, and chip thickness ratio λ on deformation temperature T is summarized in Figure 3.4. At fixed λ, T increases with increasing V_0 and then becomes saturated at ~ 1 m/s. With decreasing λ, T increases when V_0 is constant. By increasing T_0, a wide range of T (from 150 to 450 ℃) can be achieved in a single step. Similar phenomenon was observed in LSEM on Fe-Si alloys [53] and deformation temperature as high as 830 ℃ can be obtained by controlling T_0 and V_0.

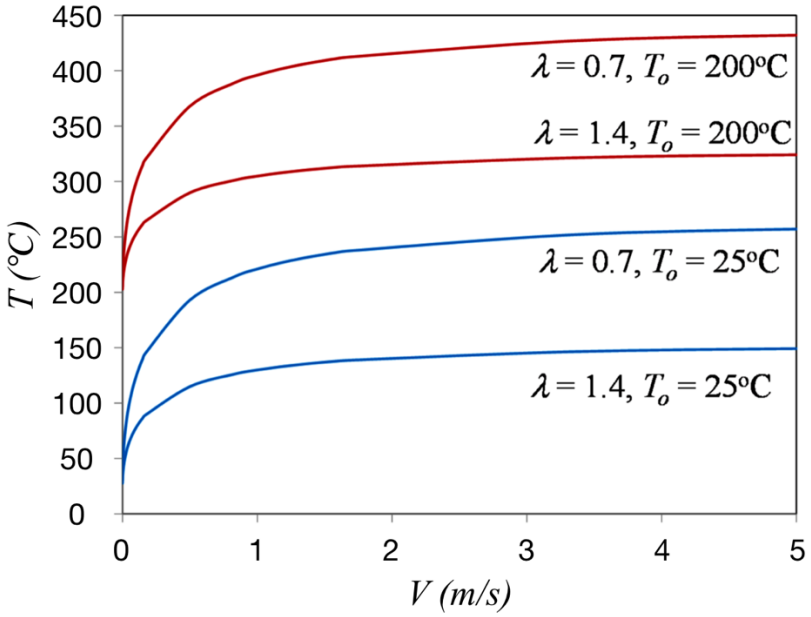

Figure 3.4 Dependence of T on V_0, T_0 and λ in LSEM of Mg AZ31B alloy. The machining parameters were: $t = 250$ μm, $\alpha = 5°$ (After [55], with permission of Elsevier)

3.2.3 Deformation path and controlling on texture

High-speed imaging and image analysis technique, particle image velocimetry (PIV), were employed to investigate the deformation path and material flow during LSEM process. Pure lead was chosen as the model system for linear LSEM and the experiment was performed at $\alpha = 10°$, $t_0 = 250$ μm, $V = 10$ mm/s, with different chip thickness ratio (λ = 2.5, 1.6, 1 and 0.6). In PIV analysis, the measurement of strain and strain rate is determined by the tracking the displacement of material elements passing through the narrow deformation zone [51]. So, in linear cutting on lead, in-situ tracking along pathline abcd (Figure 3.5) was carried out by high speed camera and a series of images containing information of surface asperities were obtained. By PIV analysis on the images, the information of the strain rate tensor, strain fields and shear direction can be obtained, as shown in Figure 3.5. At $\lambda > 1$, the deformation zone is quite localized and relatively uniform. With decreasing λ to 0.6, the deformation zone is more spread, especially near the rake face, where intensive friction develops with increasing constraint level. But still, deformation is confined in a narrow deformation region.

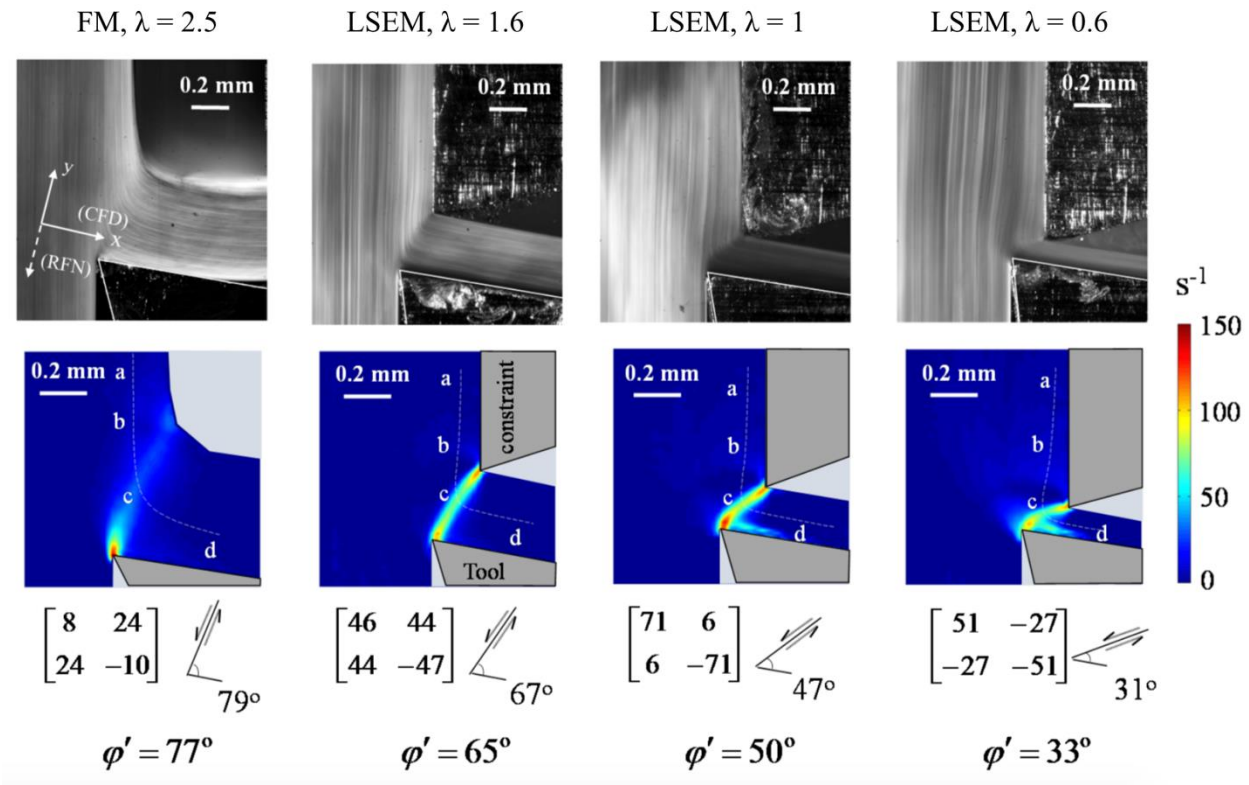

Figure 3.5 PIV analysis showing side view of shear deformation in FM and LSEM. The top four images indicate material flow in machining process and the bottom four show the resultant stain rate fields. The strain rate tensor and shear direction for point c are compared (After [51], with permission of Elsevier)

Using PIV analysis, we can obtain the strain-rate tensor and shear direction in the deformation zone. The shear plane angle, φ', which is measured counter-clockwise from the tool rake face, is expressed by:

$$\varphi' = {}^{\pi}/_{2} + \alpha - \varphi \tag{3.5}$$

where $\varphi = \tan^{-1}({}^{\cos\alpha}/_{\lambda - \sin\alpha})$. According to the measurements in Figure 3.5, the shear direction obtained by PIV analysis fits well with the calculation mentioned above from $\lambda = 0.6$ to $\lambda = 2.5$. So, a wide range of strain path can be achieved by LSEM process through controlling λ and α.

For soft materials, such as pure aluminum, the natural λ is so large that a shear angle as large as 85° can be achieved. For harder materials, this angle is smaller. In this study, cold rolling is also employed as a further deformation processing method to modify the texture and surface roughness of the FM/LSEM strip and investigate how the texture evolves when the deformation mode changes from simple shear to plane strain compression.

In summary, LSEM is a shear-based, single-step technique to produce sheet material. By manipulating the machining parameters, a wide range of microstructures and textures can be obtained. The ability of LSEM to produce strip materials from alloys with low workability, such as Fe-Si and Mg alloys, has been proved in our group by previous study [52-53]. So, in this study, LSEM was performed on 6013 aluminum alloy both in age-hardened and as-cast (without homogenization) condition, to see whether we can produce continuous strip materials, and investigate the microstructure, texture and mechanical property of the strips.

4. THERMOMECHANICAL CONTROL OF MICROSTRUCTURE IN LARGE STRAIN EXTRUSION MACHINING ON AGE-HARDENED ALUMINUM ALLOY

4.1 Introduction

Aluminum alloys have long been employed in aircraft, especially age-hardenable 2xxx and 7xxx high-strength alloy mainly because of their high strength to weight ratio. Now, in order to decrease energy consumption, the automotive industry is again showing increasing interest in aluminum alloys. Work-hardenable 5xxx aluminum alloys have traditionally been used for automotive applications due to their relatively low cost and high formability. But the appearance of Lüders bands during forming processes prevent them being employed as exterior panels, which are very critical for surface finish [16-17]. As a result, heat-treatable 6xxx aluminum alloys are particularly attractive to the automotive industry for body panels because of their good combination of formability, surface finishing, and mechanical properties.

Aluminum alloy 6013 is an automotive/aerospace alloy developed by ALCOA in the early 1980s with higher Cu and Mg contents for higher strength compared with other 6xxx aluminum alloys due to the stronger precipitation-hardening effect [56-57]. The strength of this alloy in T6 condition is higher than most other 6xxx aluminum alloys. The tensile strength and yield strength of AA6013-T6 are 405 and 370 MPa, respectively, compared to 310 and 275 MPa for AA6061-T6, for example. Dent resistance is a significant criterion for automotive body panels, so 6013 aluminum alloy is a potential candidate.

Previous studies in our group have demonstrated the ability of LSEM to produce continuous strips from low workable hcp (magnesium AZ31B) [52] and bcc (6.5Si-Fe) [53] alloys. In this chapter, FM/LSEM are performed on AA6013-T6 both at room and high temperature to

investigate the possibility to produce continuous strips from fcc alloys with low workability. Then the microstructure and hardness evolution of the strips under different thermomechanical parameters are investigated. Finally, microstructures and mechanical property of the strips produced by LSEM and rolling with the same effective strain are compared.

4.2 Experimental procedure

The alloy studied was commercial AA6013-T6 aluminum plate with 14 mm thickness purchased from McMaster-Carr, Elmhurst, IL. The chemical composition limits of this alloy according to ASME B211 are (in wt. %): 0.6-1.0 Si, 0.5 Fe, 0.6-1.1 Cu, 0.2-0.8 Mn, 0.8-1.2 Mg, 0.1 Cr, 0.25 Zn, 0.1 Ti, 0.15 others. The through-thickness microstructure of the as-received plate (Figure 4.1a) contains distinct fine-grain zones near the surfaces (Figure 4.1b) and coarse-grain zone in the middle (Figure 4.1c). This characteristic structure is remnant of the inhomogeneous deformation in the hot rolling process. Hardness measurements showed little difference between the fine-grained (137 kgf/mm^2) and coarse-grained (135 kgf/mm^2) regions, consistent with the dominant strengthening mechanism by age-hardening. Half of the thickness of the plate was machined off and a disk-shape workpiece with 150 mm diameter and 7 mm thickness of the plate was obtained (Figure 4.1a), allowing the response of the fine- and coarse-grained starting material to be studied under identical processing conditions in the same specimen.

Various strips 0.2 to 0.8 mm thick × 7 mm wide were obtained under different machining parameters. FM experiments, i.e., without constraint, at V_0 = 0.5 and 3 m/s with α = 5°, and LSEM experiments at 0.5 and 3 m/s with α = 5°, λ = 1.5 and 0.8 were performed on the workpiece at room temperature (T_0 = 25 ℃). High-temperature LSEM experiments were conduct at different initial temperatures. The workpiece was preheated in a furnace to about 550 ℃ for about 1 h and then assembled on the lathe for the high-temperature cutting. The experiments were conducted at

α = 5°, λ = 1.5 and V_0 = 3 m/s when the workpiece cooled in the air to T_0 = 400, 300 and 135 ℃. Strips produced using the same effective strain, but obtained at room temperature (T_0 = 25 ℃) were annealed at 572 ℃ for 1, 2, 3 and 4 min and then quenched in water to compare with ones produced by cutting at high temperature. During the annealing process, a bulk aluminum plate about 40 mm wide, 40 mm long and 10 mm thick was put in the furnace, with a thermocouple in contact with it to monitor the temperature. When the temperature reached 572 ℃, the LSEM strips were put on the surface of the bulk aluminum close to the thermocouple as soon as possible and then the furnace was closed. The transient time was about 0.5 min when the temperature was back to 572 ℃. The door of the furnace was opened a little to keep the temperature stable at 572 ± 2 ℃.

All the samples are prepared by mechanical grinding from 320 to 2000 grit silicon carbide papers and polishing with colloidal silica, followed by etching with 10% sodium hydroxide between 4-6 min. The through-thickness microstructure of the FM and LSEM strips produced at room and high temperatures and annealed strips were investigated by optical microscopy. Microhardness of the bulk and strip specimens were measured by Vickers indentation along centerline in the through-thickness microstructure with loads ranging from 50 g to 100 g to ensure that the sizes of the indentations were kept similar in all samples, from 34 to 41 μm. At least 10 indentations were measured to obtain an average of the hardness.

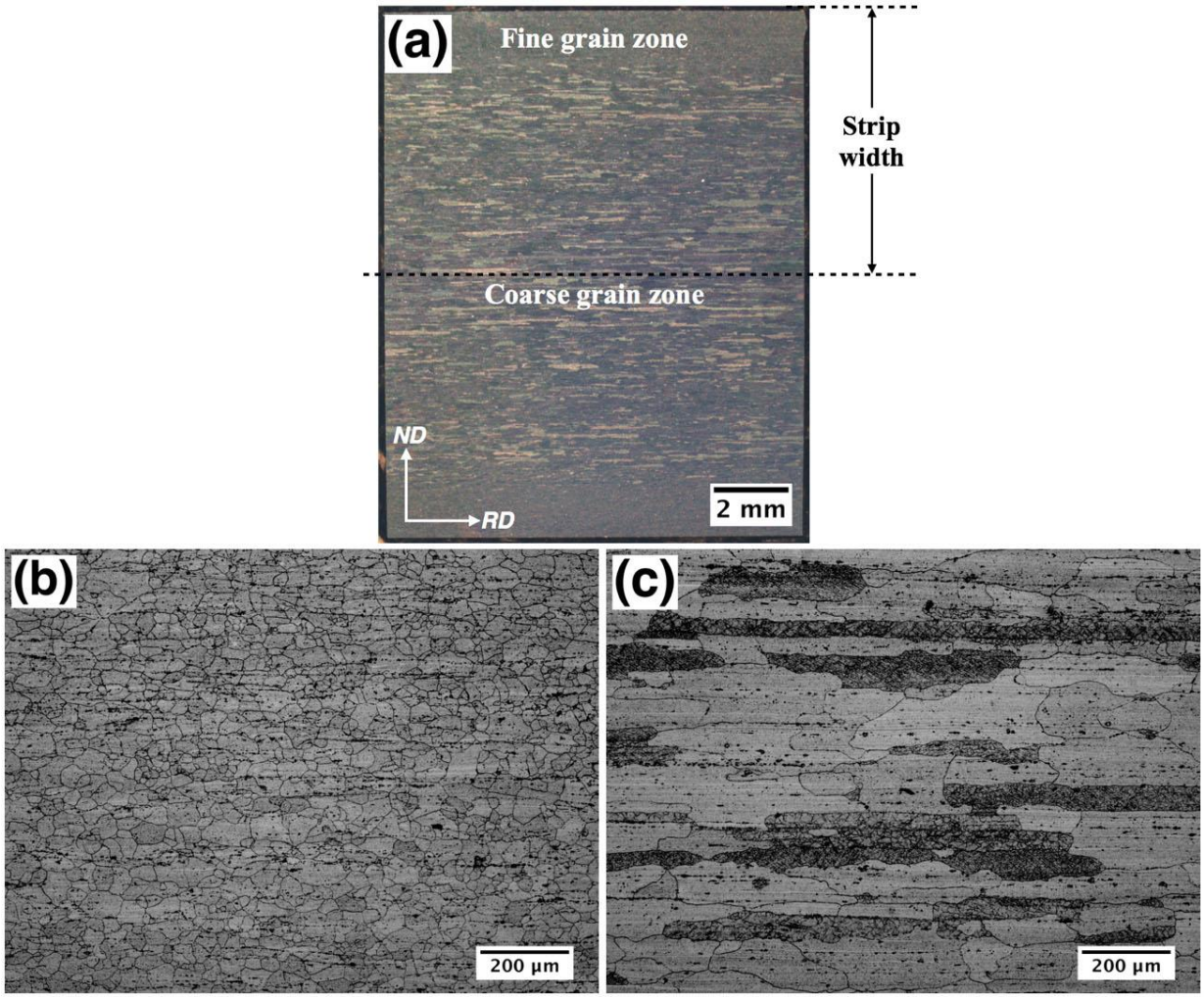

Figure 4.1 Microstructure of polished and etched cross-sections of (a) as-received 6013-T6 plate showing (b) fine-grain structure near surfaces and (c) coarse-grain structure in the middle. Half-thickness of plate removed to produce workpieces containing adjacent fine- and coarse-grain regions as indicated in (a).

4.3 Results and discussions

4.3.1 Free machining at ambient temperature

Free machining (FM) experiments were performed on the disk workpiece with the parameters shown in Table 4.1.

Table 4.1 Free machining parameters and results at room temperature

α (°)	t_0 (mm)	V_0 (m/s)	t_c (mm)	λ	ε	Hv (kgf/mm^2)
5	0.25	0.5	0.80	3.2	1.9	176
		3	0.52	2.1	1.4	161

Microstructures resulting from the fine- and coarse-grain sides of the FM strip are shown in Figure 4.2. The top surface of the FM strip is rough, whereas the tool (rake face) side is smooth. The highly elongated grains originating from the fine-grain zone in the starting material are finer than those originating from the coarse-grain zone. With increasing velocity, the thickness of the strips decreases, but at a given velocity the average thickness is independent of the starting grain size. The free surface roughness, however, does scale with the starting grain size. Since the starting material has similar hardness on both sides and they undergo the same processing condition, the initial grain size is the only reason that results in this difference in roughness. Built-up edge occurs on the tool when machining at 0.5 m/s (white arrows in Figure 4.2a and b), but not at 3 m/s. So, it is preferable to machine at higher velocity.

The second phase particles and grain structure provide clear markers of the shear flow. In contrast to rolling, where the second phase particles distribute preferably along the rolling direction, the primary shear flow in the strip is inclined to the strip faces. The inclination angle of grains at V_0 = 0.5 m/s is larger than that at 3 m/s, indicating a higher level of deformation. A narrow secondary shear zone from friction against the rake face of the cutting tool is also clearly visible, with flow aligned in the strip (chip) flow direction and a sharp transition to the primary shear zone.

The average hardness of the starting material was 136, with 135 in coarse-grain zone and 137 in fine-grain zone. After FM at 0.5 and 3 m/s, the average hardnesses increase by strain-

hardening to 176 and 161, respectively, again with negligible difference between fine- and coarse-grain regions. So in FM the initial grain size has effect on the microstructure and surface roughness of the strip, but not on the hardness, whereas the cutting speed does affect hardness. With increasing cutting speed, the strain drops while the temperature increases, so the hardness at 0.5 m/s is higher than that at 3 m/s due to a higher level of strain and lower level of dynamic recovery. The hardness increases (~20%) are significant, considering the T6 (age-hardened) condition of the workpiece.

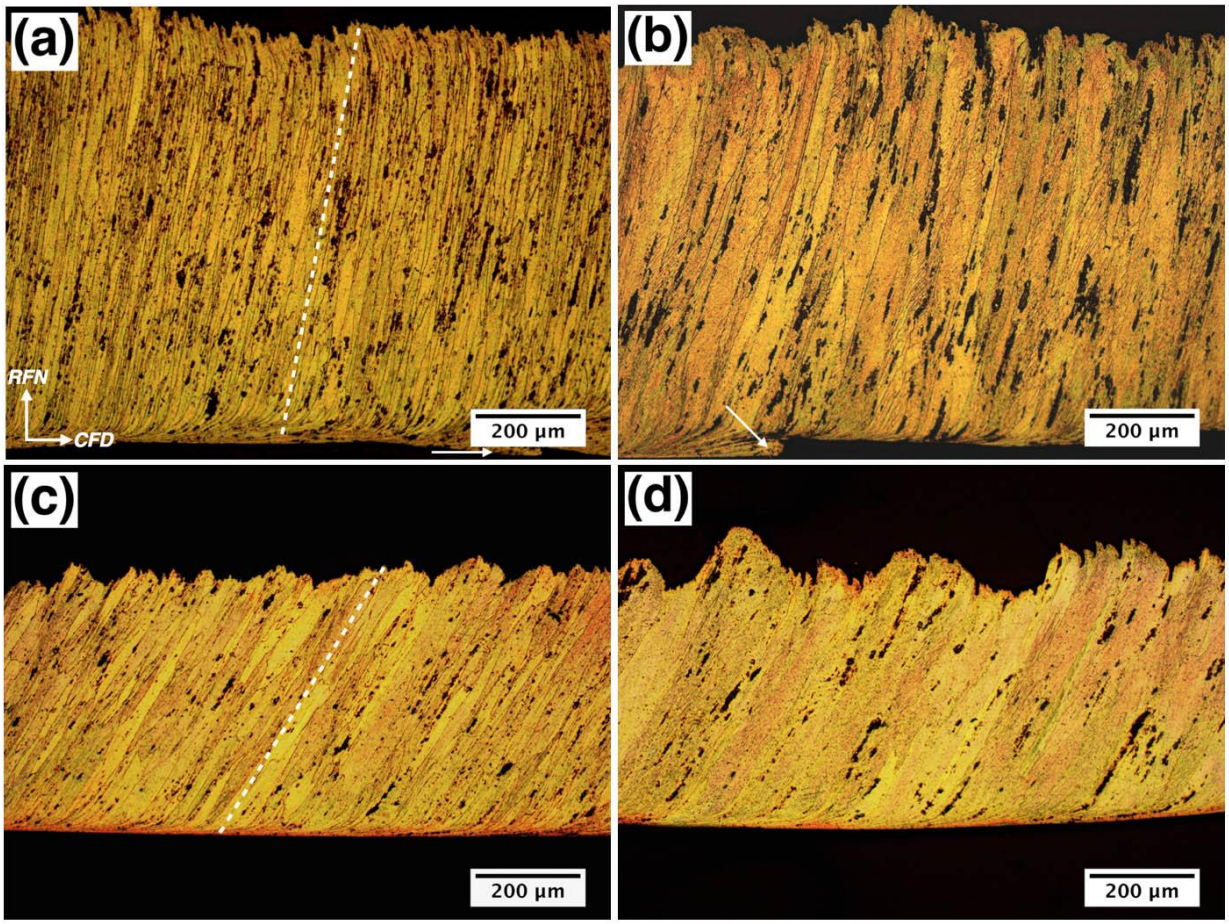

Figure 4.2 Microstructures of FM 6013-T6 strips. (a) fine-grain (b) coarse-grain side at V_0 = 0.5 m/s; (c) fine-grain (d) coarse-grain side at V_0 = 3 m/s.

4.3.2 LSEM strips at ambient temperature

Using the same workpiece as in the FM experiments, strips were produced by LSEM with two different levels of constraint at room temperature (T_0 = 25 ℃) with parameters shown in Table 4.2.

Table 4.2 LSEM parameters and results at room temperature

α (°)	t_0 (mm)	t_c (mm)	λ	ε	V_0 (m/s)	Hv (kgf/mm^2)
5	0.25	0.38	1.5	1.2	0.5	138
					3	105
		0.2	0.8	1.1	0.5	155
					3	117

LSEM strips produce with λ = 1.5 and the same velocities as in FM are shown in Figure 4.3. Unlike FM strips, both surfaces of the LSEM strips are smooth because of the constraint tool on top. During the LSEM process, the constraint confines the flow of the material and acts as an extrusion die simultaneous with cutting. The friction between the constraint and strip leads to the formation of a secondary shear zone analogous to that along the rake face of the cutting tool, referred as the “constrained zone”; the secondary shear zone from the cutting tool rake face is referred as the “secondary shear zone”. At lower cutting velocity, the friction is larger so a wider constrained zone and secondary shear zone develop. With increasing velocity, the constrained and secondary shear zones decrease and more of the primary shear zone is retained (Figure 4.3a, c). Furthermore, the built-up edge phenomenon is avoided even at 0.5 m/s, whereas build-up edge is severe in FM at the same velocity.

The starting grain size difference in the two sides of the workpiece is again reflected in the LSEM strips but, as in the case of FM, the hardness differences between the fine- and coarse-grain regions was negligible. The hardness of strips produced at 0.5 and 3 m/s are 138 and 105, much smaller than the hardness of the strip produced by FM at the same velocities, 176 and 161. Compared with FM under the same condition, λ is smaller for LSEM and temperature rise is higher. So at the same velocity, the hardness of the LSEM strip is lower than that of FM.

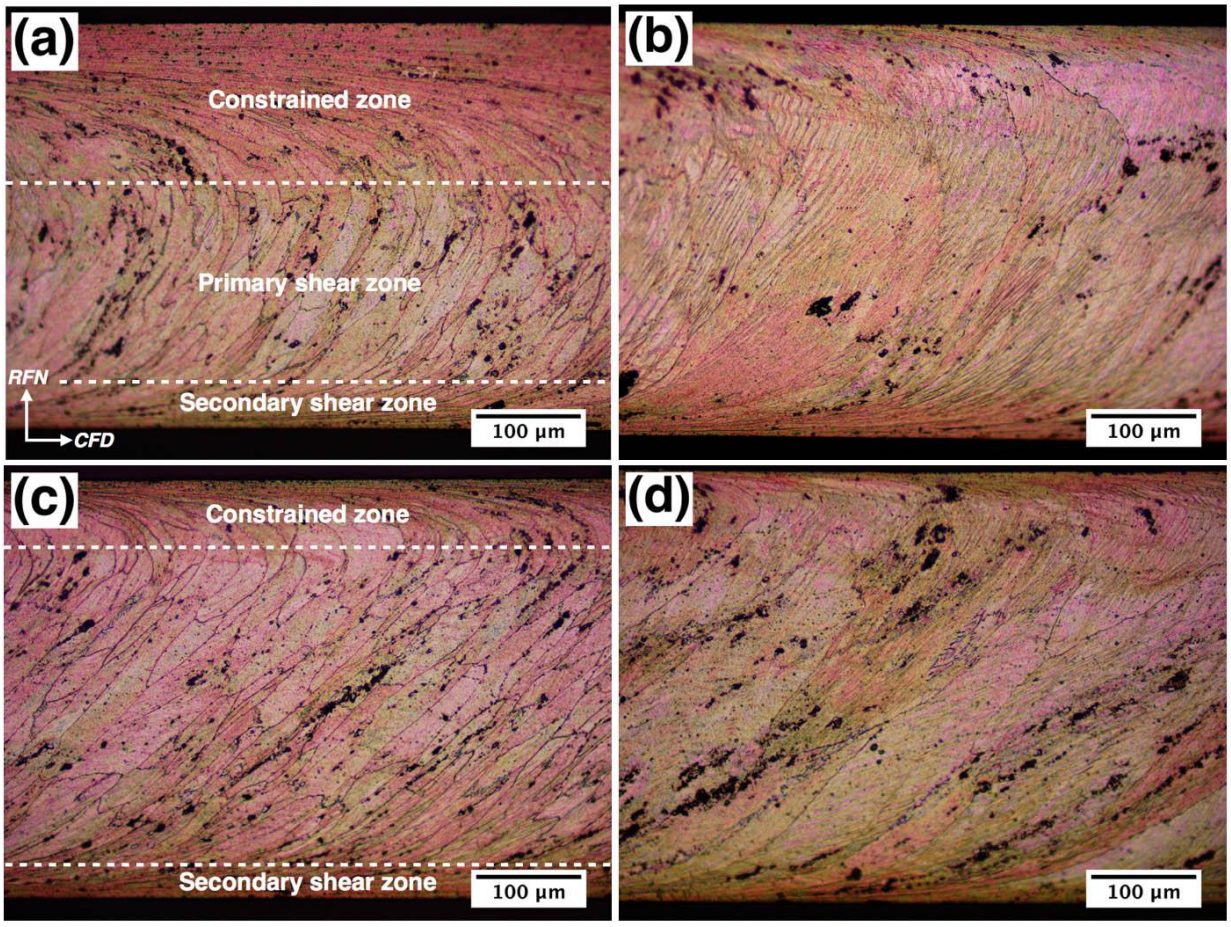

Figure 4.3 Microstructures of LSEM 6013-T6 strips at λ = 1.5. (a) fine-grain (b) coarse-grain side at V_0 = 0.5 m/s; (c) fine-grain (d) coarse-grain side at V_0 = 3 m/s.

When the LSEM experiment was performed at λ = 0.8, however, the microstructure changed significantly compared with that at λ = 1.5 (Figure 4.4 and 4.3). At λ = 0.8 the hydrostatic pressure is about 1.5 times larger than that at λ = 1.5 [55]. This effect increases the friction between the

constraint and strip, leading to the reduction, even disappearance of the primary shear zone (Figure 4.4a). With increasing velocity to V_0 = 3 m/s, the constrained zone shrinks, while the primary shear zone enlarges, as shown in Figure 4.4c.

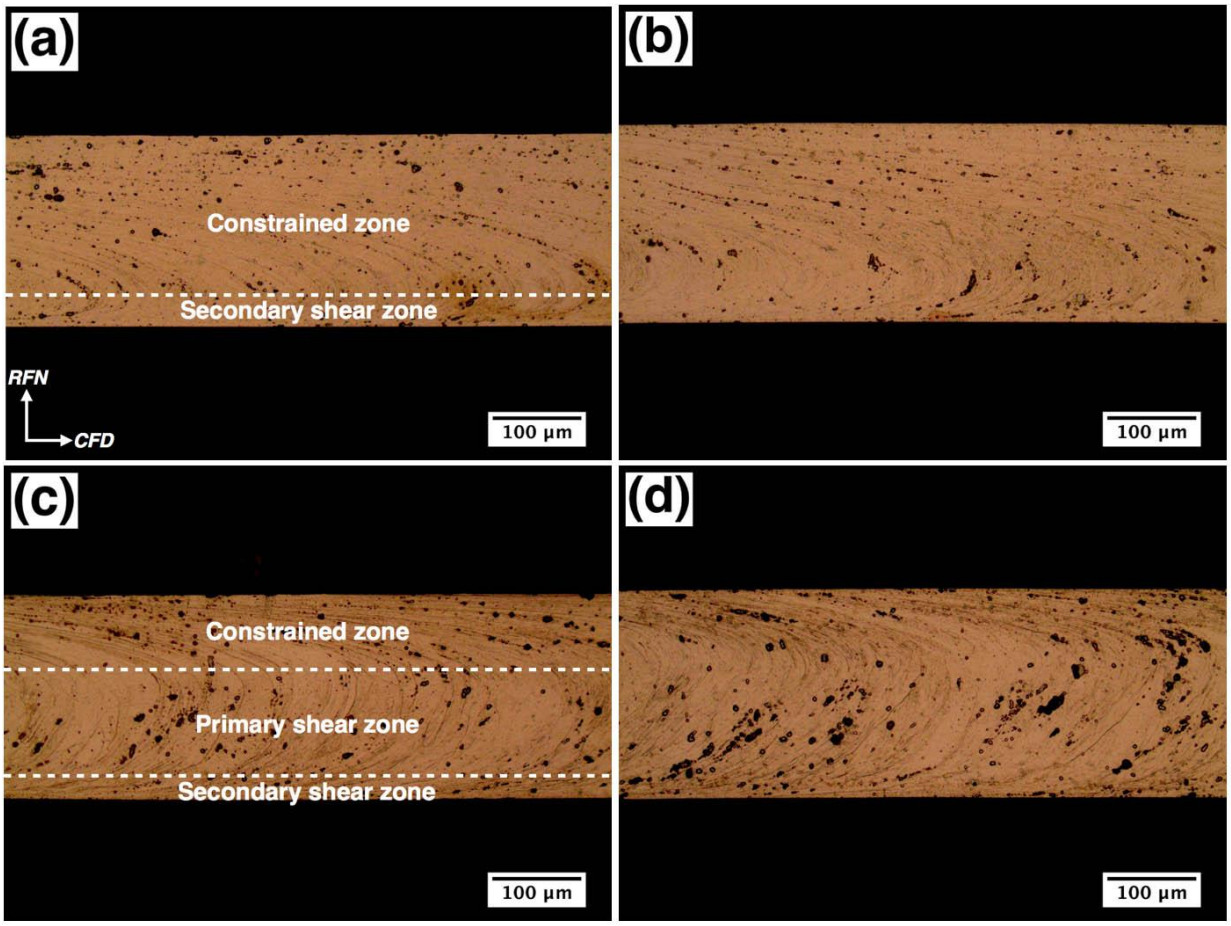

Figure 4.4 Microstructures of LSEM 6013-T6 strips at λ = 0.8. (a) fine-grain (b) coarse-grain side at V_0 = 0.5 m/s; (c) fine-grain (d) coarse-grain side at V_0 = 3 m/s.

At λ = 0.8, the inhomogeneity of the starting grain structure barely has any effect on the microstructure of the strip. That is, the microstructure originating from the fine-grain zone of the workpiece (Figure 4.4a, c) is very similar to that from the coarse-grain zone (Figure 4.4b, d) and, again, they have almost the same hardness at a given velocity. The average hardness of the strip at λ = 0.8 and V_0 = 0.5 m/s is 155, which is higher than that at λ = 1.5 with the same velocity, 138. In spite of almost the same ε, this difference can be explained by the additional redundant strain

in the constraint zone at λ = 0.8. With increasing velocity to V_0 = 3 m/s, the hardness drops to 117, below that of the starting condition, but higher than that at λ = 1.5 (105).

4.3.3 LSEM strips at high temperature

In order to observe the cutting behavior of 6013-T6 alloy at high temperatures, the workpiece was preheated and then machined under the parameters shown in Table 4.3. The resulting microstructures are shown in Figure 4.5.

Table 4.3 Parameters and results of the high-temperature LSEM experiments

α (°)	t_0 (mm)	t_c (mm)	λ	ε	V_0 (m/s)	T_0 (℃)	Hv (kgf/mm^2)
						400	89
5	0.13	0.2	1.5	1.2	3	300	74
						135	66

With LSEM at T_0 = 400 ℃, complete dynamic recrystallization happens (Figure 4.5a and b). A considerable refinement of grain size compared with the initial workpiece (Figure 4.1b and c) was achieved in just a single step of deformation after dynamic recrystallization. The grain size in the fine-grain area (Figure 4.1) of the rolled plate workpiece is around 32 μm, and that in the coarse-grain area is 240 μm along RD and 72 μm along ND. After LSEM at T_0 = 400 ℃, an, equiaxed grain structure develops with a grain size of 21 μm. This is one advantage over the conventional rolling process, which needs many hot and cold rolling steps to reach the same amount of grain refinement. The through-thickness microstructures in both sides of the strip are quite homogeneous (Figure 4.5a, b) and have the same grain size, despite the much different initial microstructures.

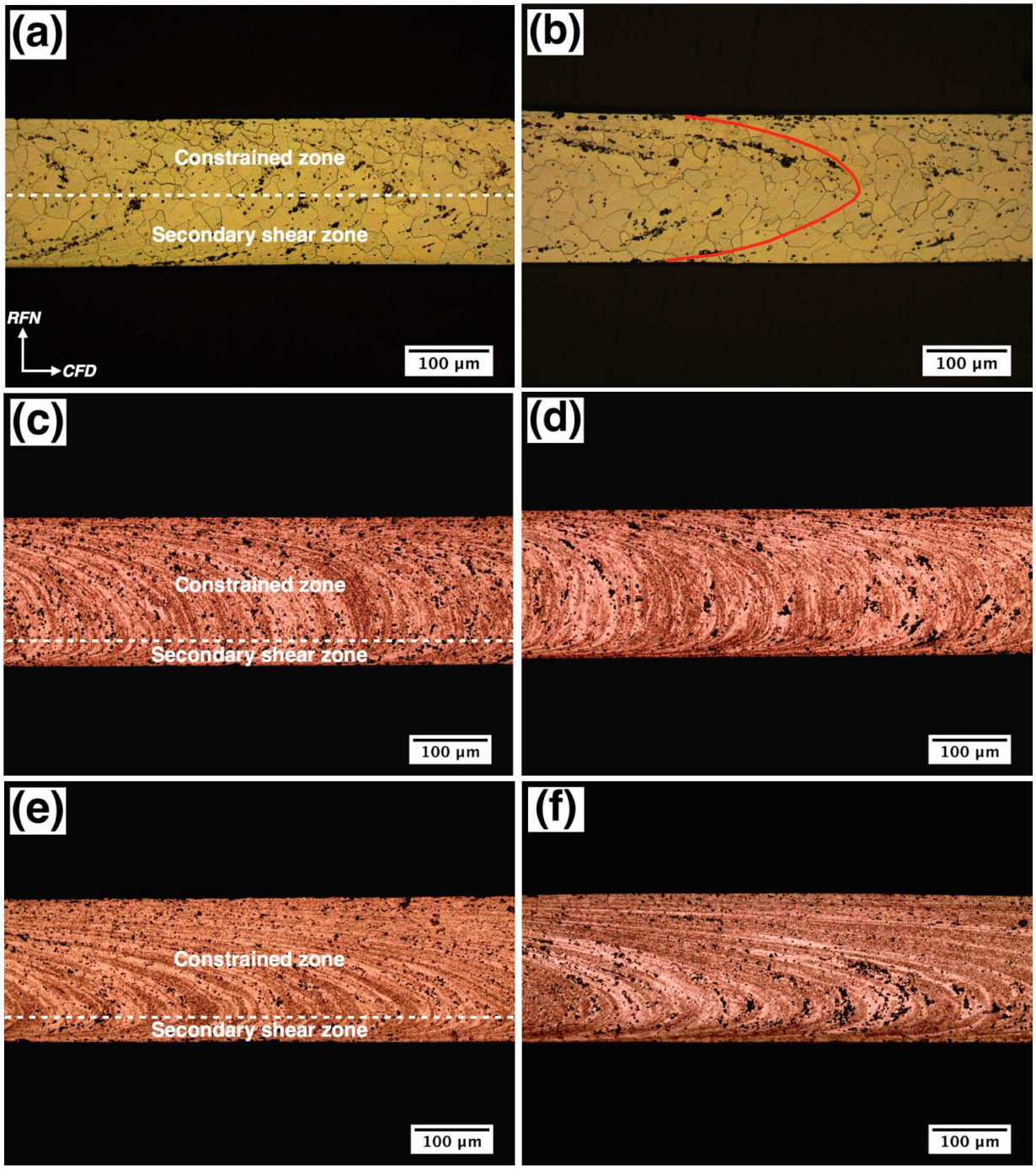

Figure 4.5 Microstructures of LSEM 6013-T6 strips at λ = 1.5. (a) fine-grain (b) coarse-grain side at T_0 = 400 ℃; (c) fine-grain (d) coarse-grain side at T_0 = 300 ℃; (e) fine-grain (f) coarse-grain side at T_0 = 135 ℃.

The microstructures of strips produced at T_0 = 300 ℃ (Figure 4.5c and d) are remarkably different from those at T_0 = 400 ℃ (Figure 4.5a and b), but similar to the deformed structures,

which contain constrained and secondary shear zones. Dynamic recrystallization is suppressed due to lower temperature and a flow-line type microstructure develops. Figure 4.5e and f show the microstructures of the LSEM strips cut at T_0 = 135 ℃ and, similar to T_0 = 300 ℃, a highly deformed flow-line type microstructure is obtained, but the inclination angle in the constraint zone is sharper due to higher level of friction.

4.3.4 Static recrystallization of LSEM strips

In order to study the recrystallization behavior further, strips produced at room temperature with λ = 1.5 and V_0 = 3 m/s (section 4.3.2) were annealed at 572 ℃ for 1 to 4 min and then water quenched. The initial microstructures of the strips were inhomogeneous, with fine- and coarse-grain structure on the two sides (Figure 4.3c and d). After annealing at 572 ℃ for 1 min the strips are completely recrystallized and a homogeneous structure with similar grain size on both sides develops (Figure 4.6a and b). So the initial non-uniform grain structure of the strip has no effect on the annealing structure, as observed when the recrystallization was dynamic at T_0 = 400 ℃ (Figure 4.5a, b). Likewise, the average grain size of the annealed strip is 20 μm, nearly the same as that of the dynamically recrystallized strip, 21 μm.

With increasing annealing time to 4 min, essentially no change in the microstructures distinguishable with only slightly larger grain size by measurement. The hardness values of both sides of annealed strips are similar and the average is about 93. And it remains constant with increasing annealing time to 4 min.

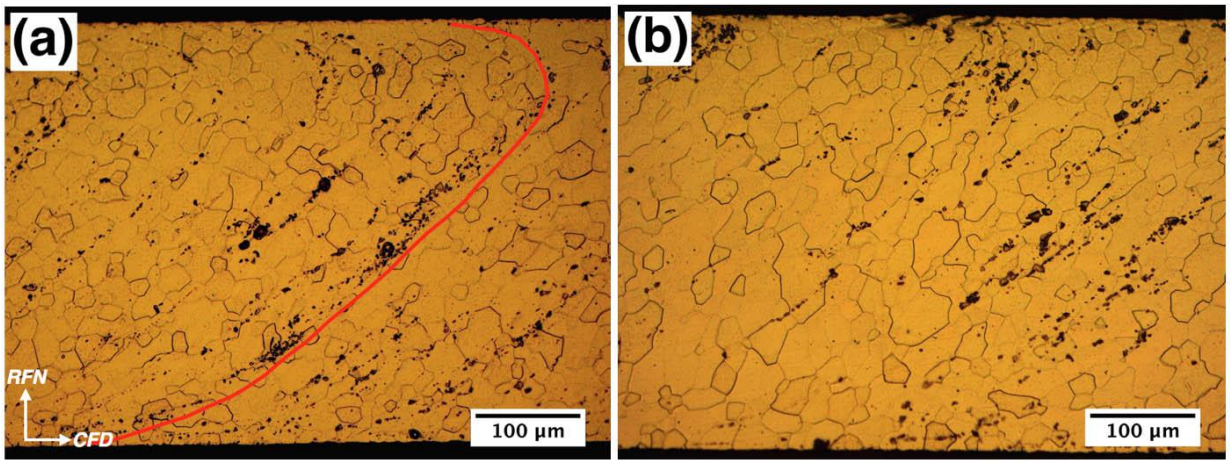

Figure 4.6 Microstructures of annealed LSEM 6013-T6 strips at 572 ℃. (a) fine-grain (b) coarse-grain side for 1 min.

4.3.5 Cold rolling on LSEM strips

The possibility of LSEM to produce strip materials from AA6013-T6 has been demonstrated and a wide range of microstructure can be obtained by controlling machining parameters. In this section, cold rolling was performed on the LSEM strips with microstructure shown in Figure 4.3d to see the workability of this highly deformed LSEM strip. In the rolling experiment, the rolling direction (RD) is the same as the chip flow direction (CFD).

The LSEM strips are cold rolled with parameters are shown in Table 4.4. As can be seen that after 60% reduction in a single step, no cracking occurs as shown in Figure 4.7. This is the limiting thickness that we can achieve in a single step by the rolling mill in the lab. By two-step rolling, 78% reduction can be imposed on the LSEM strip without any cracking (Fig. 4.7), for which the total effective strain is 2.9. This is amazing considering the initial T6 condition, which has poor workability. It seems that simple shear LSEM process makes the strips more workable.

The microstructures of the strips after cold rolling (Figure 4.8 b, c, d, e) are similar to the LSEM strip (Figure 4.8a), except the inclination angle of grain in the primary shear zone. During LSEM process, the grains are inclined with respect to CFD for about 45° as shown in blue line in

Figure 4.8a. In the subsequent cold rolling process, this angle decreases with increasing reduction to about 6° at 78% reduction.

Table 4.4 Cold rolling parameters of LSEM 6013 aluminum strips

t_i (mm)	R	t_f (mm)	ε_c	ε_t	step
0.4	10%	0.36	0.1	1.3	Single
0.4	28%	0.29	0.4	1.6	Single
0.4	60%	0.16	1.1	2.3	Single
0.4	78%	0.09	1.7	2.9	Two

Note: t_i, initial thickness, t_f, final thickness, ε_c, effective strain in cold rolling, ε_t, total effective strain (effective strain in LSEM and effective strain in cold rolling). All the cold rolling processes are performed in one step.

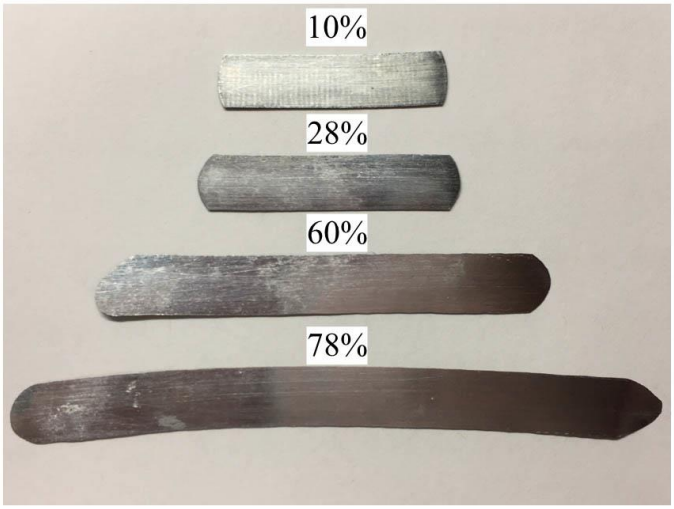

Figure 4.7 Top view of LSEM strips after different amount of cold rolling reduction.

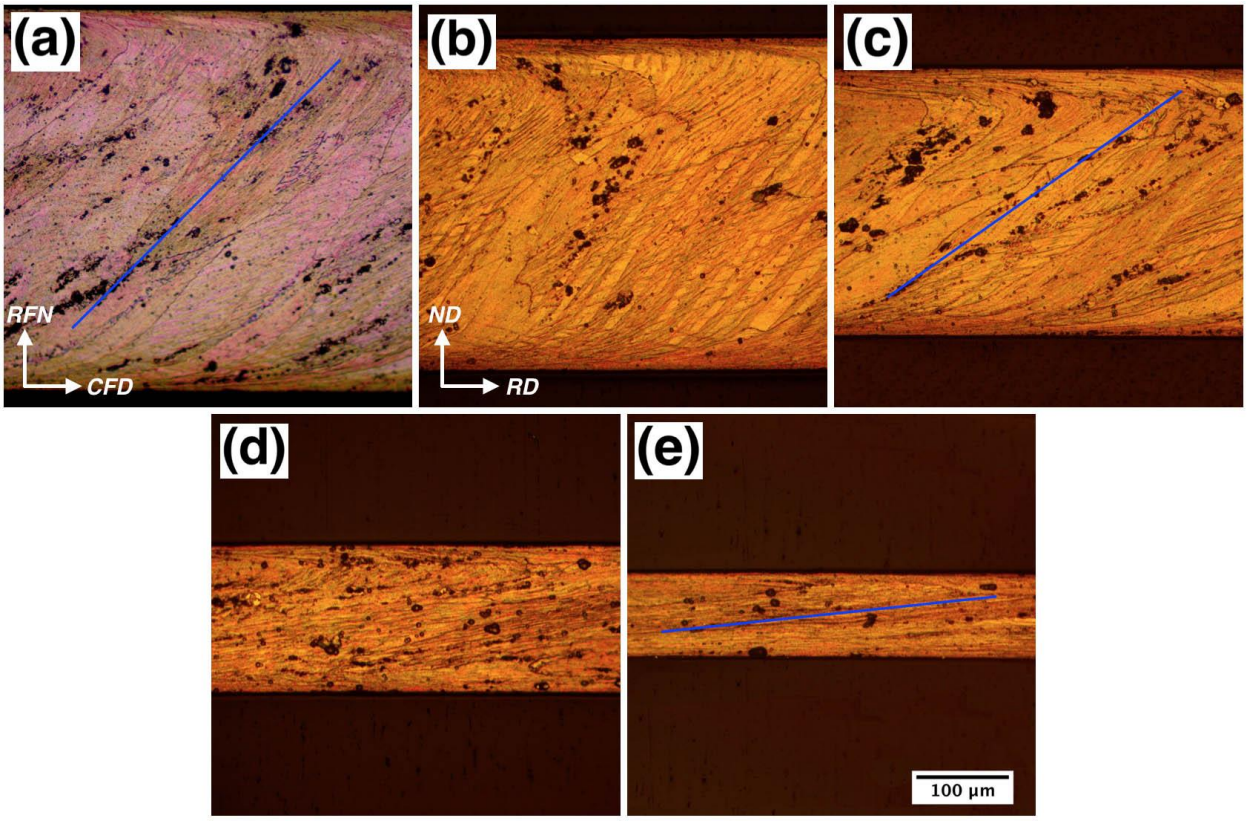

Figure 4.8 Microstructures of (a) LSEM strips after (b) 10%, (c) 28%, (d) 60% and (e) 78% reduction. After rolling, the chip flow direction (CFD) becomes rolling direction (RD) and rake face normal (RFN) becomes normal direction (ND).

4.3.6 Comparison of LSEM and rolled strips

4.3.6.1 Microstructure of the rolled and annealed strips

In order to compare the microstructure and mechanical properties of strips produced by rolling and LSEM, the as-received AA6013-T6 was warm-rolled at ~300 ℃ with the same effective strain as LSEM in section 4.3.2 (Figure 4.3c, d) and then annealed under the same condition as section 4.3.4 for 2 min. The ageing response and tensile behavior of the strips were measured and compared.

The microstructures of the warm-rolled and annealed strips are shown in Figure 4.9. Unlike LSEM process (Figure 4.3c), the grains are elongated along rolling direction (Figure 4.7a). After solution treated and quenched, equiaxed grains with grain size around 20 µm develops, similar to

that of annealed LSEM strips (Figure 4.6), due to the same effective strain. The hardness of the warm-rolled strip after annealing is 93, same as that of annealed LSEM strip, indicating a complete solution treatment.

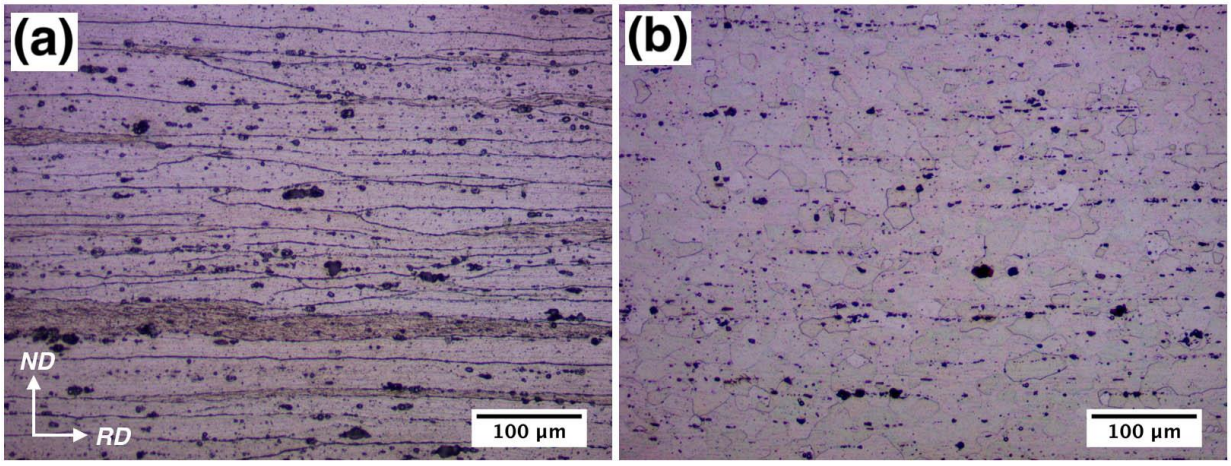

Figure 4.9 Microstructure of the strips after (a) warm-rolled with the same effective strain as LSEM strips and then (b) annealing, where ND and RD are normal and rolling direction.

4.3.6.2 Ageing response of the strips

Generally, with increasing ageing time from 20 min to 420 min, the hardness of warm-rolled and LSEM strips increase at the beginning stage and then decrease slowly, as can be seen in Figure 4.10. A significant increase in hardness is obtained after ageing at 190 ℃ for 20 min for both strips. But interestingly, the hardness of the LSEM strip is 9% higher than that of warm-rolled strip. With increasing ageing time, the hardness of the LSEM and warm-rolled strips drops; but still, the LSEM strip has a higher hardness (~ 5% higher). The explanation behind this remains unknown now due to the lack of time, but it might be related to the texture of the materials by speculation, since this is the only difference between these annealed strips. More experiments will be focused on this part to investigate the precipitation behavior of these two materials by TEM.

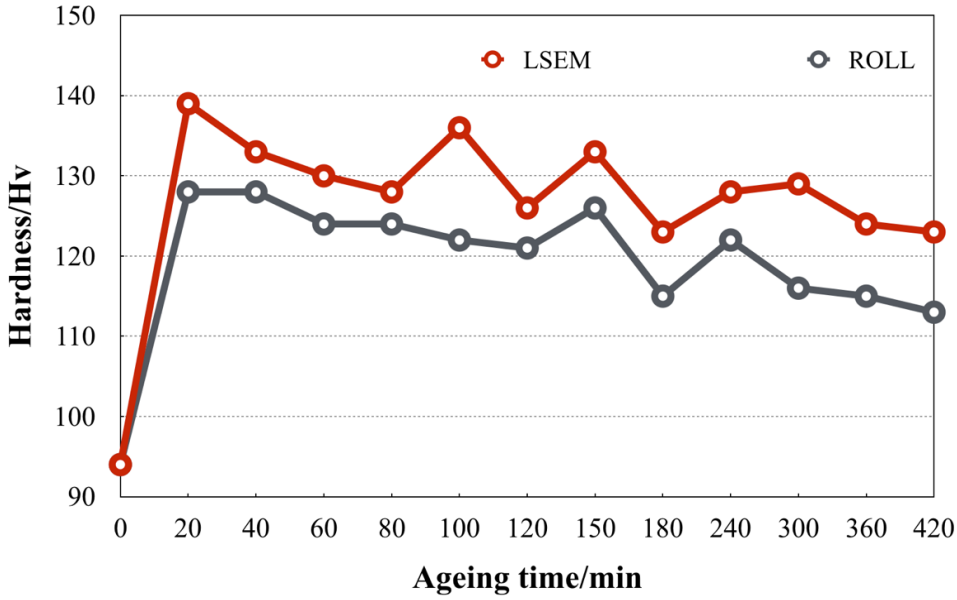

Figure 4.10 Ageing response of the LSEM and warm-rolled strips after heat treatment at 190 ℃ for up to 420 min.

4.3.6.3 Mechanical properties of the strips

Tensile stress - strain of the solution treated strips was tested in a MTS machine with strain rate $5 \times 10^{-3}\ s^{-1}$ and the elongation measured by a quarter-inch extensometer. The tested specimen has a total length of 30 mm, with 10 mm gauge length, 3 mm gauge width, and 0.37 mm thickness. Figure 4.11 is the engineering stress-strain curve of these strips and some important data are shown in Table 4.5. During uniaxial tension process, the annealed LSEM strip yield first and then strain hardening occurs. Fracture occurs on annealed warm-rolled strip at 19.7% elongation, while the LSEM strip keeps gain strength by strain hardening until fracture happens at 28.3% elongation. The yield strength (YS) of LSEM is 140 MPa, 10% smaller than the rolled strip, but they have nearly the same tensile strength (UTS). The uniform elongation (elongation before necking minus the elastic elongation) of the LSEM strip is 26.9, 59% larger than the warm-rolled strip. It is interesting to observe a big increase in ductility without losing strength in LSEM strip and the reason will be revealed in the next chapter.

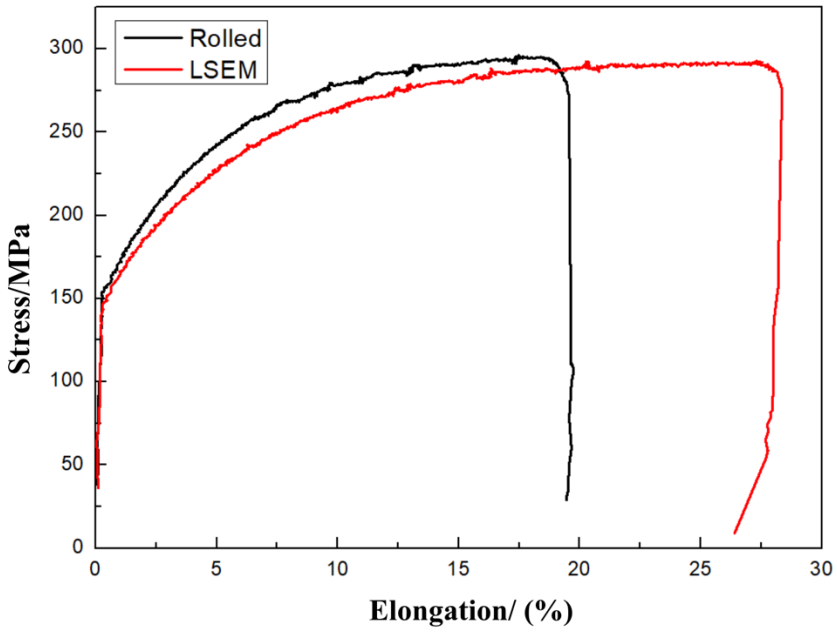

Figure 4.11 Engineering stress-strain curve of the LSEM and warm-rolled strips after solution treatment at 472 ℃ for 2 min.

Table 4.5 Tensile properties of solution treated LSEM and warm-rolled strips

	YS/MPa	UTS/MPa	Uniform elongation	Total elongation
Warm-rolled	156	296	16.9	19.7
LSEM	140	293	26.9	28.3
Comparison	-10%	-1%	+59%	+44%

4.4 Implications

The results in this chapter indicate that continuous strip can be produced from an age-hardened aluminum alloy (AA6013-T6), even without preheating, using the single-step LSEM process. By controlling deformation parameters (strain, strain rate and temperature), a wide range of microstructures is obtained. The observations have broad implications for controlling sheet microstructure and properties.

4.4.1 Controlling microstructure in LSEM

During the LSEM process at low temperatures, a flow-line type microstructure develops through the thickness of the strip. This microstructure is usually divided into three different zones: the primary shear zone coming from the shear in the deformation zone (Figure 4.3a and c); secondary shear zone originating from the friction between the cutting tool and strip, and constrained zone resulting from the friction between the constraint and strip. The zones are analogous to those developed in conventional extrusion, but distinctly different from the flow in-plane flow and structure development in rolling. In LSEM, λ and V_0 are two main factors that control these three zones. At a fixed λ, the constrained and secondary shear zone shrink, while the primary shear zone enlarges, with increasing V_0 (Figure 4.3a, c), and at low velocity, the primary shear zone even vanishes and constrained zone dominates (Figure 4.4a). At low velocity, friction on the top and bottom of the strip are so large that the primary shear zone is swallowed by secondary shear and constraint zone. With increasing V_0, however, the temperature rise increases and the natural λ decreases, leading to a smaller friction coefficient and lower hydrostatic pressure, so friction decreases. This reduction in friction results in the shrinkage of the constrained and secondary shear zone.

At high-temperature cutting, the yield strength of the materials drops and this makes the primary shear zone easy to deform. At T_0 = 400 ℃, the material is so soft that the friction can penetrate the primary shear zone easily and finally the primary shear zone completely partitioned into constrained and secondary shear zones (Figure 4.5b). With decreasing temperature to T_0 = 300 ℃, the yield stress increases, but friction effect dominates. Part of the secondary shear zone begins to transform into constrained zone (Figure 4.5c) and at T_0 = 135 ℃, the strip mainly consists of constrained zone (Figure 4.5e). The ability to control the shear flow fields and associated textures is an attractive attribute of the LSEM process to obtain a wider range of desired properties.

4.4.2 Dynamic and static recrystallization

Typically, dynamic recovery is the main softening mechanism during hot working of aluminum alloy due to the high stacking fault energy. For 6xxx aluminum alloys, plenty of second phase particles precipitate and/or coarsen in the matrix during various thermomechanical processing steps. These precipitations impede the movement of grain boundaries and dislocations, making dynamic recrystallization behavior even harder to occur [58]. In commercial production of 6xxx aluminum alloy sheets, dynamic recrystallization happens in the reversible (breakdown) hot rolling process due to the high temperature (entrance temperature ~500 ℃) and strain rate. But in the following multi-stand (finish) hot rolling process, dynamic recrystallization is suppressed due to the pinning effect of the second phase precipitations, in spite of the relatively high strain rate and temperature (entrance temperature ~400 ℃) [59].

In high-temperature LSEM experiment on AA6013-T6, complete dynamic recrystallization happens at T_0 = 400 ℃. In conventional rolling process, however, highly deformed microstructure develops during tandem hot rolling, where the entrance temperature is 400-500 ℃ [24]. The adiabatic heating during LSEM process makes it possible for dynamic recrystallization to occur at

a lower temperature than in hot rolling process. Static annealing was performed on the LSEM strip produced with the same condition as the high-temperature cutting but at room temperature, and a homogeneous microstructure is obtained with grain size very similar to the dynamically recrystallized strips. Thus, the thermomechanical history of the strip does not have any effect on the final grain size of the strip, as long as the effective strain remains the same. But regarding the different yield stress of this alloy under various temperatures, friction between cutting tool and strip, and friction between constraint and strip, etc., the flow path of this alloy during LSEM process is likely to be different and this can be seen from the alignment of the constituent particles in red line in Figure 4.5b and 4.6a. So the textures of the dynamically recrystallized and static recrystallized strips are probably different.

4.5 Conclusions

(1) Free machining (FM) and large strain extrusion machining (LSEM) experiments were performed on AA6013-T6. Continuous strip can be obtained through FM and LSEM with a flow-line type microstructure.

(2) The through-thickness microstructure of the as-received AA 6013-T6 workpiece was inhomogeneous, containing fine-grain zone near surface and coarse-grain zone in the middle, but have similar hardness. After FM/LSEM, the nonuniform microstructure was inherited to the strip and this inhomogeneity vanishes gradually with decreasing λ. But this grain size difference has no effect on the hardnesses of both sides of the strip.

(3) Completely dynamic recrystallization occurs when the workpiece was LSEM at T_0 = 400 ℃ and both sides of the strip have almost the same microstructure and hardness in spite of an inhomogeneous starting microstructure (grain size difference) in the workpiece. With decreasing initial temperature T_0, the fully annealed microstructure transformed into deformed,

but highly recovered microstructure and the hardness of the strip decreases.

(4) The microstructure and hardness of the strip solution treated at 572 ℃ for 1 min and for 4 min are almost the same. The statically recrystallized and dynamically recrystallized strips have very similar microstructure. The hardness of dynamically recrystallized strip is a little lower than that of the statically recrystallized strip due to coarsening of the second phase.

(5) The ageing response of the annealed LSEM strip is better than annealed warm-rolled strips. The yield strength of annealed LSEM strip is lower than warm-rolled strip, but they have almost the same tensile strength. The LSEM strip has enhanced ductility with 59% higher elongation than that of warm-rolled strip, most likely due to texture. Detailed discussions will be focused in the next chapter.

5. ENHANCED WORKABILITY OF ALUMINUM STRIPS PRODUCED BY CUTTING-EXTRUSION ON AS-CAST AA6013

5.1 Introduction

In the last chapter, the focus was on producing strip materials from AA6013-T6 and continuous strips were produced by LSEM process. By controlling machining parameters, a wide range of microstructures can be obtained and the final strips have better properties than rolled ones, such as ageing response, tensile ductility. As-cast aluminum alloy is another category that is notorious for low workability and homogenization is required for the following deformation process, such as rolling, extrusion. However, researches of LSEM on as-cast aluminum alloys are very limited according to literatures. For example, Efe et al. studied the mechanics of LSEM and demonstrated that continuous strips can be obtained on poor workable MgAZ31B alloy [55]; Kustas et al. conduct LSEM on high-silicon iron plate and showed that shear texture develops in this simple shear process [53]. So, in this chapter, LSEM experiments were performed directly on the as-cast 6013 aluminum alloy without homogenization for the first time. And a subsequent cold rolling process was followed to study the workability of these highly-deformed LSEM strips. The microstructures and hardness evolution during subsequent cold rolling process were investigated. Finally, the textures of the LSEM and annealed strips are studied and implication on formability of aluminum alloys are discussed.

5.2 Experimental procedure

The materials that used for casting were commercial AA6013-T6 aluminum plate purchased from ThyssenKrupp, Miamisburg, Ohio. The chemical composition (wt. %) of this alloy is: 0.66 Si, 0.27 Fe, 0.62 Cu, 0.29 Mn, 0.94 Mg, 0.021 Cr, 0.008 Ni, 0.024 Zn, 0.017 Ti and 0.15

others. The alloy was remelted in air and cast into disk shape with 150 mm diameter and 16 mm thickness in a copper mold and cool in the air and the through-thickness microstructure along the radius direction is investigated.

Free machining (FM) experiments were performed on a lathe and continuous strips were obtained with rake angle α = 5°, cutting velocity V_0 = 3 and 6 m/s, and then LSEM experiments were conduct with chip thickness ratio λ = 2.5 (t_0 = 0.25 mm, t_c = 0.63 mm) and V_0 = 6 m/s. The LSEM strips were cold rolled to different thicknesses in a single step with 17%, 44%, 65% and 73% reduction in a laboratory rolling mill with roll diameter 100 mm.

The as-cast, FM, LSEM and cold-rolled samples were prepared by mechanical grinding from 320 to 2000 grit SiC abrasive paper, and then polished with 0.05 μm alumina and 0.02 μm colloidal silica. A 10-weight percent sodium hydroxide was employed to etch the samples for times of 2-5 min with mechanical agitation to reveal the microstructures. The through-thickness microstructure of the as-cast 6013 alloy, FM, LSEM and rolled strips were investigated by optical microscopy. Grain structure of as-cast alloy was studied by EBSD inverse pole figure color mapping and grain size was determined by intercept procedure according to ASTM E112-12.

Texture measurements were performed through the thickness of the sample using FEI XL40 scanning electron microscopy with EBSD detector. At least two scans were obtained for each sample to ensure the reliability of the measurement. Data from the scans were considered acceptable when the confidence index values (CI) are greater than 0.1. The data were analyzed and the pole figures were generated by EDAX OIM software.

5.3 Results

5.3.1 Casting of AA6013

The as-cast microstructure along the radial direction reveals a fine equiaxed grain structure. The grain size in the surface and middle of the workpiece are very similar and the average is around 200 μm (Figure 5.1a), as measured by linear intercept method on the EBSD image. A low pouring temperature (~700 ℃) was controlled during casting process to decrease the solution of hydrogen and gas porosity. A small amount of porosity, however, still appears in the casting process (arrows in Figure 5.1b), as expected.

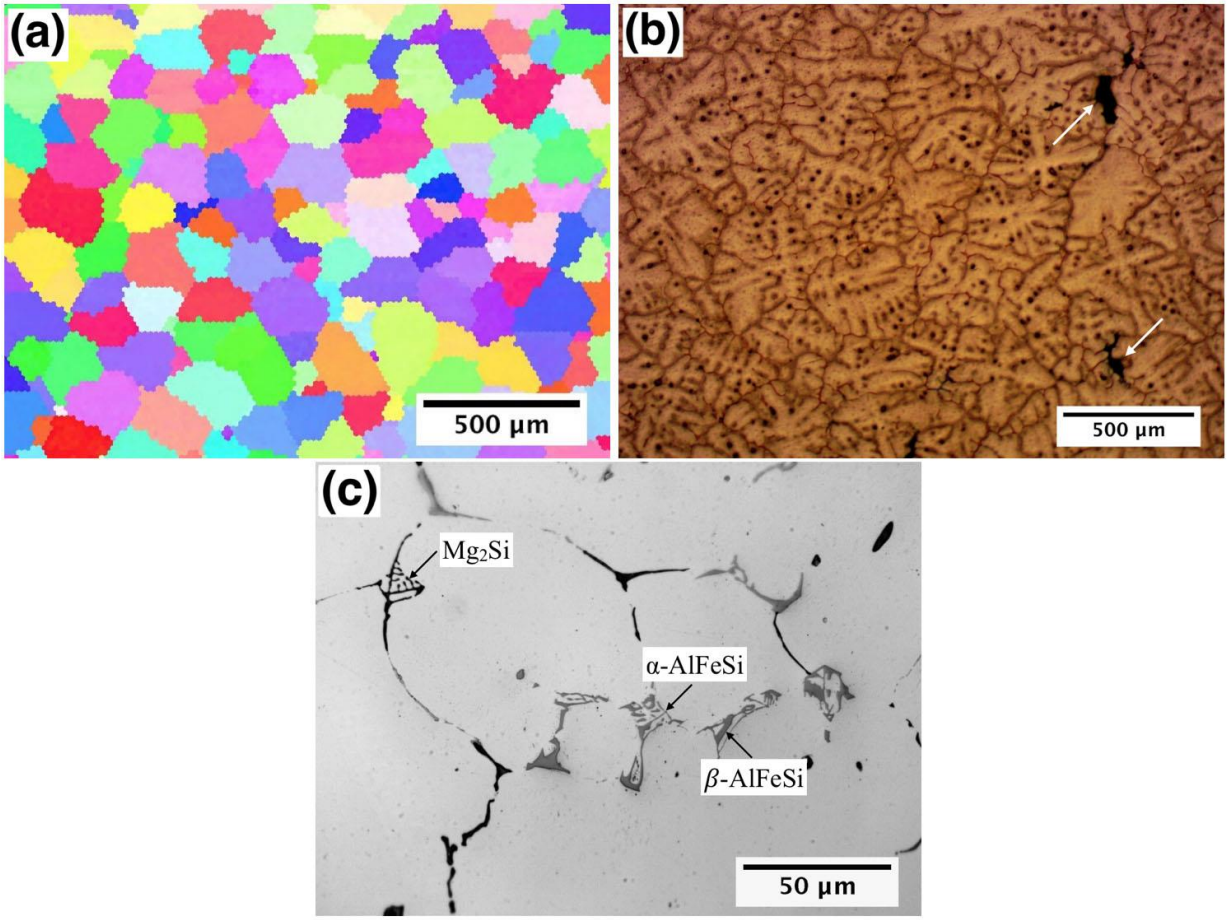

Figure 5.1 Microstructure of the as-cast 6013 alloy: (a) EBSD inverse pole figure map, clearly showing grain size, (b) optical micrograph showing dendritic grain structure and porosity, and (c) showing the morphology of interdentritic phase α-AlFeSi and β-AlFeSi.

Solidification occurs by dendrite growth and towards the end of this process, constituent phases tend to form between the dendrites. In 6xxx aluminum alloy, these constituent phases include α-AlFeSi, β-AlFeSi and Mg_2Si (Figure 5.1c) as well as other non-equilibrium phases [60]. The plate-like β-AlFeSi particles are detrimental to the following hot deformation (hot rolling, hot extrusion) process. During homogenization process, however, the transformation from β-AlFeSi to α-AlFeSi occurs [19-23]. So homogenization is usually critical to increase the workability of as-cast 6xxx alloy.

5.3.2 FM and LSEM of as-cast 6013 alloy

FM and LSEM experiments are performed on the as-cast 6013 alloy and continuous strips are obtained under various parameters shown in Table 5.1. In conventional production of 6xxx aluminum alloy sheets, homogenization is required in preparation for the following hot rolling process. And in reversing hot rolling, the ingots are hot rolled at temperatures more than 500 ℃ with rolling reductions around 10% for up to 25 steps. In the LSEM experiment on the as-cast 6013 alloy, however, continuous strips with smooth surfaces are obtained in a single step with effective strain as large as 1.6 at room temperature without any cracking, as shown in Figure 5.2a. The surface roughness of the LSEM strip is measured by 3-D Zygo View 8000 optical profilometer system. After LSEM, the top surface and back surface (rake face) have a surface roughness $Sa = 0.928$ μm and $Sa = 0.174$ μm, respective. The top surface is very smooth, but still not as good as the rake face.

Table 5.1 FM and LSEM parameters at room temperature

	α (°)	t_0 (mm)	V_0 (m/s)	t_c (mm)	λ	ε
FM	5	0.25	3	0.85	3.4	2.0
			6	0.71	2.8	1.7
LSEM	5	0.25	6	0.63	2.5	1.6

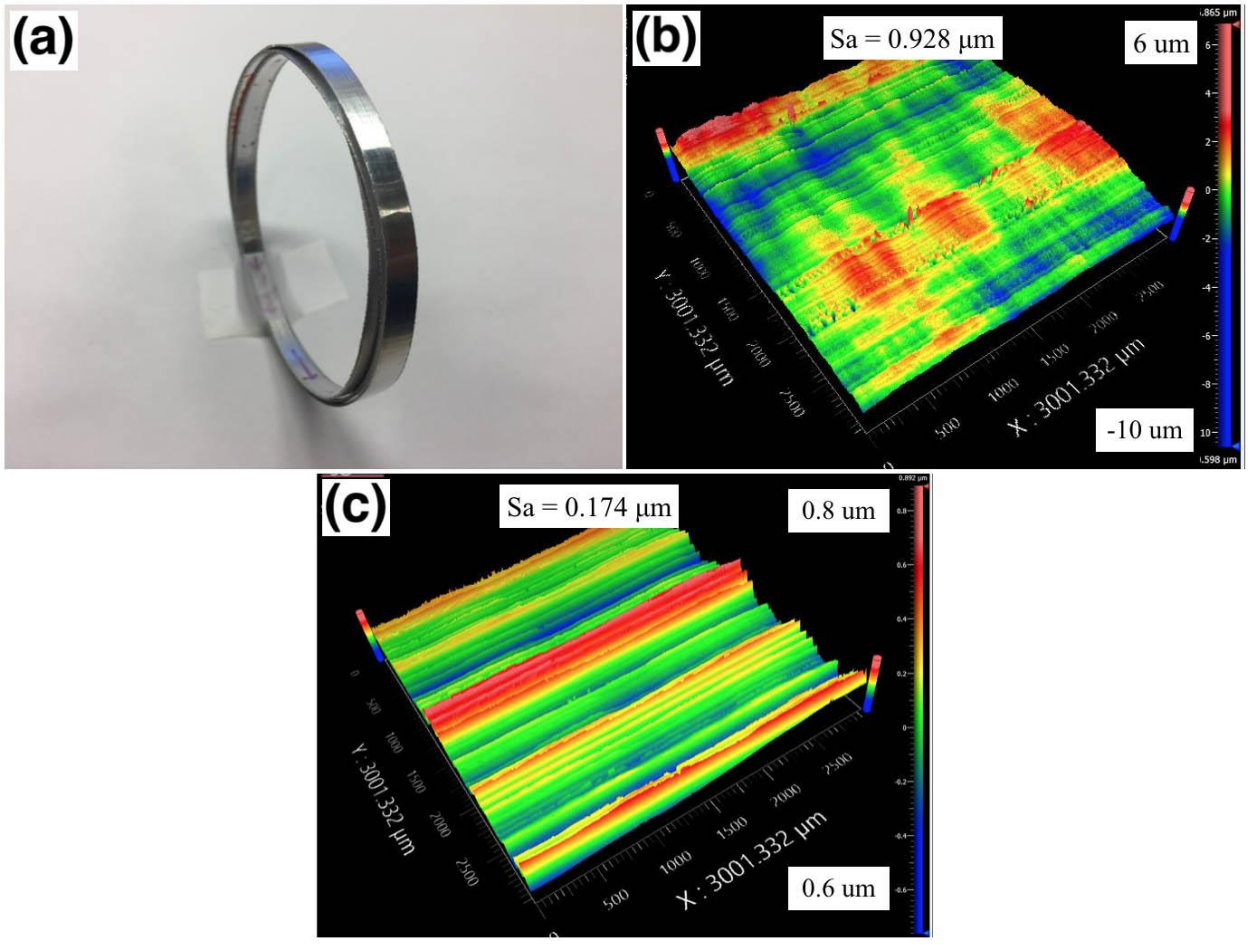

Figure 5.2 (a) Continuous strip produced by LSEM on as-cast 6013 alloy with effective strain 1.6 and surface roughness of (b) top surface and (c) rake face.

Figure 5.3 shows the flow-line type microstructures of FM and LSEM strips from as-cast 6013 alloy. During FM process, grains with various orientations in the as-cast alloy undergo

different degrees of rotation, so the top surface of the FM strip is rough. The thickness of the strip at 3 m/s is larger than that at 6 m/s, indicating a higher strain. And this is in accordance with the inclination angles of grains under these two conditions. At 3 m/s, the inclination angle is 76°, higher than that at 6 m/s, 65°. Build-up edge occurs in the strips machined at 3 m/s (Figure 5.3a), while strips at 6 m/s are free of it (Figure 5.3b). So, LSEM experiments are conduct at 6 m/s.

During LSEM process, however, the constraint confines the flow of the material on the free surface and acts as an extrusion die simultaneous with cutting, so both surfaces of LSEM strips are smooth (Figure 5.3c). During the casting process, pores formed between dendrites (Figure 5.1b), while after FM and LSEM, these pores are not observable. So, machining-based process is also a way to close pores. In FM and LSEM experiments at 6 m/s, the inclination angles (blue lines in Figure 5.3b, c) in primary shear zone are very similar, around 65°. The inclination angle of the grains is different from the shear angle: the shear plane angle of FM and LSEM strips at 6 m/s are 74° and 73° by calculation, which are larger than inclination angles of grains in these two conditions. During LSEM process, grains aligned in the direction of maximum elongation imposed and this direction is inclined at an angle to the shear plane. With increasing strain, this angle becomes smaller and smaller.

The hardness of the LSEM strip is 88, lower than that of FM strip, 98, but both are higher than as-cast material, 64, due to work-hardening effect. In LSEM experiment with $\lambda = 2.5$, the temperature rise in the strip is higher than that in FM strip because of the larger hydrostatic pressure. Besides, the effective strain in FM strip is larger. So, the hardness of LSEM strip is lower than that of FM strip due to smaller strain and higher level of recovery.

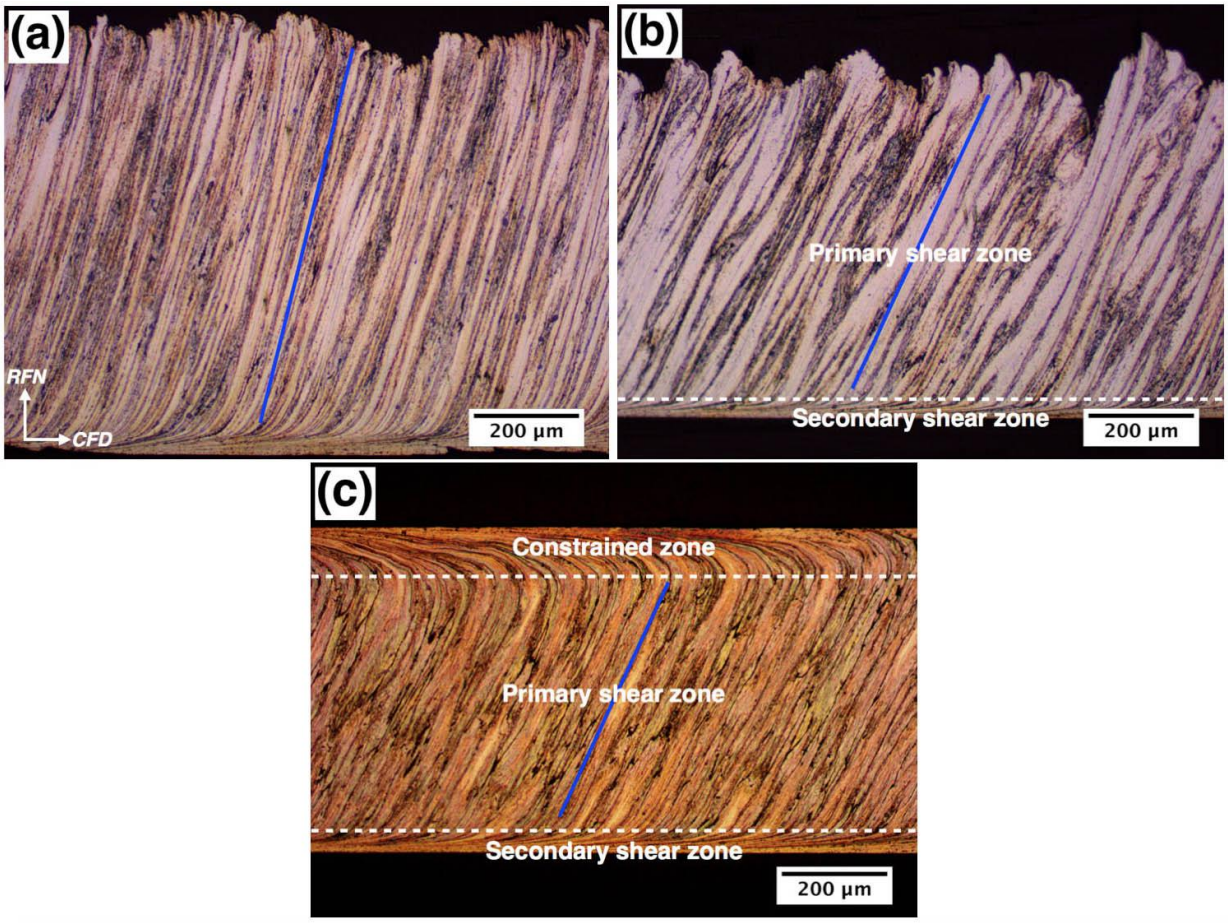

Figure 5.3 Microstructures of strips produced by FM and LSEM. (a) and (b) are microstructures of FM strips at 3 and 6 m/s, respectively, (c) is the microstructure of LSEM strip at V_0 = 6 m/s with λ = 2.5.

5.3.3 Cold rolling of LSEM strips

In commercial production of aluminum alloy sheets, hot band is cold rolled to final gauge to obtain a better surface finish. Similarly, cold rolling is performed on LSEM strips without preheating, with one goal to improve the surface finish. As can be seen from Figure 5.2b and c that the top surface of the strip is not as smooth as the rake face, so cold rolling is performed on the LSEM strip to improve the surface roughness. But most importantly to investigate the workability of this highly-deformed strips and determine whether annealing is required for the following cold

rolling process. The thickness of the starting LSEM strips were 0.63 mm and cold rolling experiments were performed on these strips with parameters in Table 5.2 in laboratory rolling mill.

Table 5.2 Rolling parameters of LSEM 6013 aluminum strips

t_i (mm)	R	t_f (mm)	ε_c	ε_t	Hv (kgf/mm^2)
0.63	17%	0.52	0.2	1.8	94
0.63	44%	0.35	0.7	2.3	98
0.63	65%	0.22	1.3	2.9	99
0.63	73%	0.17	1.5	3.1	100

Note: t_i, initial thickness, t_f, final thickness, ε_c, effective strain in cold rolling, ε_t, total effective strain (effective strain in LSEM and effective strain in cold rolling). All the cold rolling processes are performed in one step.

It is interesting to see from Table 5.2 that LSEM strips are amazingly workable. In LSEM process, continuous strip is obtained without preheating from as-cast 6013 alloy with the effective strain ε = 1.6 and this highly deformed strip can be cold rolled with 73% reduction in one step without any cracking (Figure 5.4a) at room temperature, for which the total effective strain is ε_t = 3.1. After 73% reduction, the thickness of the strip is 170 μm. This is the limit thickness of the rolling mill in our laboratory, but not the rolling limit of the LSEM strips. Clearly, intermediate annealing is not needed for the LSEM strips in cold rolling process.

The hardness of the strip increases with increasing reduction, but after cold rolled for more than 44% reduction, it remains very stable, changing from 98 in 44% reduction to 100 in 73% reduction. The possible reason is that the work-hardening effect saturates at such a high strain. During deformation process, plenty of new dislocations form; in the meantime, recovery occurs to reduce the stored energy by removal or rearrangement of defects and primarily dislocations. With increasing strain to a certain level, these two processes reach a dynamic balance. The LSEM strip

is already highly deformed with effective strain ε = 1.6. With increasing rolling reduction, the dislocation density increases, but reaches saturation gradually after 44% reduction. So, the hardness of the strip after 44% reduction is very stable.

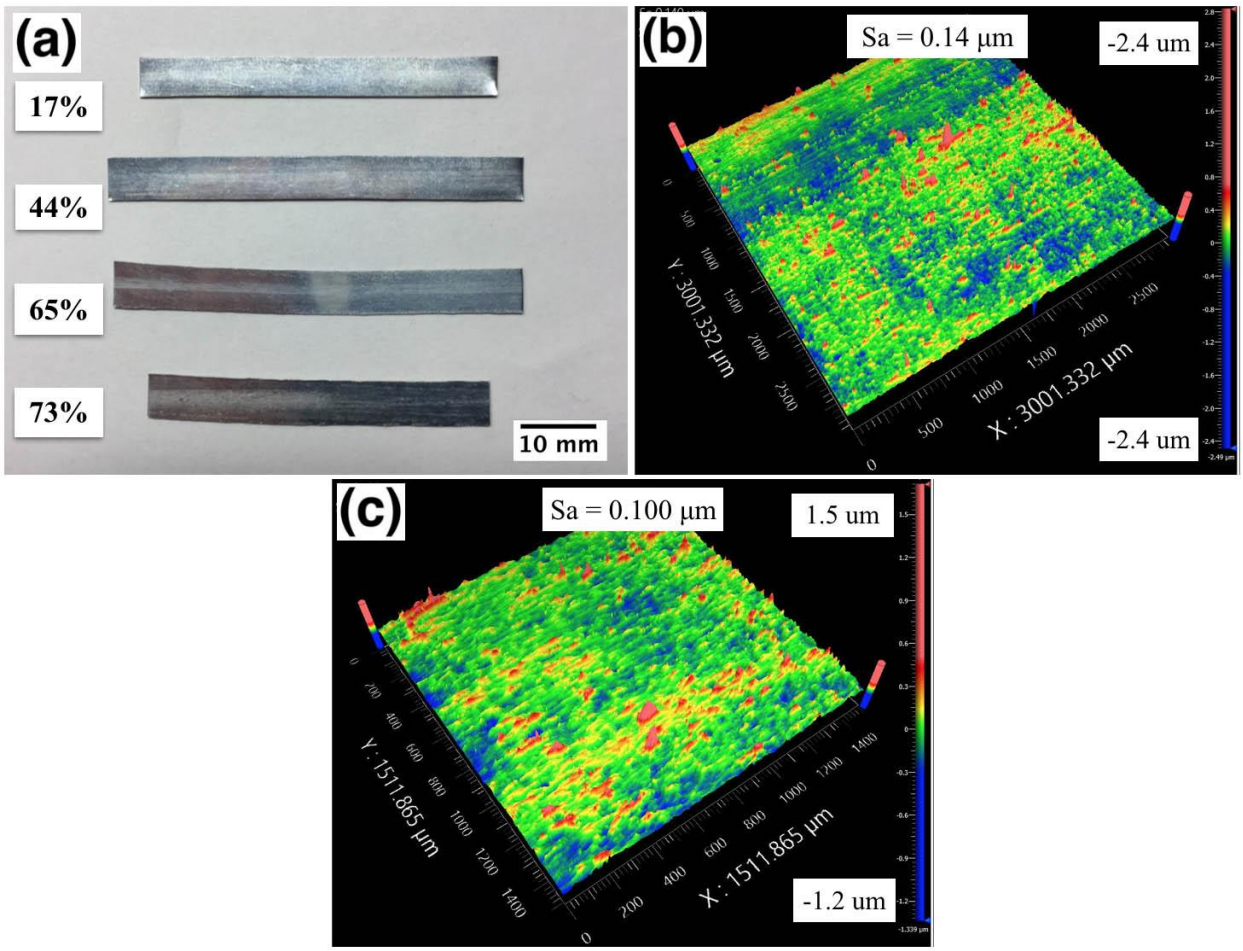

Figure 5.4 Top view of LSEM strips after cold rolling for 17%, 44%, 65% and 73% reduction and surface roughness of the top surface after (b) 44% and (c) 73% reduction.

The surface roughness of the top surface of LSEM strip is $Sa = 0.928$ µm (Figure 5.2b). After cold rolled for 44% reduction, the roughness becomes $Sa = 0.14$ µm as shown in Figure 5.4b, even better than the rake face of the LSEM strip (Figure 5.2c). With increasing reduction to 73%, this value decreases to $Sa = 0.1$ µm (Figure 5.4c), only 1/9 of the initial roughness and as good as that of the commercially rolled strips, which is about 0.1 µm.

The microstructures of the strips after cold rolling are similar to the flow-line type LSEM microstructures (Figure 5.5). They all have constrained zone, primary shear zone, and secondary shear zone, except that the secondary shear zone is hard to distinguish after cold rolled for high reductions (Figure 5.5d, e). But still there are some differences, such as the inclination angle and thickness of the grains in the primary shear zone. The inclination angle of the grain in LSEM strip is about 65. With increasing reduction, this angle decreases from 54° after 17% reduction to 11° after 73% reduction, as shown in Figure 5.5. So, cold rolling is an effective way to improve the surface quality of LSEM strip and also to control the microstructure of the strips.

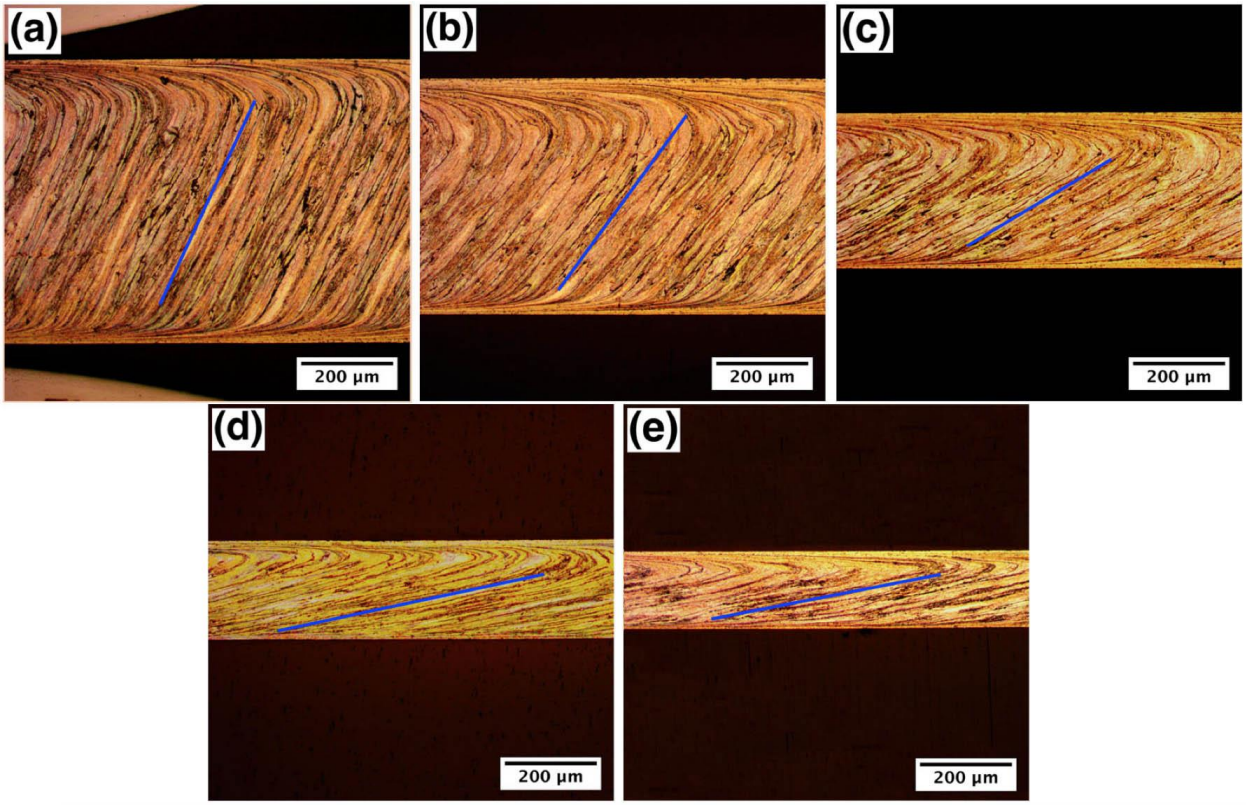

Figure 5.5 Microstructures of (a) LSEM strips after cold rolling for (b) 17% (c) 44% (d) 65% and (e) 73% reduction in a single step at room temperature.

The as-cast 6013 alloy has an equiaxed grain structure with grain size around 200 µm (Figure 5.1). After LSEM experiment, the grains are elongated toward the maximum tensile

direction and the thickness of the grains reduces to 35 μm due to this shear deformation. In the following cold rolling process, with increasing reduction, the thickness changes from 30 μm in 17% reduction to as small as 13 μm in 65% reduction. This considerable reduction in grain size along certain direction may play an important role in the annealing process.

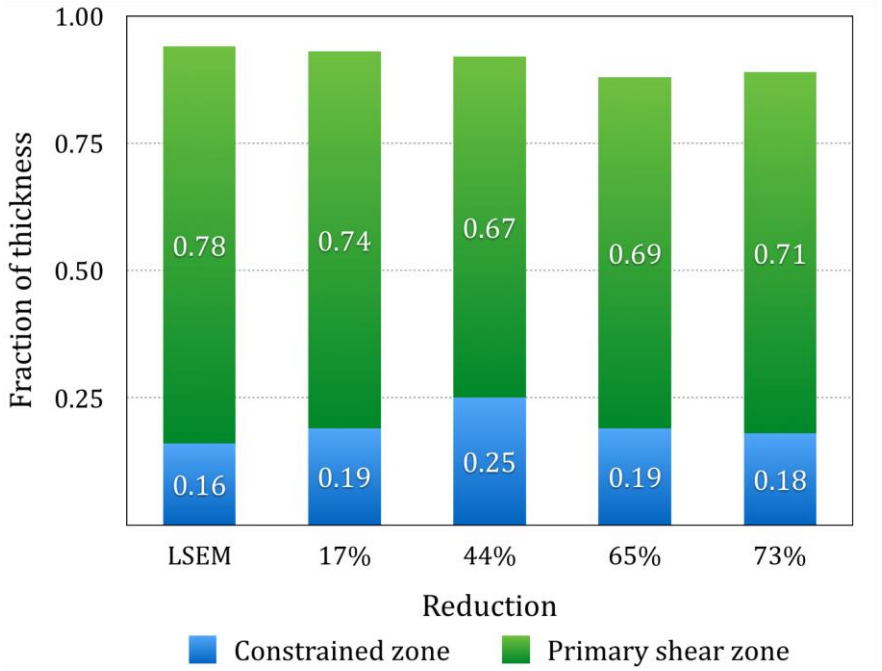

Figure 5.6 Relative thickness of constrained and primary shear zone of the LSEM strips after 17%, 44%, 65%, and 73% reduction.

Another difference is the thickness fraction of primary shear and constrained zones in the strips, as shown in Figure 5.6. The actual size of secondary shear zone is hard to distinguish after high reduction, so here we only discuss constrained and primary shear zones. The relative thickness of primary shear zone in LSEM strip is 0.78. In the following cold rolling process, with increasing rolling reduction to 44%, the relative size of this zone decreases to 0.67, but then it increases to 0.71 when it is cold rolled with 73% reduction. The relative size of constrained zone is the opposite of primary shear zone. It increases with increasing reduction to 44%, and then decreases with increasing reduction. The actual size of the constrained zone in LSEM strip is about

100 μm (Figure 5.3c), but interestingly, after cold rolled for 17% reduction, the size of constrained zone remains almost the same. After 44% reduction, the size of constrained zone only drops to 86 μm. So only 14% reduction occurs in this zone, much smaller than overall 44% reduction. Thus, it is safe to conclude that after cold rolling for 17% reduction, deformation only happens in the primary shear zone and after 44% reduction, only part of deformation occurs in constrained zone.

5.3.4 Texture of LSEM strips

In the as-cast LSEM AA6013 strip, a homogeneous flow-line type microstructure is developed in the strip with constrained, primary shear and secondary shear zone as shown in Fig. 3c. The texture data measured by EBSD from these zones is shown in Figure 5.7 using (111) pole figures, obtained from the sheet thickness cross-section (RFN-CFD plane in Figure 3.2). The textures in these zones are dominated by two partial fibers, {111} fiber and <110> fiber, highlighted by the dotted lines in the (111) pole figures for reference. In fact, these fibers are characteristic of the simple shear deformation texture for FCC systems. The ideal {111} fiber results from an alignment of the (111) plane in a direction parallel to the shear plane, and the ideal <110> fiber arises from [110] direction aligning along the shear direction [65-68]. Due to different shear plane angles in these zones, however, their textures have different rotation angles with respect to CFD in the RFN-CFD plane. In secondary shear and primary shear zone, the rotation angles are about 14° and 70°, counter-clockwise about CFD. While in the constrained zone, the rotation is clockwise and the rotation angle is about 42°.

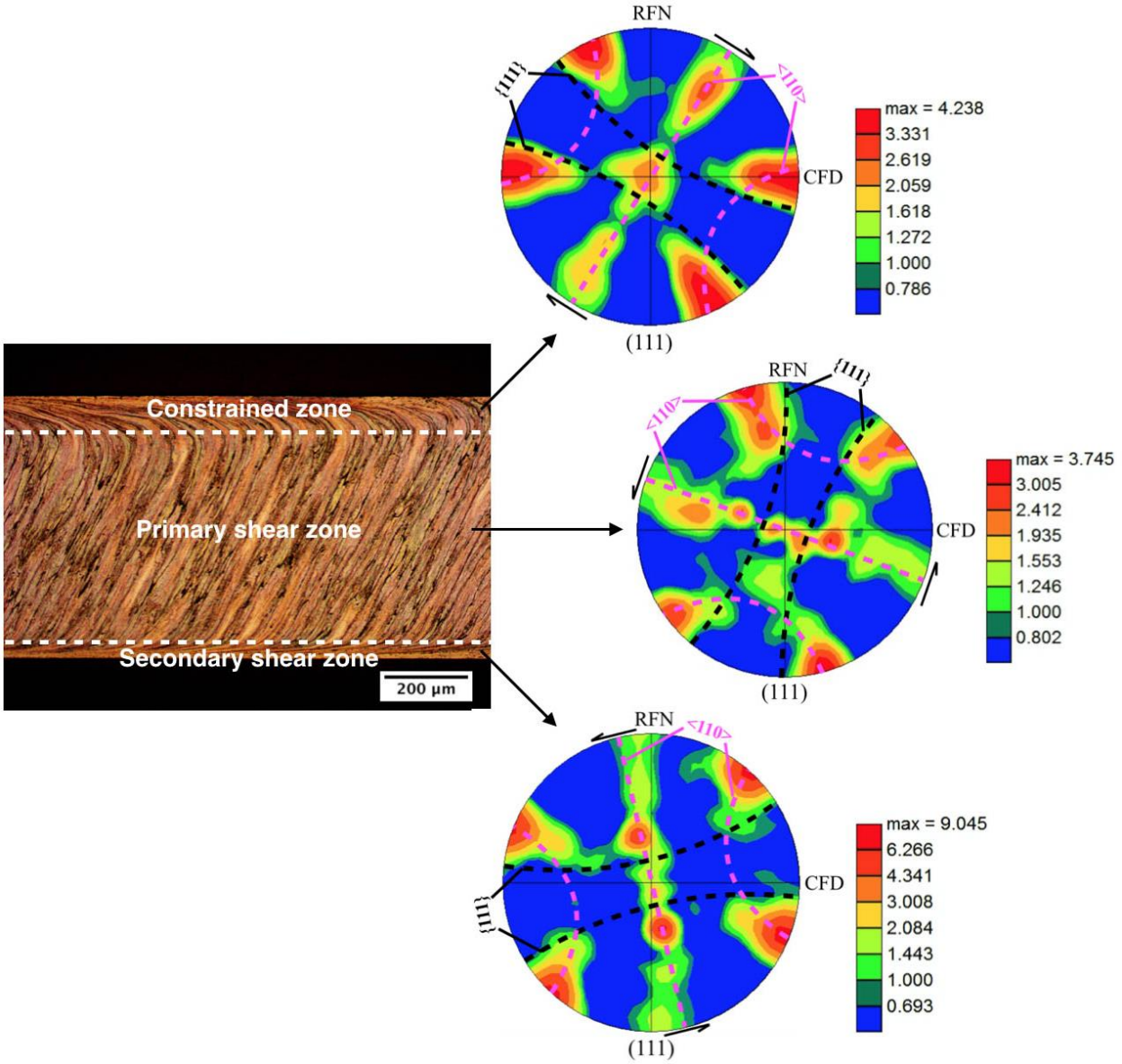

Figure 5.7 EBSD analysis showing texture data in constrained, primary shear and secondary shear zone in LSEM 6013 strip. The {111} and <110> shear texture fibers are highlighted in the (111) pole figures by black and magenta dotted lines, respectively.

In LSEM experiment as shown in Figure 3.2, grains in the primary shear zone are sheared counter-clockwise around TD for φ' degree with respect to CFD and this shear angle φ' is a function of rake angle α and chip thickness ratio λ. In our LSEM experiment at α = 5°, V_0 = 6 m/s and λ = 2.5, the shear plane angle in primary shear zone is 73° by calculation. Based on the analysis

of the pole figure in primary shear zone, the rotation angle is 70°, which is very close to the shear plane orientation for this process condition.

5.3.5 Microstructure and texture of annealed LSEM strip

The LSEM strip of as-cast AA6013 is annealed at 568 ℃ for 2 min and then solution treated and quenched to observe the microstructure. In commercial production of aluminum sheets, the grain size of the as-cast ingot is around 200 μm. This coarse ingot undergoes homogenization, breakdown and multi-stand hot rolling, cold rolling, and solution treatment to obtain an equaixed grain structure with grain size about 20 μm in the final sheets. In the LSEM experiments, however, the same refinement of grain size can be achieved in a single step, as shown in Figure 5.8.

The texture of the annealed strip is also measured by EBSD and the (111) pole figure of the texture is shown in Figure 5.8. Compared with the texture in the primary shear zone of the LSEM strip, the {111} and <110> fiber are inherited in the annealed strip from the deformation texture because of continuous recrystallization. Similar phenomenon was observed in ECAP on pure aluminum.

Besides the simple shear texture, we can also see some other texture components. When the second-phase precipitations are present in aluminum alloys, the recrystallization process is influenced by the precipitation state, since large particles can promote recrystallization by acting as nucleation sites. The particle stimulated nucleation (PSN) takes place in the so-called deformation zones that form around particles that are larger than 1 μm by interaction between dislocations and particles and the resulting recrystallization textures of PSN are usually very weak, almost random. In the as-cast material, large constituent phases form during solidification process (Figure 5.1c), so it is possible that during annealing process, these large particles act as nucleation

sites and PSN occurs. As was introduced in chapter 1, very weak texture develops during PSN process and this agrees well with the texture of the annealed LSEM strip.

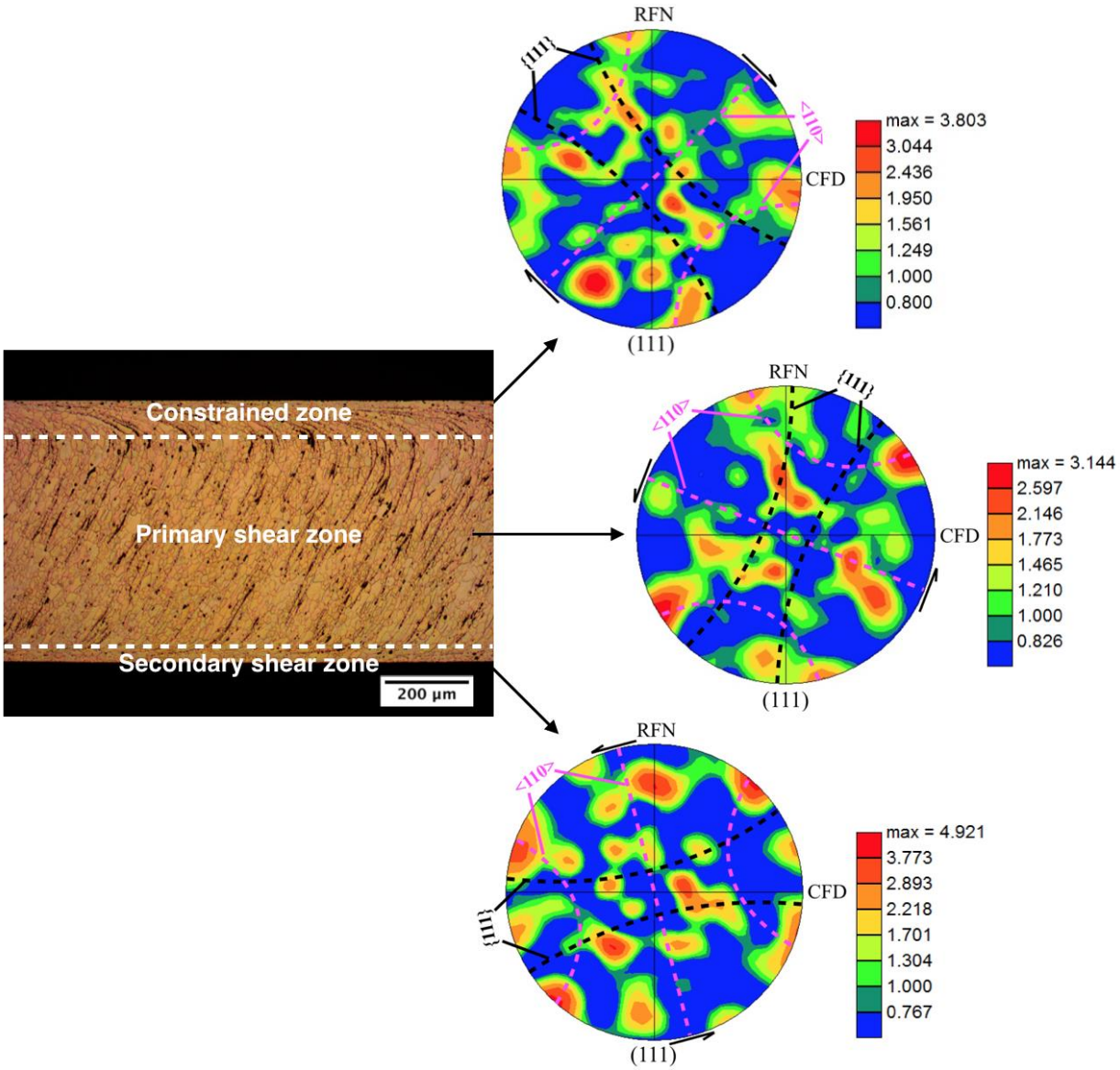

Figure 5.8 Microstructure of LSEM strip annealed at 568 ℃ for 2 min, showing uniform structure with grain size around 20 μm.

5.4 Discussion

The results in this chapter have shown that continuous strip with thickness around 600 μm can be produced from as-cast 6013 aluminum alloy without homogenization using single-step shear deformation LSEM. And this deformed strip can be cold rolled with reduction as large as 73% in a single step without any cracking. Unlike textures in rolled sheet, textures in LSEM strips are demonstrated to be rotated simple shear textures and the rotation angles in constrained, primary shear and secondary shear zones are different. In the annealed strip, a mixed texture containing simple shear texture and other weak components develops. The observations have broad implications for creation of sheet metals and controlling of sheet microstructures.

5.4.1 LSEM vs Hot rolling

Conventional production of aluminum alloy sheets starts from cast ingots and in preparation for the following hot rolling process, the ingots are homogenized at temperatures around 550 ℃ for up to 48 h to remove micro-segregation and dissolve soluble phases. Also, the transformation of the plate-like β-AlFeSi to Chinese script-like α-AlFeSi particles is important for the following hot working process, such as hot rolling and hot extrusion. In reversing hot rolling process, the ingot is hot rolled at temperature between 500 and 600 ℃with rolling reduction about 10% reduction for up to 25 passes. And in the following tandem hot rolling, the transfer slab is hot rolled between 400-500 ℃ with about 50% reduction per pass. In this chapter, however, the possibility of LSEM to produce strip materials directly from as-cast 6013 aluminum alloy without homogenization were demonstrated and continuous strips were obtained in a single step with effective strain as large as 1.6 at ambient temperature. This is a big advantage over conventional rolling process in which homogenization and multi-stage hot rolling (including reversing and tandem hot rolling) consume a large amount of energy and need massive infrastructure.

5.4.2 Cold rolling after LSEM

The surface of the strip produced by LSEM is very flat, but still not as smooth as ones produced by rolling process. So, similar to conventional rolling process, cold rolling is employed to reach the final gauge after LSEM process. In conventional rolling process, the exit temperature of hot band after tandem hot rolling is between 250 and 350 ℃ and then this hot band is coiled and cooled down to room temperature. In the following cold rolling process, this highly recovered hot band is usually cold rolled in 3-4 passes with about 50% reduction in each pass. During our LSEM experiment, the effective strain is as large as 1.6. And amazingly, this highly deformed strips can be further cold rolled down to at least 73% reduction (effective strain 1.5) to 170 μm in thickness in a single step without cracking, which means the as-cast 6013 alloy can withstand total effective strain 3.1 at ambient temperature without failure. This is impossible for conventional rolling process, especially for as-cast aluminum alloy without homogenization. Note that 170 μm is the limit of rolling mill in our lab, but it is not the limit of our LSEM strips. And the hot bands for conventional cold rolling process are highly recovered while our LSEM strips are produced at ambient temperature.

5.4.3 Shear texture and workability

In commercial production of aluminum alloy sheets, β fiber textures, which consists of Brass, Copper and S texture, develop during rolling process [61-64]. In our LSEM process, however, simple shear texture {111} fiber and <110> fiber develop with different rotation angles regarding to CFD in constrained, primary shear and secondary shear zone (Figure 5.7). In FCC materials, such as aluminum alloy, {111} <110> is the slip system where {111} is the slip plane and <110> is the slip direction. During the simple-shear type processes such as LSEM and ECAP (equal channel angular pressing), {111} slip plane tends to align parallel to the shear plane and

<110> slip direction tends to align parallel to the shear direction since shear is the driving force for deformation. Plenty of grains rotate and adjust themselves to align toward this condition during shear deformation and then {111} fiber and <110> fiber form [65-68]. Due to the friction effect between the cutting tool and strip, constraint and strip, the rotation angles in secondary shear and constrained zone are different from primary shear zone.

Slip is the main mechanism for plastic deformation and due to restricted slip systems, deformation is usually confined in certain crystallographic planes and directions. In polycrystalline material, such as aluminum alloy, deformation is rather complex and inhomogeneous, although it appears uniform macroscopically. At low level of strain, the amount of deformation in each grain varies depending on the individual orientation, local Schmid factor, and confinement imposed by neighboring grains [69-72]: in grains with favorable orientations for slip, deformation will primarily occur by single slip in the interior regions of grains; in grains whose crystallographic orientations are not as favorable for slip, however, deformation will tend to localize in the grain boundary regions because additional shear displacements are required to produce grain rotation for slip. With increasing strain, the localized strain in grain boundary becomes more and more severe in order to maintain grain-to-grain contiguity and finally fracture occurs. In strips produced by LSEM process from as-cast 6013 alloy, partial {111} fiber and <110> fiber dominate. And in fact, most of the fiber components spread about the intersection of {111} fiber and <110> fiber (Figure 5.7). That is, most of the grains orient with {111} approximately parallel to shear plane and <110> parallel to shear direction, which is the same as the slip system of FCC materials, {111} <110>. So, grains in LSEM strips are well oriented, nearly perfectly oriented for further deformation and due to this unique shear texture, rotations of grain boundaries are very limited, which prevent the occurrence of fracture effectively. That is a reason why the LSEM strip can be

further cold rolled with 73% reduction in a single step without cracking and after annealing, the LSEM strips have enhanced ductility as have shown in Chapter 4.

5.4.4 Microstructure evolution of cold rolled strip

The microstructure of LSEM (Figure 5.3c) and cold-rolled strips (Figure 5.5) contains constrained, primary shear, and secondary shear zone. The size of the constrained zone in LSEM strip at λ = 2.5 is about 100 μm (Figure 5.3c) and after cold rolling for 17% reduction, the size of constrained zone remains nearly constant. Regarding the relatively small size of secondary shear zone, here we only focus on primary shear and constrained zone as shown in Figure 5.9. During LSEM process, {111} fiber and <110> fiber develop with different rotation angles in different zones. Assume β and θ are rotation angles in constrained and primary shear zone; σ is the stress imposed during rolling process. So, the resolved shear stress that drives plastic deformation during rolling process in constrained zone is:

$$\sigma_s = \sigma \sin \beta \tag{5.1}$$

And the resolved shear stress in primary shear zone is:

$$\sigma_s = \sigma \sin \theta \tag{5.2}$$

In LSEM strip, the rotation angles of shear textures in constrained and primary shear zone are $\beta = 42°$ and $\theta = 70°$. According to the above equations, σ_s in primary shear zone is larger than that in constrained zone. That is, deformation in primary shear zone occurs first. During cold rolling process for 17% reduction, the inclination angle of grains in primary shear zone decreases to 54°. The inclination angle of grains in LSEM strip is 65°, close to the rotation angle of the shear texture, 70°. So here we assume the rotation angle of texture is close to the inclination angle of grains. Under this assumption, after 17% reduction, σ_s in primary shear zone is still larger than that in constrained zone and that is why the size of constrained zone remains almost unchanged

after cold rolled for 17% reduction. With increasing reduction, the inclination of grains decreases while the constrained zone stays undeformed. And when σ_s in constrained zone and primary shear zone are the same ($\theta = \beta = 42°$), slip in constrained zone starts to initiate and deformation in constrained and primary shear zone occurs simultaneously. After cold rolled for 44% reduction, the inclination angle of grains in primary shear zone drops to 27° and the size of constrained zone becomes 86 μm. The reduction in constrained zone is 14%, much smaller than actual cold rolling reduction 44% because deformation starts in constrained zone only when θ is smaller than 42°, so only part of deformation occurs in this zone. This is the same case at 65% and 73% reduction, where the reduction in constrained zone is 58% and 66%, respectively.

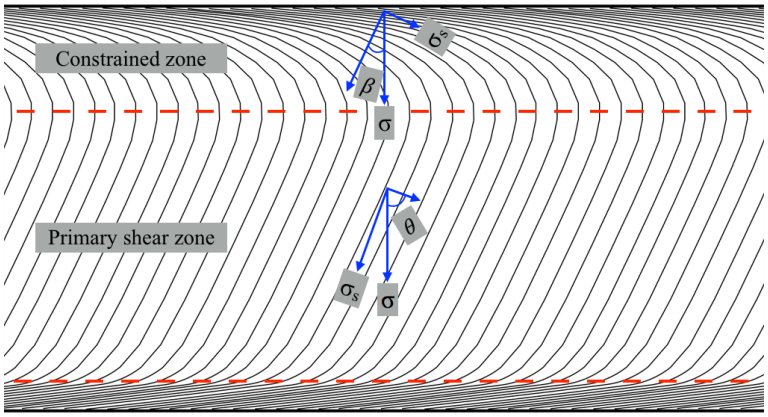

Figure 5.9 Schematic showing flow line-type microstructure after LSEM process. Here σ, the compression imposed on the strip during rolling; σ_s, resolved shear stress along shear plane direction; β and θ are rotation angles of textures in constrained and primary shear zone.

5.4.5 Shear texture and formability

For sheet materials, the Lankford parameter R determines their necking resistance. R is the ratio of the strain in width direction to the strain in thickness direction $R = {\varepsilon_w}/{\varepsilon_t}$. A large value of R indicates a high resistance to thinning in the thickness direction, and thus greater drawability.

For most rolled sheets, the elastic and plastic properties in the plane of the sheet are usually

different due to crystallographic texture developed in the rolling and annealing process. So, an averaged $\bar{R}$ value (R values at 0, 45 and 90° inclined with rolling direction) is employed to measure the formability, and the higher the $\bar{R}$ value, the better the formability.

$$\bar{R} = \frac{R_0 + 2R_{45} + R_{90}}{4} \tag{5.3}$$

The calculated $\bar{R}$ values of some common sheet texture components according to the literatures [73-74] are listed in the Table 5.3. We can see that Cube component, {001} <100> has a much smaller $\bar{R}$ value than {111} fiber. So, in FCC metal sheets, such as aluminum sheets, where the final texture is dominated by Cube component, the $\bar{R}$ is rather small and the formability is bad. Actually this is one of the main barrier that prevents the application of aluminum alloys on the automotive outer body panels. For BCC metal sheets with {111} fiber texture such as drawing quality steel, however, the $\bar{R}$ is much larger and the corresponding formability is better.

In the LSEM strip, based on the EBSD measurement the texture after annealing contains partial {111}, <110> fiber and some other non-Cube components, so the strips are expected to have better formability. More experiment will be done once we have wider strip to validate this.

Table 5.3 Calculated R values for common sheet texture components

Orientation	R_0	R_0	R_0	$\bar{R}$
{001} <100>	1.0	0	1.0	0.53
{111} <110>	1.84	1.89	1.95	1.91
{111} <112>	1.95	1.89	1.84	1.91

5.5 Conclusions

(1) Large strain extrusion machining (LSEM) was employed to produced aluminum strips directly from as-cast 6013 alloy without homogenization and continuous strips were obtained in a single step with effective strain as large as 1.6 at room temperature, which is impossible for conventional rolling process.

(2) The highly-deformed strips from as-cast 6013 alloy can be cold rolled with reduction as large as 73% in a single step without cracking due to the unique shear texture develops during LSEM process. Besides, cold rolling is a good way to improve the surface quality of the LSEM strips.

(3) The strip produced by LSEM is characterized by simple shear textures with partial {111} and <110> fibers and the rotation angles in constrained, primary shear, and secondary shear zone are different. After annealing, the simple shear textures are inherited to the annealed strip. Besides, some other weak components also develop in the strip possibly due to particle stimulated nucleation. But the overall texture is quite different from commercial rolled strips, so the final strips were expected to have better formability.

6. A NOVEL WAY TO PRODUCE ALUMINUM STRIPS BY MACHINING AND ROLLING PROCESS

6.1 Introduction

In the last chapter, LSEM experiments were conduct directly on the as-cast 6013 aluminum alloy without homogenization to produce aluminum strips. Continuous strips were obtained at room temperature and the highly deformed strips have enhanced workability due to the unique shear texture developed in the LSEM process. In this chapter, the non-homogenized as-cast 6013 alloy was warm rolled with the same effective strain and temperature as in LSEM process to demonstrate whether we can produce strip materials directly from as-cast alloys by warm rolling. Then, the resulting warm-rolled strips were cold rolled with the same reduction as cold rolling on LSEM strips in a single step to investigate the workability of the warm-rolled strips. At last, the possibility of LSEM process to take the place of conventional homogenization and hot rolling (including reversing hot rolling and tandem hot rolling) process is discussed and a novel way to produce aluminum alloy sheets, even other types of alloys, such as steel, magnesium alloy, is introduced.

6.2 Experimental procedure

Warm rolling experiments were performed on a lab rolling mill (roll diameter 100 mm) with the same effective strain and temperature as the LSEM experiments in chapter 5. The as-cast samples with 40 mm × 27 mm × 4.8 mm (L × W × T) and 40 mm × 27 mm × 4.2 mm in size were preheated in the furnace to 300 ℃ and transferred to the rolling mill quickly to minimize the heat lose (The distance from the furnace to rolling mill is around 2 m). Then the warm-rolled strips were cold rolled in a single step with about 17%, 44%, 65% and 73% reduction (same reduction

as cold rolling on LSEM strips in chapter 5) in a laboratory rolling mill with roll diameter 100 mm.

The as-cast, warm-rolled and cold-rolled samples are prepared by mechanical grinding from 320 to 2000 grid sand paper and final polishing colloidal silica, followed by etching with 10 wt.% sodium hydroxide between 2-5 min. The through thickness microstructure of the as-cast 6013 alloy, FM, LSEM and rolled strips were investigated by optical microscopy. Microhardness of the bulk and strip specimens were measured by Vickers indentation with loads ranging from 50 g to 100 g to ensure a similar indentation size and at least 10 indentations are measured to obtain an average of the hardness.

6.3 Results and discussions

6.3.1 Casting of 6013 aluminum alloy

The as-cast microstructure along the radial direction reveals a fine equiaxed grain structure with an average grain size around 200 μm (Figure 6.1a), as measured by linear intercept method. During solidification process, dendrite grow along heat flow direction and porosity forms (arrows in Figure 6.1a) between the dendrites because the flow of the liquid is confined. But this small amount of porosity can be removed in the deformation processes such as rolling and extrusion. Large constituent phases (arrow in Figure 6.1b) with size as large as 4 μm forms in the solidification process and in the following cooling process, small second-phase particles precipitate preferably along grain boundary as shown in Figure 6.1b.

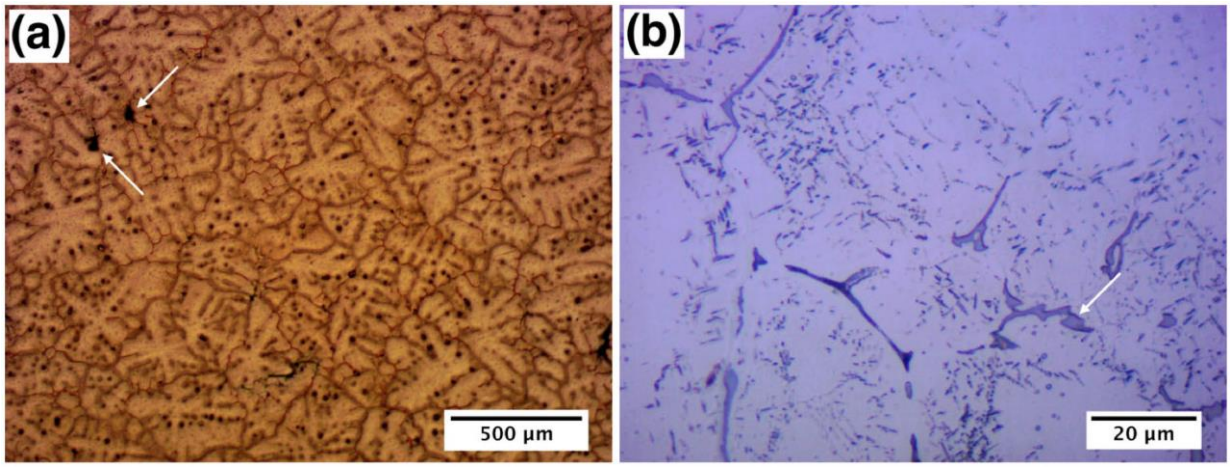

Figure 6.1 Microstructure of the as-cast 6013 alloy with (a) dendritic grain structure and (b) precipitations along grain boundary.

6.3.2 Warm rolling of as-cast alloy

The as-cast 6013 alloy can be deformed by LSEM with effective strain as large as 1.6 in a single step without cracking. To demonstrate whether the cast alloy is as workable in rolling, the sample is warm rolled with the same effective strain as the LSEM strip. In LSEM process, the material is heated adiabatically in a highly localized primary shear zone due to large strain and strain rate. In our LSEM experiment on as-cast 6013 alloy, the temperature rise is estimated around 150 ℃, so in warm rolling experiment, samples are preheated to 300 ℃ to make sure that the deformation temperature during warm rolling process is not less than that in LSEM process. The warming rolling parameters are shown in Table 6.1 (ε_w, effective strain in warm rolling).

Table 6.1 Warm rolling parameters on the as-cast 6013 workpieces

t_i (mm)	R/pass	No. of passes	t_f (mm)	ε_w
4.8	12%	11	1.2	1.6
4.2	16%	8	1.1	1.5

For sample rolled with 12%/pass, fracture happens in the 9th pass, while it occurs in the 6th pass for sample rolled with 16%/pass. In sample rolled with 12%/pass, fractures on edges are much smaller than those of sample with 16%/pass (Figure 6.2a) although they undergo the same strain. Slip is the main mechanism for plastic deformation and due to limited slip systems, deformation is usually restricted in certain crystallographic planes and directions. For grains whose orientations are not favorable for slip, grain rotation occurs to adjust themselves for slip. Thus, deformation will tend to localize in the grain boundary and with increasing strain, the shear displacements in grain boundary is more and more severe [69-72]. Besides, in the as-cast 6013 alloy, constituent particles with size as large as 4 μm form preferably along grain boundary (Figure 6.1b). During the following warm rolling process, regions with high dislocation density and large orientation gradient develop around these particles and this further intensify the occurrence of fracture [58, 75-76]. Finally, crack forms and propagates along grain boundary as shown in arrow in Figure 6.2b. In sample rolled with 16%/pass, the localized strain in grain boundary is more severe than sample rolled with 12%/pass so fracture initiates earlier. For LSEM strips with the same effective strain, however, no fracture appears although such a large strain is achieved in a single step, compared with 11 steps in warm rolling with 12%/pass and 8 steps with 16%/pass.

During LSEM process on as-cast 6013 alloy, the grains are sheared uniformly and this shear, together with the hydrostatic pressure imposed by the constraint, suppress the initiation of cracks effectively, so no cracking occurs even after undergoing such a large strain in a single step and a homogeneous microstructure is obtained (Figure 5.3c). In the warming rolling process, however, due to the large constituent particles, especially ones along grain boundaries, shear strain develops around these particles and penetrates through several grains, so a wavy grain structure is obtained along rolling direction (Figure 6.2c).

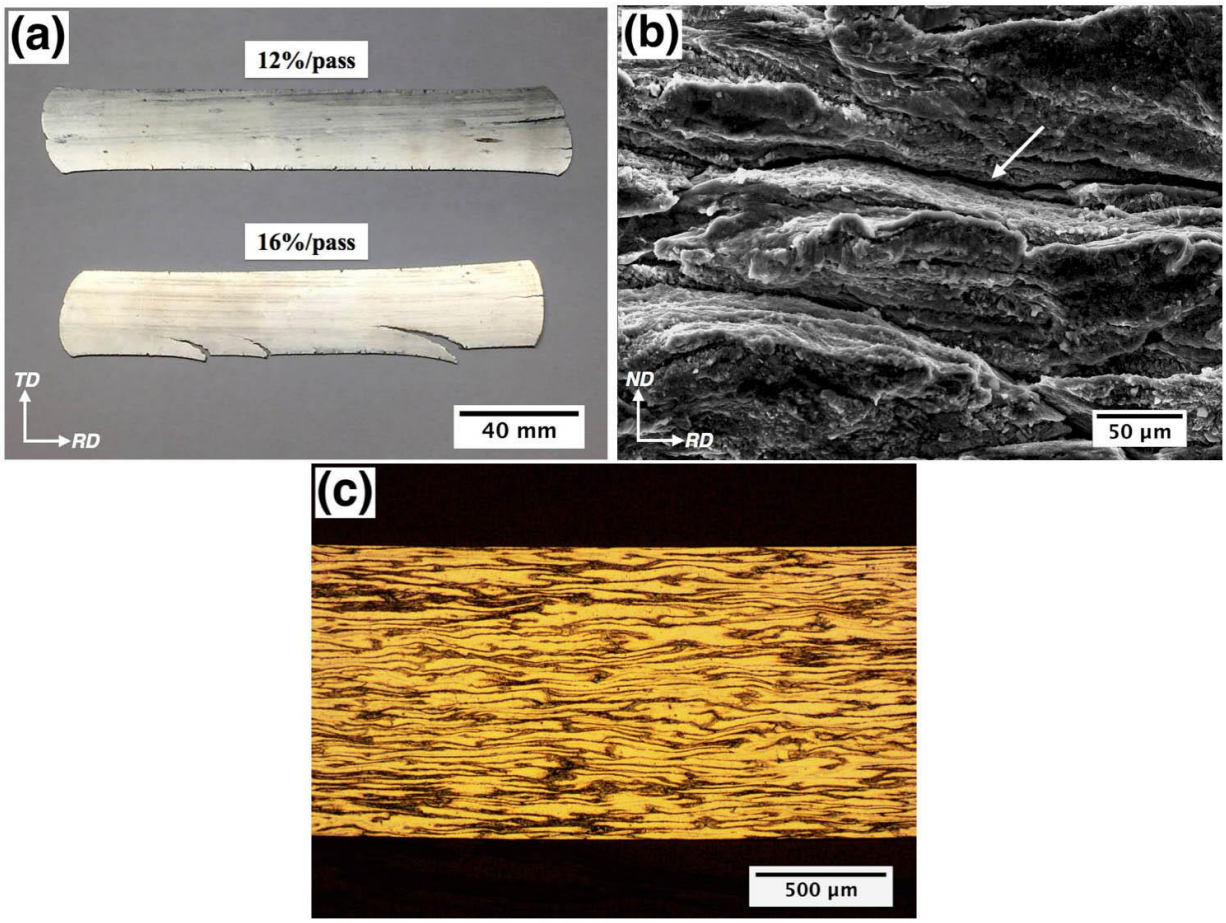

Figure 6.2 (a) Top view of warm-rolled strips with 12% and 16% reduction per pass; (b) fracture surface of the sample rolled with 16%/pass; (c) through-thickness microstructure of the warm-rolled sample with 16%/pass, showing wavy grain structure along RD.

6.3.3 Cold rolling of warm rolled strips

Cold rolling is performed on LSEM strips and no crack develops on the strip even after 73% reduction in a single step (Figure 5.4). So, in comparison, cold rolling experiment is conduct on warm-rolled strips with the same reduction imposed on LSEM strips, as shown in Table 6.2. Here ε_t is the total effective strain (effective strain in warm rolling plus effective strain in cold rolling). The samples used for cold rolling are cut from warm rolled strips (both 12%/pass and 16%/pass) with size about 40 mm × 8 mm × 1.1 mm (L × W × T) and then perform cold rolling process with 17%, 26%, 46%, 65% and 72% reduction in a single step.

Table 6.2 Cold rolling parameters on warm-rolled 6013 aluminum strips

t_i (mm)	R	t_f (mm)	ε_c	ε_t
1.1	17%	0.91	0.2	1.8
1.1	26%	0.81	0.3	1.9
1.1	46%	0.59	0.7	2.3
1.1	65%	0.38	1.3	2.9
1.1	72%	0.31	1.5	3.1

Figure 6.3 shows the top view of warm-rolled strips (12%/pass) cold rolled with different amount of reduction. Similar to cold rolling of LSEM strips, the strip is free of crack after 17% reduction (Figure 6.3a). When cold rolled with 46% reduction, however, fracture happens along the centerline of the strip (Figure 6.3b). In order to determine how the crack propagates, the sample is cold rolled with a smaller reduction, 26%. Under this reduction, a small fracture develops on the head of the strip (arrow in Figure 6.3a). So, the maximum cold rolling reduction can be imposed on the warm-rolled strip without cracking must be less than 26% reduction. During cold rolling of warm-rolled strips, the length of the center portion increases faster due to the friction effect on the edges (red circle in Figure 6.3a, b). This inhomogeneous deformation leads to a compression in the center and tension in the edges. With increasing reduction, this difference in strains becomes more severe and finally crack occurs and propagate along centerline of the strip, even across the whole sample at large reduction (Figure 6.3c). Compared with cold rolling of LSEM strips, however, no crack appears even after 73% reduction in a single pass (Figure 5.4).

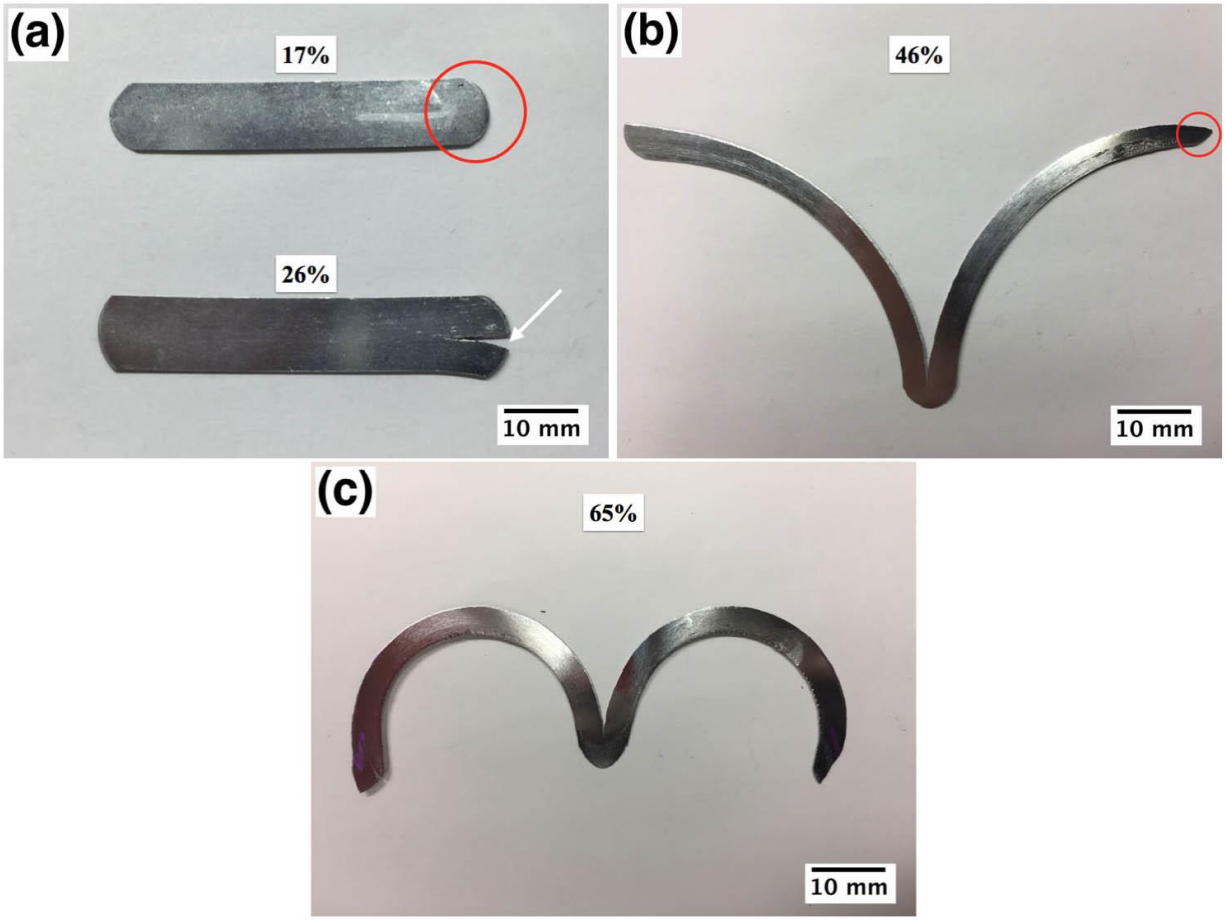

Figure 6.3 Top view of strips after cold rolling with (a) 17% and 26% (b) 46%, and (c) 65% reduction, showing the development of crack during cold rolling.

The microstructures of the warm-rolled strips after cold rolling are distinct from those of the cold-rolled LSEM strips. The grains in the warm-rolled strips after cold rolling are elongated along RD (Figure 6.4), while grains in the cold-rolled LSEM strips are aligned along the maximum tensile direction. The average thickness of grains in Figure 6.4a and b are 28 μm and 14 μm, similar to the that of the cold-rolled LSEM strips with the same reduction, 30 μm (Figure 5.5b) and 15 μm (Figure 5.5d). The homogeneity of microstructure, however, varies considerably. For the LSEM strips, the grain structures are rather uniform after cold rolling, and even after 73% reduction in a single pass, the microstructure are still homogeneous (Figure 5.5e). For the warm-

rolled strips, however, wavy grain structure occurs after 17% reduction (Figure 6.4a), and after 63% reduction, the microstructure is so inhomogeneous that crack propagates along the centerline and cross the whole sample (Figure 6.3c).

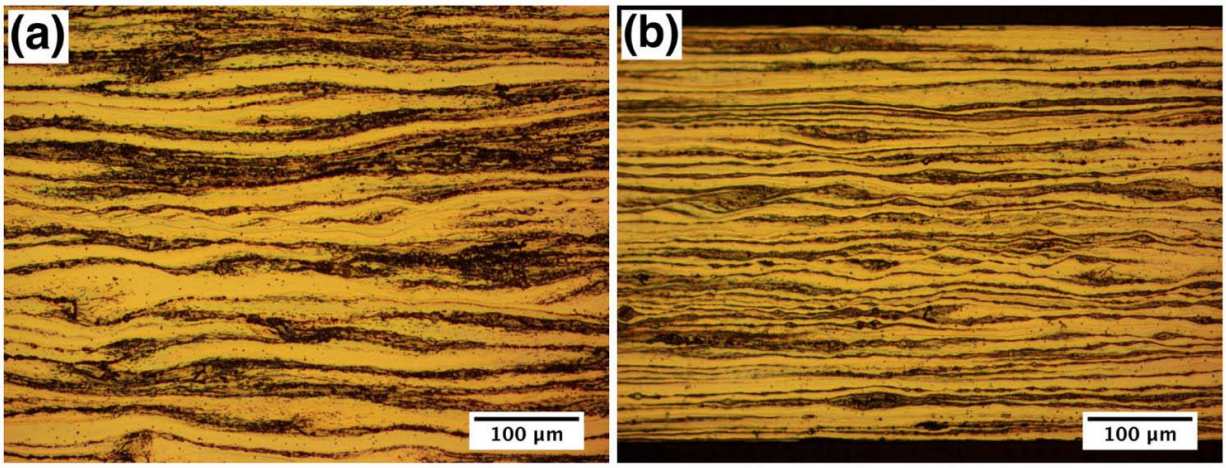

Figure 6.4 Cross-section microstructures of warm-rolled strips (12%/pass) after cold rolling for (a) 17% and (b) 65% reduction.

The cross sections of the warm-rolled and LSEM strips are fine-polished and then cold rolled to study the slip behavior of these two strips. The observation indicates two distinct slip behaviors (Figure 6.5). In the warm-rolled strip, two set of slip lines develop in the cold rolling process as shown in Figure 6.5a. These two set of slip lines intersect with each other, leading to the occurrence of fracture with increasing reduction, especially in the intersections where lie the second phase particles (white arrow in Figure 6.5a). The observation agrees well with references [77-79]. In LSEM strip, however, only one set of slip line develops (Figure 6.5b) and this kind of slip prevents the initiation of fracture, even if in second phase particles (white arrow in Figure 6.5b). This single slip bands have never been seen in the literature before and the reason is the unique shear texture developed in the LSEM process as discussed in chapter 5.

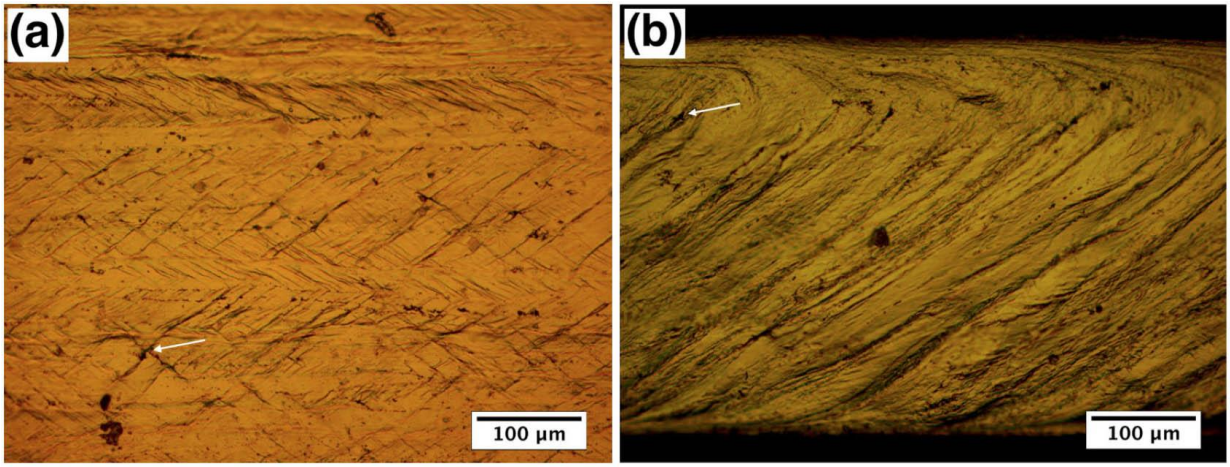

Figure 6.5 Slip patterns of the (a) cold rolled of warm-rolled strips and (b) LSEM strips after 44% reduction in a single step.

6.4 Discussion

6.4.1 LSEM vs warm rolling

Conventional production of aluminum alloy sheets starts from cast ingots and in preparation for the following hot deformation, the ingots are homogenized at temperatures around 550 ℃ for up to 48 h to remove micro-segregation and dissolve soluble phases, but most importantly, to transform the plate-like β-AlFeSi to Chinese script-like α-AlFeSi particles, which is critical for the hot working process, such as hot rolling and hot extrusion. The warm rolling experiments in this chapter demonstrate this. The as-cast samples without homogenization are heated to 300 ℃ and then warm rolled with 12% and 16% reduction per pass. For sample rolled with 12% reduction per pass, fracture happens in the 9th pass, and the same phenomenon occurs in the 6th pass for sample rolled with 16% reduction per pass. In the LSEM experiment on as-cast sample without homogenization, however, continuous strips free of cracking are produced in a single step at room temperature. This is a big advantage over conventional rolling process where homogenization and hot rolling (including reversing and tandem hot rolling) consume plenty of energy. Besides, such a large strain is achieved in only one step during LSEM process, compared

with 11 passes with 12% reduction per pass and 8 passes with 16% reduction per pass, where crack occurs in both cases. The width of the strip produced by LSEM in this study is 7 mm, but wider strips can be made by lathe with higher power. So width is not a problem in the application of this LSEM process.

6.4.2 Cold rolling of LSEM and warm-rolled strips

The surface of the strip produced by LSEM is very flat, but still not as smooth as ones produced by rolling process. So, similar to conventional rolling process, cold rolling is employed to reach the final gauge after LSEM process. During the LSEM experiment, the effective strain is as large as 1.6. And amazingly, this highly deformed strips can be further cold rolled for at least 73% reduction (effective strain 1.5) to 170 μm in thickness without any cracking, which means the non-homogenized as-cast AA6013 can withstand total effective strain 3.1 at ambient temperature without failure. This is impossible for conventional rolling process on non-homogenized aluminum alloys. In comparison, cold rolling of warm-rolled strips is done with almost the same reduction as that on LSEM strips. The results, however, show that fracture occurs on the head of sample at 26% reduction. With increasing reduction, crack propagates along the centerline of the strips as shown in Figure 6.3. So, LSEM strips are much more workable than warm-rolled strips under the same condition.

One possible reason is homogeneity of the microstructure. During solidification process, constituent phases, such as Mg_2Si, α-AlFeSi and β-AlFeSi, distribute preferably along grain boundaries (Figure 6.1b). In the rolling process, the deformed matrix adjacent to constituent particles is relatively homogeneous at low strains; at high strains, however, large scale structural heterogeneities in the form of deformation zones develops around constituent particles. With increasing strain, these microstructural heterogeneities near large particles become more severe

[80-82]. Finally, crack initiates around these large particles and propagates along grain boundary (Figure 6.2b). This can be seen from the microstructure of warm-rolled strip that significant local distortions of the deformed microstructure develop after cold rolled for 65% reduction (Figure 6.4b). In LSEM process, cracks are suppressed effectively by the large hydrostatic pressure and the microstructure is very uniform (Figure 5.3c). Even after cold rolled with 73% reduction in a single step, the microstructure is still rather homogeneous (Figure 5.5e).

The other possible reason for unexpectedly high workability from LSEM is the texture. The effect of simple shear texture on the workability of strip materials produced by LSEM has been studied in chapter 5 and the results showed that the texture developed in the LSEM process enhances the workability of the strip. During rolling process, however, all the initial textures rotate to the final stable β fiber rolling texture. So it is possible that unlike shear texture, β fiber rolling texture does not contribute as much on the workability of the strips.

6.4.3 Homogenization and solution treatment of LSEM strips

In commercial rolling production of aluminum alloy sheets, homogenization has been demonstrated an integral part of the processing route. This high-temperature heat treatment is usually performed after casting, and benefit not only for the following hot deformation, but also for the final ageing process, because of the homogenous distribution of alloy elements, such as Mg, Cu and Si. In LSEM process, continuous strips are obtained from as-cast alloys without homogenization, and this LSEM strip can be cold rolled with at least 73% reduction in a single step. So, homogenization is not needed for this deformation process, which saves plenty of energy. The question, however, is that after cold rolling of LSEM strip, the coring effect still exists. This segregation in alloy elements is not favorable for the ageing process, unless homogenization is achieved during solution treatment process, which occurs at high temperatures for several minutes.

The chemical gradients in a dendritic structure can be reduced by annealing at high temperature for a sufficient time. As a conservative approximation to Fick's law, the relationship between the required time for homogenization and the rate of diffusion is shown as follow equation [83]:

$$x^2 \cong Dt \tag{6.1}$$

where x is the distance between the regions of low and high concentration in the dendrite cell, which is half of the cell size; D is the diffusion rate. The as-cast AA6013 possesses an equiaxed grain structure with grain size around 200 μm, after LSEM at $\lambda = 2.5$, the thickness of the grain reduces to 35 μm. In the following cold rolling process with 65% reduction, the grain thickness further decreases to 15 μm. According to the above equation, the homogenization time of the as-cast AA6013 alloy is around 30 times as large as that of the LSEM strip, 167 times as large as that of cold rolled strip with 65% reduction. Much less time is needed to achieve the same level of homogenization, which saves plenty of energy. So, it is highly possible that homogenization can be accomplished in the solution heat treatment process.

The index of residual microsegregation δ_i is usually employed to discuss the homogenization of microsegregation [84]:

$$\delta_i = \frac{C_M - C_m}{C_M^0 - C_m^0} \tag{6.2}$$

where C_M= maximum solute concentration of element i (in interdendritic spaces) at time t

C_M= minimum solute concentration of element i (in center of interdendritic arms) at time t

C_M^0= maximum initial solute concentration of element i

C_m^0= minimum initial solute concentration of element i

δ_i = index of residual micorsegregation of element i

Before the homogenization process, δ_i = 1 and after fully homogenization, δ_i = 0.

The solution of Fick's second law for the change in the concentration profile with time yields:

$$\frac{C-C_0}{C_M^0-C_0} = \sin\frac{\pi x}{l} e^{-\pi^2(D_s t/{l_0}^2)} \tag{6.3}$$

where D_s is the diffusion coefficient of element i in the solid at homogenization temperature, t is the homogenization time, l_0 is one-half of the dendrite arm spacing. Combining Eq. 6.2 and 6.3 at $x = l_0/2$, $C = C_M$, the following equation is obtained:

$$\delta_i = e^{-\pi^2(D_s t/{l_0}^2)} \tag{6.4}$$

Equation 6.4 is useful for predicting the residual microsegregation of element i at certain temperature for a given amount of time. The times required to homogenize a given cast structure at certain temperatures is shown as:

$$t = -\frac{{l_0}^2 \ln(\delta_i)}{\pi^2 D_s} \tag{6.5}$$

The diffusion coefficient of copper in aluminum is given by [84]:

$$D_s = 0.29e^{-(31120/RT)}\text{cm}^2/\text{s} \tag{6.6}$$

where $R = 1.99$ cal/(mol)(°K).

At 530 ℃, the diffusion coefficient of copper in aluminum is $1.01 \times 10^{-9}\text{cm}^2/\text{s}$ according to Eq. 6.6. Assuming $l_0 = 200$ μm in the as-cast AA6013, the time needed for 95% homogenization at 530 ℃ is 506 min. In the LSEM and cold rolled sample with 65% reduction, however, the $l_0 = 15$ μm and the time required for 95% homogenization at the same temperature is only 11 min. So, it is possible that complete homogenization can be achieved in the solution treatment process.

Based on the analysis above, a novel way to produce aluminum strips is introduced as shown in Figure 6.6. The alloys are static casting into large disk shape workpiece. The workpiece is then scalped on the surface and transferred to LSEM facility without homogenization. In the LSEM

process, continuous strips are obtained at ambient temperature. The LSEM strips are then cold rolled for 1-3 passes to reach the final gauge. Finally, the cold-rolled strips are solution treated at temperatures around 560 ℃ for several minutes to obtain both maximum age hardening response and good formability. Compared to the conventional process of aluminum alloy sheets (Figure 1.1), the homogenization and hot rolling process, including breakdown and tandem hot rolling, are replaced by LSEM process, which has a great potential to save energy.

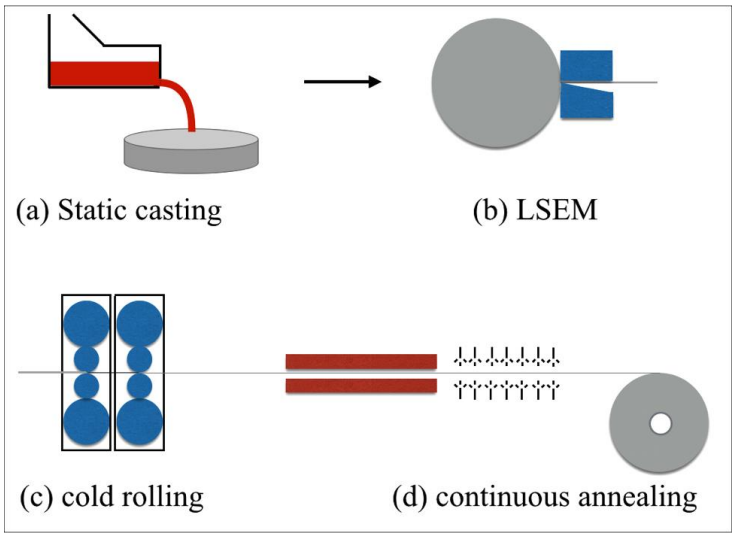

Figure 6.6 Novel way to make aluminum strips by machining and rolling process.

6.5 Summary

(1) Warm rolling of as-cast AA6013 was conduct with the same effective strain at 300 ℃ to compare with the LSEM strip. The as-cast samples were warm-rolled with 12% and 16% reduction per pass and after 9 and 6 passes, respectively, crack occurs on each sample. The warm-rolled samples were then cold rolled with the same reduction as employed in cold rolling of LSEM strips. Obvious cracking happens on the head of the sample only after 26% reduction, much less than 73% reduction of LSEM strip.

(2) A novel way to produce aluminum strips is introduced in this chapter. Compared with

commercial rolling method, the homogenization and hot rolling (including breakdown and tandem hot rolling) process are substituted by a single-step LSEM process. The alloys are static cast into disk-shape workpiece. The workpiece is scalped on the surface and then transferred to the LSEM line. After LSEM, the strips are cold rolled to the final gauge. The cold-rolled strips are solution treated in a continuous annealing line for further deformation processing.

7. CONCLUSIONS AND RECOMMENDATIONS FOR FUTURE WORK

7.1 Conclusions

In this dissertation, conventional free machining (FM) and large strain extrusion machining (LSEM) were employed to produce continuous strips from a variety of AA6013 conditions, which are famous for their limited workability in conventional rolling process. By a proper controlling of cutting parameters (strain, strain rate and temperature), a wide range of deformation microstructures were developed with primary shear zone, secondary shear zone and constraint zone.

AA6013-T6 was used to produce strip materials via FM and LSEM experiments. Continuous strip with thickness from 0.4-0.8 mm were obtained in a single step with a flow-line type microstructure. The initial AA6013-T6 workpiece possessed a fine-grain zone on the surface and coarse-grain zone in the middle. After LSEM, the nonuniform microstructure (difference in grain size) was inherited to the strip and this inhomogeneity vanishes gradually with decreasing λ. But this inhomogeneous microstructure has no effect on the hardnesses of the strip. Complete dynamic recrystallization occurs when the workpiece was LSEM at T_0 = 400 ℃, which is lower than commercial hot rolling process (~ 500 ℃). The LSEM and warm-rolled strips with the same effective strain and same heat treatment history were compared to reveal the difference in microstructure and properties. They have similar microstructure and hardness, but distinct ageing response and tensile properties. The ageing response of the annealed LSEM strip is better (average 6% higher in hardness) than annealed warm-rolled strips; the yield strength of annealed LSEM strip is lower than warm-rolled strip, but they have almost the same tensile strength. The LSEM strip is much more ductile than warm-rolled strip.

Large strain extrusion machining (LSEM) was employed to produced aluminum strips directly from as-cast AA6013 alloy without homogenization and continuous strips were obtained in a single step with effective strain as large as 1.6 at room temperature, which is impossible for conventional rolling process. Interestingly, this highly-deformed strips could be cold rolled with reduction as large as 73% in a single step without cracking due to the unique shear texture developed during LSEM process. Meanwhile, the surface quality of the LSEM strips was improved considerably by subsequent cold rolling process. The texture of LSEM strip from as-cast AA6013 was characterized by partial {111} and <110> fibers inclined relative to the strip surface. The inclination angle matches closely with the prediction from a geometric shear plane model. After annealing, the simple shear textures are inherited to the annealed strip. Besides, some other weak components also develop in the strip, possibly due to particle stimulated nucleation. But the overall texture is quite different from commercial rolled strips, so the final strips were expected to have better formability.

Warm rolling of as-cast AA6013 was conduct with the same effective strain at 300 ℃ to compare with the strip produced by LSEM. The as-cast samples were warm-rolled with 12% and 16% reduction per pass and cracking occurs on each sample. The warm-rolled samples were then cold rolled with the same reduction as employed in cold rolling of LSEM strips. Obvious cracking happens on the head of the sample only after 26% reduction, much less than 73% reduction of LSEM strip without cracking.

A novel way to produce aluminum sheets was introduced and compared with commercial production of aluminum sheets. The alloys are static cast into disk-shape workpiece. The workpiece is scalped on the surface and then transferred to the LSEM line. In this line, continuous strips with highly deformed microstructure and simple shear texture are produced. After LSEM,

the strips are cold rolled to the final gauge. The cold-rolled strips are solution treated in a continuous annealing line for further heat treatment or deformation processing. Compared with commercial rolling process, the homogenization and hot rolling (including breakdown and tandem hot rolling) process are substituted by a single-step LSEM process.

7.2 Future work

6xxx aluminum alloys, owning to their balanced properties, such as high strength-to-weight ratio and good corrosion resistance, have been considered as a potential candidate for automotive outer body panels. The current dissertation provides a novel way to produce 6xxx aluminum sheet materials and investigate the microstructure and texture evolution during large shear deformation process. However, some new questions are raised and some more experiments need to be done to fully understand the phenomenon in this dissertation.

In chapter 4, a comparison of the microstructure and mechanical property of the LSEM and warm-rolled strips was made and the results showed that the ageing response and ductility of the LSEM strips are better than the warm-rolled strips. The better ductility can be explained by the texture developed in the LSEM and following annealing process. But it is hard to illustrate the ageing response of the LSEM strips. Since the only difference between the LSEM and warm-rolled strips is the initial texture, it is speculated that the texture plays a role in the ageing process. So TEM study of the ageing behavior is recommended in the future to investigate the orientation relationship between the precipitates and the matrix. It is possible that certain textures influence the size, distribution, even coherency of the precipitates during ageing process.

Homogenization is very important for age-hardenable aluminum alloy such as AA6013 and the maximum strength of these alloys cannot be achieved unless they are completely homogenized. In the new way to make aluminum sheet materials, however, homogenization is avoided to save

energy, but it may affect the final ageing response of the strips. After LSEM and cold rolling, the sheet materials are solution treated, which typically occurs at temperatures about 550 °C for several minutes. So it is important to find out whether or not complete homogenization can be obtained in the short solution treatment process and If not, how much time is needed to reach a complete homogenization.

In commercial rolling process of 6xxx aluminum alloy, the so-called β fiber texture, including Brass, Copper, and S texture develops. And in the annealing process, Cube, Goss, and R texture forms. In LSEM process, however, shear texture forms and in the following annealing process, a mixed texture containing shear texture and non-Cube component develops. Cube and Goss texture are detrimental to the formability of aluminum sheets, but in the LSEM strips, completely different texture develops. In the future, the following experiments are suggested to perform on this part, if possible:

1. Study the texture related properties of the LSEM strips, such as formability, roping performance and deep drawability.
2. Investigate the texture evolution during LSEM and rolling process and figure out the role of rolling in controlling the texture of the LSEM strips. We have some good results on this part, but more experiments need to be done.
3. Study the microstructure, texture, mechanical property, texture related properties (formability, roping performance, deep drawability and so on).

REFERENCE

[1] Benedyk, J. C. (2010). *Aluminum alloy for light weight automotive structures,* Woodhead Publishing Series in Composites Science and Engineering.

[2] Scheps, R. (Alcoa, representing ALTG), *The Battle for Market Share,* presentation made at the American Metal Market's 3rd Annual Automotive Metals Conference, Oct. 28-30, 2008, detroit, MI.

[3] Bull, M. (Novelis, representing ALTG), *Going Green: The Aluminum Perspective,* presentation made at the American Metal Market's 3rd Annual Automotive Metals Conference, Oct. 28-30, 2008, detroit, MI.

[4] Martchek, K. (Alcoa), *Keys to the Climate in the Aluminum Supply Chain,* presentation made at the American Metal Market's 3rd Annual Automotive Metals Conference, Oct. 28-30, 2008, detroit, MI.

[5] *Aluminum Standards and Data 2008 (standard and metric)*, The Aluminum Association.

[6] Davis, J.R. (1993). *Aluminum and Aluminum Alloys*, ASM Specialty Handbook, ASM International.

[7] Hesse, W. (2007). *Aluminium Material Data Sheets*, Aluminium-Verlag Marketing & kommunikation GmbH, düsseldorf, Germany, 5th edition.

[8] Heinz, A., Haszler, A., Keidel, C., Moldenhauer, S., Benedictus, R., & Miller, S. W. (2000). Recent development in aluminum alloys for aerospace applications. *Materials Science and Engineering A*, 280, 102-107.

[9] Williams, J. C., & Jr. Starke, E., A. (2003). Progress in structural materials for aerospace systems. *Acta Materialia*, 51, 5775-5799.

[10] Dursun, T., & Soutis, C. (2014). Recent developments in advanced aircraft aluminum alloys. *Materials and Design*, 56, 862-871.

[11] Zhen, L., Hu, H., Wang, X. Y., Zhang B. Y., & Shao W. Z. (2009). Distribution characterization of boundary misorientation angle of 7050 aluminum alloy after high-temperature compression. *Journal of Materials Processing Technology*, 209, 754-761.

[12] Nakai, M., & Eto, T. (2000). New aspects of development of high strength aluminum alloys for aerospace applications. *Materials Science and Engineering A*, 285, 62-68.

[13] Hirsch, J. (2004). Automotive trends in aluminum-The European perspective. *Materials Forum*, 28, 15-23.

[14] Hirsch, J., & Al-Samman, T. (2013). Superior light metals by texture engineering: Optimized aluminum and magnesium alloys for automotive applications. *Acta Materialia*, 61, 818-843.

[15] Ma, W. Y., Wang, B. Y., Yang, L., Tang, X. F., Xiao, W. C., & Zhou, J. (2015). Influence of solution heat treatment on mechanical response and fracture behavior of aluminum alloy sheets: An experimental study. *Materials Design*, 88, 1119-1126.

[16] Kang, J., Wilkinson, D. S., Jain, M., Embury, J. D., Beaudoin, A. J., Kim, S., Mishira R., & Sachdev, A. K. (2006). On the sequence of inhomogeneous deformation process occurring during tensile deformation of strip cast AA5754. *Acta Materialia*, 54, 209-218.

[17] Halim, H., Wilkinson, D. S., & Niewczas, M. (2007). The Portevin-Le Chatelier effect and shear band formation in an AA5754 alloy. *Acta Materialia*, 55, 4151-4160.

[18] Engler, O., & Hirsch, J. (2002). Texture control by thermomechanical processing of AA6xxx Al-Mg-Si sheet alloys for automotive applications-a review. *Materials Science and Engineering A*, 336, 249-262.

[19] Couto, K. B. S., Claves, S. R., Van Geertruyden, W. H., Misiolek, M. Z., & Goncalves, M. (2005). Effects of homogenization treatment on microstructure and hot ductility of aluminum alloy 6063, *Material Science and Technology,* 21, 263-268.

[20] Kuijpers, N. C. W., Tirel, J., Hanlon, D. N., & van der Zwaag, S. (2002). Quantification of the evolution of the 3D intermetallic structure in a 6005A aluminum alloy during a homogenization treatment. *Materials Characterization,* 48, 379-392.

[21] Kuijpers, N. C. W., Kool, W. H., Koenis, P. T. G., Nilsen, K. E., Todd, I., & van der Zwaag, S. (2003). Assessment of different techniques for quantification of a-Al(FeMn)Si and b-AlFeSi intermetallics in AA 6xxx alloys. *Materials Characterization,* 49, 409-420.

[22] Rinderer, B. (2011). The metallurgy of homogenization. *Materials Science Forum,* 693, 264-275.

[23] Rosefort, M., Matthies, C., Buck H., & Koch, H. (2011). Using SEM and EDX for a simple differentiation of a- and b-AlFeSi-phases in wrought aluminum billets. *Light Metals,* 711- 716.

[24] Totten, G. E., Funatani, K., & Xie, L. (2004). *Handbook of Metallurgical Process Design.* Marcel Dekker, Inc.

[25] Bryant, J. D. (1999). The effects of presaging treatments on aging kinetics and mechanical properties in AA6111 aluminum autobody sheet. *Metallurgical and Materials Transactions A,* 30A, 1999-2006.

[26] Murayama, M., & Hono, K. (1999). Pre-precipitate clusters and precipitation process in Al-Mg-Si alloys. *Acta Materialia,* 47(5), 1537-1548.

[27] Engler, O., & Randle, V. (2010). *Introduction to Texture Analysis, Macrotexture, Microtexture and Orientation Mapping-2nd edition,* Taylor & Francis Group.

[28] Hirsch, J., & Lücke, K. (1988). Mechanism of deformation and development of rolling textures in polycrystalline ccc metals. *Acta Metallurgica et Materialia*, 36, 2863-2882.

[29] Engler, O., Hirsch, J., & Lücke, K. (1989). Texture development in Al 1.8 wt% Cu depending on the precipitation state. *Acta Metallurgica et Materialia*, 37, 2743-2753.

[30] Hollinshead, P.A., & Sheppard, T. (1989). Development of rolling textures in aluminum alloy 3004 subjected to varying hot-rolling deformation. *Metallurgical and Materials Transactions A*, 20A, 1495-1507.

[31] Daaland, O., & Nes, E. (1996). Recrystallization texture development in commercial Al-Mn-Mg alloys. *Acta Materialia*, 44, 1413-1435.

[32] Hirsch, J., Nes, E., & Lücke, K. (1987) Rolling and recrystallization textures in directionally solidified aluminium. *Acta Metallurgica*, 35, 427-438.

[33] Engler, O., & Huh, M. Y. (1999) Evolution of the cube texture in high purity aluminum capacitor foils by continuous recrystallization and subsequent grain growth. *Materials Science and Engineering A*, 271, 371-381.

[34] Engler, O., Hirsch, J., & Lücke, K. (1995) Texture development in Al-1.8 wt% Cu depending on the precipitation state-Recrystallization textures. *Acta Metallurgica et Materialia*, 43, 121-138.

[35] Weiland, H., & Hirsch, J. R. (1991) Microstructure and local texture in hot rolled aluminum. *Textures and Microstructures*, 14-18, 647-652.

[36] Doherty, R. D., Kashyap, K., & Panchanadeeswaran, S. (1993) Direct observation of the development of recrystallization texture in commercial purity aluminum. *Acta Metallurgica et Materialia*, 41, 3209-3053.

[37] Daaland, O., & Nes, E. (1996) Recrystallization texture development in commercial AlMnMg alloys. *Acta Materialia,* 44, 1413-1435.

[38] Dalland, O., & Nes, E. (1996) Origin of cube texture during hot rolling of commercial AlMnMg alloys. *Acta Materialia,* 44, 1389-1411.

[39] Vatne, H. E., Furu, T., & Nes, E. (1996) Nucleation of recrystallised grains from cube bands in hot deformed commercial purity aluminium. *Materials Science and Technology,* 12, 201-210.

[40] Jensen, D. J. (1995) Growth rates and misorientation relationships between growing nuclei/grains and the surrounding deformed matrix during recrystallization. *Acta Metallurgica et Materialia,* 43, 4117-4129.

[41] Doherty, R. D. (1997) Recrystallization and texture. *Progress in Material Science,* 42, 39-58.

[42] Engler, O. (1998) On the influence of orientation pinning on growth selection of recrystallization. *Acta Materialia,* 46, 1555-1568.

[43] Engler, O. (1999) On the origin of the R orientation in the recrystallization textures of aluminum alloys. *Metallurgical and Materials Transactions A,* 30A, 1517-1527.

[44] Engler, O. (2013) Nucleation and growth druing recrystallization of aluminum alloys investigated by local texture analysis. *Materials Science and Technology,* 12(10), 859-872.

[45] Humphreys, F. J. (1977) The nucleation of recrystallization at second phase particles in deformed aluminum. *Acta Metallurgica,* 25(11), 1323-1344.

[46] Vatne, H. E., Engler, O., & Nes, E. (1997) Influence of particles on recrystallization texture and microstructures of aluminum alloy 3103. Materials Science and Technology, 13(2), 93-102.

[47] Nes, E., & Hutchinson, W.B. (1989) Texture and grain size control during processing of metals. Proceedings of 10th Risø International Symposium on Material Science, 233-250.

[48] Engler, O., Chavooshi, A., Hirsch, J., & Gottstein, G. (1994) Formation of recrystallization textures and plastic anisotropy in Al-Mg-Si alloys. *Materials Science Forum,* 157-162, 939-944.

[49] Brown, T. L., Swaminathan, S., Chandrasekar, S., Compton W. D., & Trumble K. P. (2002) Low-cost manufacturing process for nanostructured metals and alloys. *Journal of Materials Research,* 17, 2484-88.

[50] Swaminathan, S., Shankar, M. R., Lee, S., Hwang, J., King, A. H., Kezar, R. F., Rao, B. C., Brown, T. L., Chandrasekar, S., Compton W. D., & Trumble K. P. (2005) Large strain deformation and ultra-fine grained materials by machining. *Materials Science and Engineering A,* 410-411, 358-363.

[51] Guo, Y., Efe, M., Moscoso, W., Sagapuram, D., Trumble K. P., & Chandrasekar S. (2012) Deformation field in large-strain extrusion machining and implication for deformation processing. *Scripta Material,* 66, 235-38.

[52] Sagapuram, D., Efe, M., Moscoso, W., Chandrasekar S., & Trumble K. P. (2013) Controlling texture in magnesium alloy sheet by shear-based deformation processing. *Acta Materialia,* 61, 6843-6856.

[53] Andrew, K., Sagapuram, D., Trumble, K. P., & Chandrasekar, S. (2016) Texture development in high-silicon iron sheet produced by simple shear deformation. Metallurgical and Materials Transactions A, 47A, 3095-3108.

[54] Huang, C., Murthy, T. G., Shankar, M. R., M'Saoubi, R., & Chandrasekar, S. (2008) Temperature rise in severe plastic deformation of titanium at small strain-rates. *Scripta*

Materialia, 58, 663-666.

[55] Efe, M., Moscoso, W., Trumble, K. P., Compton W. D., & Chandrasekar S. (2012) Mechanics of large strain extrusion machining and application to deformation processing of magnesium alloys. *Acta Materialia,* 60, 2031-2042.

[56] ALCOA Aerospace Technical Fact Sheet: Alloy 6013 Sheet, Bettendorf, Iowa.

[57] ALCOA, Aluminum Alloy 6013. (1987). *Alloy Digest,* Orange, NJ.

[58] Humphreys, F. J., & Hatherly, M. (2004). *Recrystallization and related annealing phenomena.* Elsevier.

[59] Bai, X. L., & Trumble, K. P. *Materials Science and Engineering A,* prepare for publish.

[60] Liu, Y. L., Kang, S. B., & Kim, H. W. (1999). The complex microstructures in an as-cast Al-Mg-Si alloy. *Materials Letter,* 41, 267-272.

[61] Zhen, L., Chen, J. Z., Yang, S. J., Shao, W. Z., & Dai, S. L. (2009). Development of microstructures and texture during cold rolling in AA7055 aluminum alloy. *Materials Science and Engineering A,* 504, 55-63.

[62] Mishin, O. V., Bay, B., & Jensen, D. J. (2000). Through-thickness texture gradients in cold-rolled aluminum. *Metallurgical and Materials Transaction A,* 31, 1653-1662.

[63] Liu, W. C., Man, C. S., Raabe, D., & Morris, J. G. (2005). Effect of hot and cold deformation on the recrystallization texture of continuous cast AA5052 aluminum alloy. *Scripta Materialia,* 53, 1273-1277.

[64] Panchanadeeswaran, S., & Field, D. P. (1995). Texture evolution during plane strain deformation of aluminum. *Acta Metallurgical Materialia,* 43, 1683-1692.

[65] Wang, S. C., Starink, M. J., Gao, N., Qiao, X. G., Xu, C., & Langdon, T. G. (2008). Texture evolution by shear on two planes during ECAP of a high-strength aluminum alloy. *Acta Materialia,* 56, 3800-3809.

[66] Ei-Danaf, E. A. (2008). Texture evolution and fraction of favorably oriented fibers in commercially pure aluminum processed to 16 ECAP passes. *Materials Science and Engineering A,* 492, 141-152.

[67] Gazder, A. A., Torre, F. D., Gu, C. F., Davies, C. H. J., & Pereloma, E. V. (2006). Microstructure and texture evolution of bcc and fcc metals subjected to equal channel angular extrusion. *Materials Science and Engineering A,* 415, 126-139.

[68] Li, S. Y., Beyerlein, I. J., & Bourke, M. A. M. (2005). Texture formation during equal channel angular extrusion of fcc and bcc materials: comparison with simple shear. *Materials Science and Engineering A,* 394, 66-77.

[69] Taylor, G. I. (1938). Plastic strain in metals, *Journal of the Institute of Metals,* 62, 307-324.

[70] Eshelby, J. D. (1957). The determination of the elastic field of an ellipsoidal inclusion, and related problems. *Proceedings of Royal Society A,* 241, 376-396.

[71] Ashby, M. F. (1970). The deformation of plastically non-homogeneous materials. *Philosophical Magazine,* 21, 399-424.

[72] Stoudt, M. R., & Ricker, R. E. (2002). The relationship between grain size and the surface roughening behavior of Al-Mg alloys. *Metallurgical and Materials Transactions A,* 33A, 2883-2889.

[73] Qin, L., Seefeldt, M., & Houtte, P. V. (2013). Meso-scale modelling on ridging or roping of aluminum alloys. *Materials Science and Technology,* 1274-1283.

[74] Jin, H., & Gupta A. K. (2012). The effect of through-thickness texture inhomogeneity on roping behavior in AA6111 Al-Si-Mg-alloy. *Materials Science Forum,* 702-703, 273-278.

[75] Liu, Q., Yao, Z. Y., Godfrey, A., & Liu, W. (2009). Effect of particles on the microstructural evolution during cold rolling of the aluminum alloy AA3104. *Journal of Alloys and Compounds*, 482, 264-271.

[76] Doherty, R. D., Hughes, D. A., Humphreys, F. J., Jonas, J. J., Jensen, D. J., Kassner, M. E., King, W. E., Mcnelley, T. R., McQueen H. J., & Rollett, A. D. (1997). Current issurs in recrystallization: a review. *Materials Science and Engineering A,* 238, 219-274.

[77] Davis K. G., Teghtsoonian, E., & Lu, A. (1966). Slip band continuity across grain boundaries in aluminum. *Acta Metallurgica,* 14(12), 1677-1684.

[78] Hahn, G. T., & Rosenfield, A. R. (1975). Metallurgical factors affecting fracture toughness of aluminum alloys. Materials and Metallurgical Transactions A, 6A, 653-668.

[79] Vasudevan, A. K., & Doherty, R. D. (1986). Grain boundary ductile fracture in precipitation hardened aluminum alloys. *Acta Metallurgica*, 35(6), 1193-1219.

[80] Kim, H. W., Kang, S. B., Tsuji, N., & Minamino, Y. (2005). Deformation textures of AA8011 aluminum alloy sheets severely deformed by accumulative roll bonding. *Metallurgical and Materials Transactions A,* 36A, 3151-3163.

[81] Humphreys, F. J., & Kalu, P. N. (1987). Dislocation-particle interactions during high temperature deformation of two-phase aluminum alloys. *Acta Metallurgica,* 35(12), 2815-2829.

[82] IIdefonse, B., & Mancktelow, N. S. (1993). Deformation around rigid particles: The influence of slip at the particle/matrix interface. *Tectonophysics*, 221(3-4), 345-359.

[83] Brooks, C. R. (1991). *Principles of heat treating of nonferrous alloys*, *ASM handbook*, 4, 823-840.

[84] Flemings, M. C. (1974). *Solidification processing,* McGraw-Hill, 328-355.

VITA

Xiaolong Bai was born and raised in Fuyang, Anhui Province, China, where he attended Taihe No.1 High School. He received his bachelor of Engineering degree in Inorganic Non-metallic Materials Science and Engineering in 2011 from Hefei University of Technology. Then he continued as a master student there and received his master's degree in 2014 in Materials Science. In 2014, he began his graduate studies at Purdue University in West Lafayette, in School of Materials Engineering, working with Prof. Kevin Tumble and Prof. Srinivasan Chandrasekar. He is expecting to receive his Ph.D degree in December, 2018.